# REFINING FIELD PORTABLE TECHNOLOGY: QUANTIFICATION OF ARSENIC FIELD TEST KITS

by

Brian Battaglia

Bachelor of Engineering, Ryerson University, Toronto, Canada, 2015

A thesis

presented to Ryerson University

in partial fulfillment of the

requirements for the degree of

Master of Applied Science

in the Program of

Mechanical and Industrial Engineering

Toronto, Ontario, Canada, 2015

AUTHOR'S DECLARATION FOR ELECTRONIC SUBMISSION OF A THESIS

I hereby declare that I am the sole author of this thesis. This is a true copy of the thesis, including any required final revisions, as accepted by my examiners. I authorize Ryerson University to lend this thesis out to other institutions or individuals for the purpose of scholarly research. I further authorize Ryerson University to reproduce this thesis by photocopying or by other means, in total or in part, at the request of other institutions or individuals for the purpose of scholarly research. I understand that my thesis may be made electronically available to the public.

# Abstract

REFINING FIELD PORTABLE TECHNOLOGY:
QUANTIFICATION OF ARSENIC FIELD TEST KITS

Masters of Applied Science, 2015

Brian Battaglia

Mechanical and Industrial Engineering
Ryerson University

This thesis investigates issues related to the detection of arsenic from water sources and the analysis performed to quantify its presence. Through the literature it is shown that colourimetric means of analysis are essential, but current techniques suffer quantitatively, generally relying on a technicians' ability to visually discern colour. An increased level of control, over the Gutzeit method, would serve to drastically improve the existing means of analysis. With reliance being placed on simple field portable technologies, considerable room has been left for misclassifications. Methodology and means of using these commercial products must therefore be tuned, if they are to be globally accepted as a means of quantification.

This thesis compared both benchmark and colourimetric technologies, to redefine in-field analysis. Here the goals were to improve both the classification of arsenic concentrations in water and alleviate the need for technical proficiency. A framework was built under ideal conditions, moving away from the qualitative state of existing colourimetric analyses. A combination of cameras and imaging apparati were put to use, in the acquisition of colourimetric indicator images. MATLAB algorithms were applied to quantitatively discern samples with assembled calibration curves.

# Acknowledgments

I would like to thank my two supervisors, Dr. Beau Standish and Dr. Scott Tsai, for providing me the opportunity to collaborate with them.

I would also like to thank my colleagues, Alireza Rahimnejad, Bryan Bonici, Hiep Nguyen, Nevetha Yogarajah, Omar Rodriguez, Steve Jones, Vaskar Gnyawali and Vineet Missra for their invaluable support throughout the course of the performed research.

Lastly, I would like to thank Grand Challenges Canada, Ontario Grant Scholarship and Ryerson University's Faculty of Engineering and Architectural Science for Financial Support.

# Dedications

I dedicate this thesis to my parents and close friends, who have both supported and encouraged me throughout this period of my education.

# Table of Contents

# List of Tables

# List of Figures

# List of Terms and Abbreviations

| | |
|---|---|
| AAS | Atomic Absorption Spectroscopy |
| Analyte | A substance or chemical constituent that is undergoing analysis. |
| ANNs | Artificial Neural Networks |
| CCD | Charge-coupled Device |
| Chroma | Short for chrominance, signal used to convey colour |
| Covariance | A measure of how much two random variables change together |
| CMYK | Subtractive colour model with cyan, magenta, yellow, and black channels |
| CTAB | Cetrimonium bromide surfactant |
| DIA | Digital image analysis |
| DI-$H_2O$ | Deionized water |
| DMA | Dimethylated Arsenic |
| DOF | Depth of Field, the region of exceptionally sharp optical focus |
| DSLR | Digital single-lens reflex camera |
| EPA | Environmental protection agency |
| FTKs | Field test kits |
| Gamut | A model for colour that is defined in reference to the colour space |
| GFP | Green fluorescent protein |
| Gutzeit | A method to reduce arsenic in solution, releasing it as a gas |
| HG | Hydride generation |
| ICP – AES | Inductively coupled plasma-atomic emission spectroscopy |
| HSV/HSI | Colour model with hue, saturation and value channels |
| LAB | Opponent space colour model with luminance, red vs. green and blue vs. yellow channels |
| YCbCr | Discrete encoding of RGB as Luma and Chroma channels |
| Mapping | The colourimetric range that is studied in relation to arsenic concentration |
| MDL | Method Detection Limit |
| Methylation | A form of alkylation where a methyl group replaces a hydrogen atom |
| MI | Matrix Interference |
| MMA | Monomethylated Arsenic |
| MSE | Mean squared error |
| NP | Nanoparticles |
| PAD | Paper-based Analytic Devices |
| PPB | Parts-per-billion, a measure of concentration |
| POC | Point of care |
| Potable | Safe for consumption |
| PSNR | Peak Signal-to-noise ratio |
| PTFE | Polytetrafluoroethylene |
| PVDF | Polyvinylidene fluoride |
| SDDC | Silver diethyldithiocarbamate |
| SNR | Signal-to-noise Ratio |
| SML | Smartphone with macro lens attachment |

| | |
|---|---|
| RGB | Additive colour model with Red, Green, Blue channels |
| Tuples | An ordered list of elements |
| FPI | Field Portable Imaging |
| FPT | Field Portable Technology |
| WHO | World Health Organization |

# Chapter One

# 1. Introduction

The health effects caused through exposure to heavy metals has been difficult to quantify with widespread occurrences going unnoticed [1]. Heavy metal pollutants, specifically cadmium (Cd), chromium (Cr), manganese (Mn), cobalt (Co), iron (Fe), selenium (Se), nickel (Ni), copper (Cu), zinc (Zn), and arsenic (As), have become a concern for public health and safety, due to their high toxicity, pressing the need for effective monitoring and measurement [2]. Many of these heavy metals bioaccumulate, inhibiting proper cellular functions, and result in serious ailments [3]. While there are a variety of metals to quantify, the focus of this thesis will be on the detection of arsenic in water sources and the application of digital technologies.

## 1.1 Motivation and Objectives

The World Health Organization (WHO) and the US Environmental Protection Agency (EPA), have classified arsenic as a human carcinogen. While the allowable concentration of arsenic was set to 50 µg/L in severely affected areas such as Bangladesh, it is generally recommended that the threshold for arsenic be reduced to a value of 10 µg/L [4], [5]. This reduction in the threshold concentration was substantiated as the analysis of unpolluted fresh water sources typically fall within the range of 1 to 10 µg/L [4]. Analyses of industrial regions have been especially informative: those with sulfide mineralization or mining processes have demonstrated arsenic concentrations ranging from 100 to 5000 µg/L [4].

As the presence of arsenic has been perceived to be detrimental to human health, a variety of detection methods have been sought. The means of detection are generally based upon spectrometric or electrochemical methods. Some examples of the possible methods to detect the presence of arsenic include spectrophotometry, inductively coupled plasma-mass spectrometry, neutron activation analysis, optical spectrometric techniques and high-pressure liquid chromatography, among other methods [6]. This thesis has focused on one of the more sensitive techniques, Atomic Absorption Spectroscopy (AAS).

Although spectroscopy is one of the most commonly chosen means for analyzing contaminates, spectrophotometry has been shown suitable, especially where AAS fails [7]. In either case, none of the benchmark methods have been shown to meet the challenge of performing detection in the far spread regions of developing countries. To clarify, while these diagnostic tools have been well defined and can effortlessly measure the presence of a contaminant, down to the parts-per-billion (ppb) scale, they cannot simply be transported from one location to the next [8]. In addition to equipment expenses, they also place a reliance on specialized testing facility and trained experts, hardly affordable in countries that lack the necessary resources [3], [9], [10]. As developing countries generally experience variable levels of arsenic contamination, the need for a more appropriate means of detection must be implemented [11].

Moving forward, the focus has shifted towards finding simpler means of detection and tools for the quantitative analysis, with emphasis being placed on colourimetric approaches and possible biosensors [6]. Here, the focus is to drastically decrease time and associated costs through the incorporation of simple diagnostics that can be brought into the field [6]. With well-water being the only source of potable water for millions of people in Bangladesh, especially during dry season, a recurring assessment of such water sources could provide substantial detail, required in effectively reducing and monitoring exposure to arsenic [12].

Of the possible on-site diagnostics, the arsenic field test kits (FTKs) have provided the most common means of measurement for potable water sources. An example kit is shown in Figure 1 below. Most FTKs evaluate the presence of arsenic through use of the classical Gutzeit method, described in the literature review of Chapter 2 section 2.2. Once the gas has formed, it is typically made to react with mercuric bromide, impregnated on the test strips. A variety of other chemical substitutes may also be used in the production of a colour-complex, for which the colour's intensity may be matched with a specific concentration of arsenic. The Gutzeit method has so far remained the best approach in achieving a visual detection limit close to the set standard [11].

Colourimetric FTKs have distinct advantages over the various technologies used for arsenic detection. In comparison to laboratory technologies, they do not require samples to be transported

or stored with preservations at low temperature. Additionally they involve a relatively easy and rapid procedure, allowing the public to be informed within a short time span [11]. In their most basic form, FTKs originally indicated whether or not arsenic exceeded a set threshold concentration, through the presence of a coloured indicator. This process has become more specific, providing a colour palette for comparison with test results. Unlike benchmark technologies, the accurate performance of a FTK must come from improved control, which will be expanded upon in Chapter 4. Both the equipment and chemicals involved must advance, as there is a lack of sensitivity and a weak correlation to the set standard [9], [11].


*Figure 1: A field test kit used in the detection of arsenic.*

To improve upon the quantification of FTKs, a focus must be placed on how the formed colour-complexes are evaluated. While evaluation of colour variations have generally been performed by the naked eye, leading to subjective measurements, there is a growing trend to rely upon digital analysis [13]. Even so, the sample control factors have been limited, leaving considerable room for misclassifications. A more convenient means of imaging the test strips should be sought.

Colourimetric results can be variably affected by the presence of interfering species or the overall turbidity of the obtained water sample, the temperature at which the reaction is performed, and how the samples are handled during the analysis. Previous work has shown that the use of conventional flatbed scanners with software for imaging can provide densitometric measurements [7]. A potentially more cost-effective and mobile solution includes the use of modern smartphones as a simple means for image capture, on-the-spot analysis and the potential for geographic trends. As current smartphone technology is setting a path for a variety of analyses, it should hold useful for Field Portable Imaging (FPI) of arsenic [9], [14]. With them, the mass screening of samples could be made possible, as the general analysis could be performed and controlled by designated algorithms that limit user reliance, beyond the collection of test strip indicators. Though this may present a new set of challenges, in terms of the quality control, the opportunities for quantitative measure far outweigh the cons.

## 1.2 Contribution of this Thesis

The following chapters are focused around the current tools being used for the detection of arsenic. This thesis sought to simplify and significantly improve upon the quantitative potential of colourimetric detection, associated with FTKs. By advancing the incorporated FTK diagnostics, it will be possible to replace the need for cumbersome benchmark technologies.

It is proposed that one possible way of improving the precision of colourimetric determinations is to work upon digital images obtained with a smartphones Charge-Coupled Device (CCD) sensor, with a macro lens attachment for an improved Signal-to-Noise Ratio (SNR). With smartphones already providing user-friendly interfaces and a simple means of spectroscopic detection, the possibility for integrated calibrations make it reasonable for untrained personnel to perform the test.

Besides the camera being used, concern is placed on defining the physical parameters of the imaging apparatus that will be used for the analysis of coloured test strips generated by FTKs. While the imaging apparatus should provide precise control over how the samples are handled, the incorporated algorithms will provide a repetitive and reproducible analysis. The focus of this

research is not placed on the improved chemical production of colour but instead the means by which any existing FTK's response can be quantified and calibrated on the go. All of these changes should assist in reaching the eventual goal, to reduce the misclassification of FTKs to under 5 % from the current 15 to 35 % [11], [15].

## 1.3 Layout of the Thesis

The following chapters are organized as follows:

Chapter 2 provides a literature review on arsenic detection. Multiple concepts are defined in parallel, for their combined efforts will set a new baseline for the detection capabilities possible with existing colourimetric technologies. Here, the focus has been placed specifically on the field test kits that rely upon the gaseous phase of arsenic for detection.

Chapter 3 defines the benchmark technologies used as a reference point for the development of field portable solutions in the following chapters. It will furthermore define the production of standard arsenic solutions for use with the benchmark and field portable technologies being analyzed.

Chapter 4 discusses the field portable technology that will be used to develop a basis for imaging in the field, where it needs to go and a means to do so. Focus is placed on development of novel algorithms, removing user involvement.

Chapter 5 will contrast the results for both the digital single-lens reflex (DSLR) camera and smartphone with a macro lens (SML) attachment, and correlate them with the chosen benchmark of chapter 3, the Graphite Furnace-Atomic Absorption Spectroscopy (GF-AAS).

Chapter 6 provides the overall conclusions for the thesis; recommendations, and future work are presented.

The References and Appendices follow.

# Chapter Two

# 2. Literature Review

## 2.1 Characterizing Arsenic

### *2.1.1 The Presence of Arsenic*

Arsenic is a prevalent metalloid, produced by both natural and anthropogenic means [6]. Natural sources, shown below in Table 1, include sediments or soils derived from the earth's crust. In this setting, arsenic plays a role in the composition of over two-hundred minerals including arsenate, sulfides, sulfosalts, arsenites, arsenides, oxides and silicates. Besides its natural occurrence, arsenic is often made present through a variety of human activities. Recognized methods include the combustion of fuels, the inclusion of feed additives, industrial waste disposal and mining processes [4].

Table 1: Leading arsenic minerals occurring in nature, adapted from [4].

| **Mineral** | **Composition** | **Occurrence** |
|---|---|---|
| Native arsenic | As | Hydrothermal veins |
| Proustite | $Ag_3AsS_3$ | Generally one of the late Ag minerals |
| Rammelsbergite | $NiAs_2$ | Commonly in mesothermal vein deposits |
| Safflorite | $(Co,Fe)As_2$ | Generally in mesothermal vein deposits |
| Seligmannite | $PbCuAsS_3$ | Occurs in hydrothermal veins |
| Niccolite | NiAs | Vein deposits and norites |
| Realgar | AsS | Vein deposits |
| Orpiment | $As_2S_3$ | Hydrothermal veins, hot springs, volcanic sublimation product |
| Cobaltite | CoAsS | High-temperature deposits, metamorphic rocks |
| Arsenopyrite | FeAsS | The most abundant As mineral, dominantly mineral veins |
| Tennantite | $(Cu,Fe)_{12}As_4S_{13}$ | Hydrothermal veins |
| Enargite | $Cu_3AsS_4$ | Hydrothermal veins |
| Arsenolite | $As_2O_3$ | Secondary mineral formed by oxidation |
| Claudetite | $As_2O_3$ | Secondary mineral formed by oxidation |
| Scorodite | $FeAsO_4 \cdot 2H_2O$ | Secondary mineral |
| Annabergite | $(Ni,Co)_3(AsO4)_2 \cdot 8H_20$ | Secondary mineral |
| Hoernesite | $Mg_3(AsO4)_2 \cdot 8H_2O$ | Secondary mineral, smelter wastes |
| Conichalcite | $CaCu(AsO_4)(OH)$ | Secondary mineral |
| Adamite | $Zn2(OH)(AsO_4)$ | Secondary mineral |
| Domeykite | $Cu_3As$ | Found in vein and replacement deposits |
| Loellingite | $FeAs_2$ | Found in mesothermal vein deposits |
| Pharmacosiderite | $Fe_3(AsO_4)_2(OH)_3 \cdot 5H_2O$ | Oxidation product of arsenopyrite and other As minerals |

As arsenic can take on a variety of forms, exposure to it is of growing concern. Its movement through sources of food and the hydrosphere have made it difficult to track [6]. Stated prior, the focus has been placed on its presence in water sources, more specifically in aquifers. As these underground layers of permeable rock are tested and used to gather drinking water for public consumption, the registered list of arsenic sources grows, Table 2 illustrates a variety of these.

Table 2: Sources of arsenic, adapted from [4].

| **Location** | **Arsenic Source** |
|---|---|
| Bangladesh | Well waters |
| Calcutta, India | Near pesticide production plant |
| China, Shanxi, PR China | Well waters |
| Fukuoka, Japan | Natural origin |
| Hanoi, Vietnam | Arsenic-rich sediment |
| Hsinchu, Taiwan | Well waters |
| Hungary | Deep groundwater |
| Kuitun-Usum, Xinjiang, PR | Well waters |
| Lagunera region, northern | Well waters |
| Missouri, USA | Natural origin |
| Nakhon Si Thammarat | Shallow (alluvial) groundwater; mining |
| New Jersey, USA | Well waters |
| Northeastern Ohio, USA | Natural origin |
| Province, Thailand activity | Deep groundwater; mining activity |
| Southern Iowa and western | Natural origin |
| South-west Finland | Well waters; natural origin |
| South-west USA | Alluvial aquifers |
| Western USA | Geochemical environments |
| West Bengal, India | Arsenic-rich sediment |

Arsenic present in these aquifers is generally found in both inorganic and organic forms. While inorganic forms present a significant concern, the organic forms do not. Unlike the former, organic arsenic undergoes a naturally occurring methylation process, preventing bioaccumulation by lowering its affinity to tissues [16], [17]. To further narrow this concern, the essential oxidation states for inorganic arsenic species should be discussed [3]. Of these states, arsenite [+3 or As(III)] and arsenate [+5 or As (V)] are the most prevalent anions in water [4]. Their structures are shown in Figure 2 below [18].

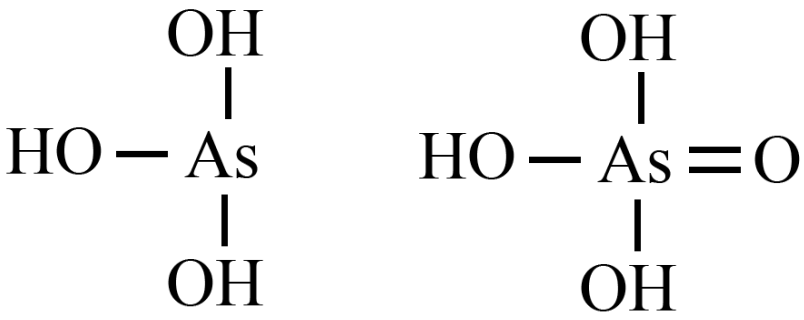

(a) (b)

*Figure 2: The chemical structures for naturally occurring (a) Arsenite – As(III) and (b) Arsenate – As(V)* [18].

### *2.1.2 Relating Arsenic to Health Concerns*

While the concern for arsenic has been narrowed to aquifers used for drinking water, for this thesis, there is a need to clarify the issues posed towards human health. The toxicity of arsenic depends on a number of factors. As already indicated, the organic forms do not pose a considerable issue when compared with the inorganic form and their oxidation states. In addition to the chemical forms and oxidation states present, the physical state plays a role on the rate it is either absorbed or excreted from the human body. All of these factors are further complicated by the present health of an individual when exposed to arsenic above recommended levels [4].

With limited control over water quality in developing countries, and a vast number of affected sites occurring worldwide as shown in Figure 3, it is understandable that the higher concentration of arsenic poses an impact to human health. Shallow wells that serve the populace, as the only source for potable water during dry season, are easily contaminated and hard to maintain [12]. In 1997 the large scale occurrence of arsenic poisoning was classified throughout Southeast Asia. During this period, 27 % of the wells tested in Bangladesh were shown to be contaminated above the EPA arsenic threshold of 50 μg/L [6], [19].


*Figure 3: The world map indicating the presence of arsenic above recommended levels* [17].

Once inorganic arsenic is present in biological tissues, its excretion is slow, generally occurring through urine, feces, and keratin-containing tissues such as skin and hair. Ingested arsenic has been shown to afflict the respiratory, pulmonary, cardiovascular, gastrointestinal, and hematological systems when found above the set WHO threshold [4]. Long-term renal accumulation, dermatologic insignias, neural injury, diabetes mellitus, and the risk of cancer in the bladder, liver, kidney or skin are all concerning factors [8]. The occurrence of these health complications have given rise to the need for preventative measures, thus detection is becoming a necessary first line of defence [20].

Focusing on Bangladesh's healthcare costs, arsenic is registered at around $2.7 billion [21]. Such health impacts and costs could be alleviated if simple means of detection are made routine and removal technologies made practical [22]. In developing countries, the continual diagnosis of water sources would make it possible to avoid unsafe conditions. This routine would be essential as the metalloids presence is time-variant, remaining in a water source for only a given period, due to its circulation through a variety of states. As shown in Figure 4, arsenic is variably released into wells depending on a variety of conditions. As such, the well water must be monitored effectively if wells are to be used when reasonable concentrations permit.

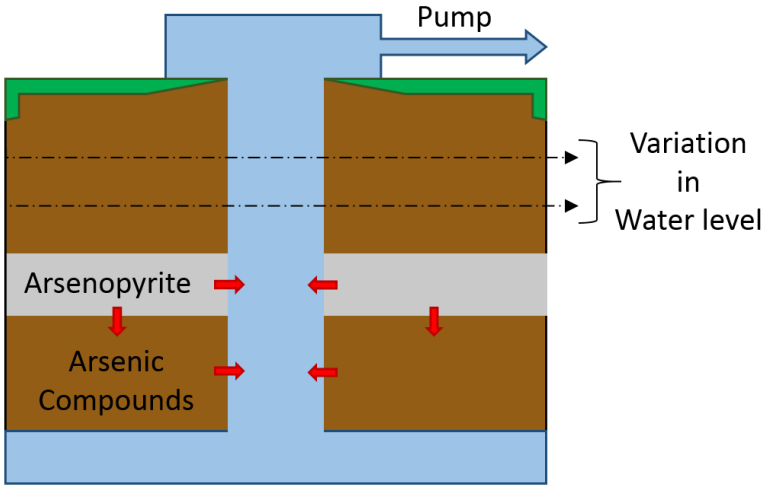


*Figure 4: The presence of groundwater arsenic in tube wells caused by the circulation throughout the year* [18].

## 2.2 Means of Arsenic Quantification

In the previous section it was stated that water sources must be monitored, more precisely their contents should be quantified. Quantitative analysis, in a broad sense, is defined by a resource used to produce an understandable measure. In terms of arsenic, its measure can be defined by a broad range of technologies, comparing it to a reference measure. Here results are further correlated to specific concentrations, estimated through experimentation [23]. Table 3 has been provided to summarize a variety of in-field technologies that have had success in the detection of arsenic. While a variety of technologies are shown in this Table, the current maximum method detection limit (MDL) and commentary illustrate the value that colourimetric tools already provide.

Table 3: Summary of promising arsenic detection techniques, adapted from [2].

| **Method** | **Medium** | **MDL** | **Commentary** |
|---|---|---|---|
| *Current technologies* | | | |
| Colourimetric [11], [24] | Liquid | 1 - 30 µg/L | *Quantitative readings obtained with spectrometer*<br>*Limited to detection of arsenite and arsenate*<br>*Promise for speciation* |
| X-ray Fluorescence (XRF) [25] | Solid | $6x10^4$ µg/L | Measures wide spectrum of metals |
| Anodic Stripping Voltammetry (ASV) [26] | Liquid | 0.1 µg/L | High sensitivity |

| *Research efforts for technologies* | | | |
|---|---|---|---|
| Colourimetric [27]–[30] | Liquid | **1 µg/L** | ***Separation technologies allow for enhanced sensitivity and speciation*** |
| Electrophoreses [31]–[33] | Liquid | 0.2 - 2000 µg/L | Some possibilities for a compact sensor unit<br>Directly measured organoarsenic compounds |
| Laser-induced breakdown spectroscopy (LIBS) [34]–[36] | Solid | $4x10^5$ µg/L | Poor sensitivity |
| ASV [37], [38] | Liquid | 0.05 - 0.5 µg/L | Literature debate over capability to measure species<br>Interference from other environmental metals a concern |
| XRF [25], [39], [40] | Liquid | $5x10^4$ µg/L | Measures a wide spectrum of metals |
| Bioassay [41], [42] | Liquid | 10 µg/L | Semi-quantitative results for species in water |

### *2.2.1 Benchmark Technologies*

The current standard for arsenic detection has been based on benchmark technologies only accessible through high-end laboratories. Such technologies include atomic absorption spectroscopy, atomic fluorescence spectrometry, inductively coupled plasma and high-pressure liquid chromatography [6]. Although, each of these diagnostic systems have been well defined, effortlessly measuring contaminates down to the parts-per-billion (ppb or in SI units µg/L) scale, they cannot easily meet the new aim for in-field diagnosis [3], [8]. Benchmark technologies suffer from a variety of difficulties. Besides the considerable operation and maintenance expenses, consideration must be made for technical proficiency of the machine and its user. Illustrating the need for change, a comparison of a set of arsenic sample solutions was made between 17 Bangladesh laboratories. Results showed that only a third of the facilities were within the expected range of concentrations [17]. Conflicting laboratory results have lowered the confidence placed upon the quality of testing facilities and their benchmark tools [11]. Further transportation challenges are met through using centralized laboratory facilities. Here, arsenic samples must be preserved, through acidification, which both dissolves the minerals, causing overestimations, and poses a considerable risk for those in contact with the acid [11].

### *2.2.2 Field Portable Technologies*

Several field-portable arsenic detection technologies are currently under development, each providing a set of advantages that offset the deficiencies of the benchmarks. As described in Chapter 1, commercially available arsenic Field Test Kits (FTKs) have become a common means of on-site measurements. Of the advantages, FTKs are best known for eliminating the lag-time involved in obtaining a discrete verdict. While obtaining results requires minimal time, the test itself still lacks a quantitative result. To expand upon this, while the process involved in generating the colour of a Test Strip Indicator (TSI) is done in a controlled manner, the TSI's analysis has been qualitative to semi-quantitative at best [11], [43]. Although recent claims state the current generation of commercial arsenic FTKs are capable of distinguishing concentrations lower than the WHO standard, a mere 10 µg/L, they have yet to be investigated in depth [11], [43]. Improving the quality and types of reagents used has been a focal point, with little attention being spent advancing the diagnostics and the protocols for analysis. As this is the case, it is optimal to begin by defining the chemistry.

#### *Generation of Arsine Gas*

The volatile formation of arsine ($AsH_3$) gas is generally used in FTKs to detect the presence of arsenic in liquid. Originally designed for toxicology, the reduction of arsenic and its release as a gas is commonly referred to as the Gutzeit Method, after its creator Ernst Wilhelm Heinrich Gutzeit. Although the materials that define the Gutzeit method have seen much change, it continues to be referred to hold the original inventors name [11]. Through its gaseous release, it becomes possible to separate the arsenic from a variety of interfering compounds, including the phosphates that commonly affect most analyses of arsenic. While arsenic is removed from solutions to lower the interference of certain chemical compounds, other elements still inhibit its release and detection. As such, if an element bonds strongly with arsenic, it must be filtered out beforehand. The general chemical process has been summarized through equations 2.1 to 2.5 below [44]:

Half Reactions:

$$H_3AsO_4 + 8H^+ + 8e^- \rightarrow AsH_3 + 4H_2O \quad \text{Eq. 1}$$

$$Zn \rightarrow Zn_2 + + 2e^- \quad \text{Eq. 2}$$

$H_3AsO_4$ Reaction:

$$H_3AsO_4 + 4Zn + 8H^+ \rightarrow AsH_3 + 4Zn_2 + 4H_2O \quad \text{Eq. 3}$$

$As_2O_3$ Reaction:

$$As_2O_3 + 6Zn + 12HCl \rightarrow 2AsH_3 + 6ZnCl_2 + 3H_2O \quad \text{Eq. 4}$$

$$H_3AsO_4 + 4Zn + 8HCl \rightarrow AsH_3 + 4ZnCl_2 + 4H_2O \quad \text{Eq. 5}$$

*Field Test Kits and the Gutzeit Method*

As the reactions proceed, the released arsine gas can be collected for study; its chemical structure is provided in Figure 5.

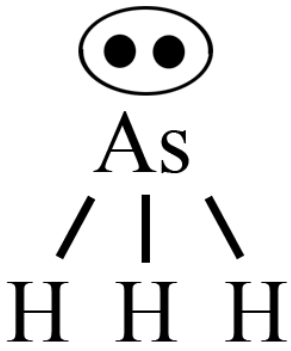


*Figure 5: The general chemical structure for arsine gas – $AsH_3$* [18].

To make the analysis of this gaseous product possible, an additional reaction must occur. Here, the arsine is made to interact with impregnated filter paper, generally in the form of a TSI. TSIs link together the arsine and gas, causing the formation of a coloured-complex. The colour is dependent on the availability of arsine released from solution. While a variety of chemicals may be used as the indicator, mercuric chloride ($HgCl_2$) or mercuric bromide ($HgBr_2$) have been the most common. Although mercuric bromide is a highly toxic material and other indicators are available, none have proven to be as efficient. Impregnated filter paper, while frequently chosen, may also

be replaced through the use of silica gel, alumina gel, or powdered porcelain [15]. The general chemical process for this colour change is described below with Equations 2.6 and 2.7 [44]:

Halogen Formation:

$$AsH_3 + HgBr_2 \rightarrow AsH_2HgBr \quad \text{Eq. 6}$$

Concentration (Low – High), Colour (Yellow – Black):

$$H(HgBr)_2As \rightarrow (HgBr)_3As \rightarrow Hg_3As_2 \quad \text{Eq. 7}$$

The classical Gutzeit method has been brought into a more quantitative state through the various iterations of reagent advancements. The increasing purity of the chemical reagents used has been an essential factor in the improvement of FTKs, with many reagents having originally contributed impurities, including arsenic, to the formation of the coloured-complex [11]. Besides increasing the purity of the reagents used, testing blank samples has played a common role in assessing a reagent's purity. Increased clarity in the results have triggered a greater desire to measure lower concentrations. Test kits are now available on the microgram per liter (µg/L) range. The improved grain size of the solid reagents has been essential in enhancing kinetics of the hydrogen generation (HG), with hydrogen extracting the arsenic as arsenic hydride [11].

The pH of the solution is also important, as strongly acidic conditions can be used to pre-reduce the various arsenic species to As(III), a form more easily extracted. However, the use of strong acids poses a problem for both transportation and handling by personnel. More recently, sulfamic acid, $H_3NSO_3$, has been seen as a possible replacement, given that it can be handled as a solid and increases reaction time for solutions with high alkalinity, generally the state of ground water [11].

In place of zinc, sodium borohydride ($NaBH_4$) is being substituted. As a strong reducing agent, it provides improved kinetics of HG for FTKs, and is common place in most laboratory analyses, such as atomic absorption spectrophotometry (HG-AAS) or inductively coupled plasma atomic emission spectrometry (HG-ICP-AES) [11].

The time associated with generating arsine gas has been analyzed for a variety of FTKs. Through increasing the time span of the reaction samples of 15 μg/L, those previously analyzed incorrectly were properly registered above a semi-quantitative concentration of 10 μg/L for both the EZ and Hach FTKs [45], [46]. Although the FTK has focused on promoting short reaction times to increase sales, it is apparent that lengthening this reaction will provide a more quantitative result.

Finally, two general practices have been used to unite arsine with TSIs. The original method passed arsine gas across the surface of the impregnated paper in a vertical tube [11]. Here, the length of paper that turned yellow was quantified. Although this method had success in wastewater treatment, it did not handle well in distinguishing exact concentrations. The second approach, now used in most FTKs, placed impregnated paper in contact for a given period of time. Within a contained vessel, the gas would interact with the filter rather than just passing across the surface. Here, the impregnated indicator was made small to concentrate the available arsine, within the defined space, increasing the colour that can be developed [11].

*Preferred Method*

It is important to note that although arsine is extremely toxic, FTKs pose little threat to the user. The low quantity of gas generated in the FTK reaction is efficiently absorbed in the formation of the colour-complex, especially through maintaining the proper protocol. The safety precaution of working in a well-ventilated environment was added as an additional measure. Other means of detection are under development to remove any concerns with current field portable technology [11]. Currently, photometric methods, incorporating either silver diethyldithiocarbamate (SDDC) or molybdenum blue have been possible [2], [27]. Unfortunately, volatile solvents used with SDDC are difficult to maintain while molybdenum blue suffers from matrix interference, ultimately limiting the sensitivity for both of these methods.

*Quantification of the Gutzeit Method*

Finding a means to gauge an indicator's colour has been sought as early as 1944 [11]. This need has generally placed a reliance upon detecting the intensity of light that is made to either pass through the coloured-complex of the test strip or be reflected off the test strips surface [11].

Currently the diagnostics used for colourimetric analysis continue to follow these trends with more sophisticated means of measuring the light intensity. One such device, a densitometer, is used to quantify the amount of light reflected [7]. These systems do not measure colour variations but instead focus solely on analyzing optical density, which is a comparison of the quantity of light that is reflected off the test strips coloured surface and compared with a reference (a blank test strip) to calculate the change in intensity.

Several types of densitometers have been applied to the analysis of arsenic as shown through the literature, including spectrophotometers, CCD cameras, and other CCD arrays. Even though colourimetric detection is possible with simple diagnostic tools, the general reliance continues to be based on visual analysis. With the current use of FTKs beginning to move away from the visual approach, colourimetric detection still has far to go before it can provide quantitative means of analysis [12], [47], [48]. Development of FTKs is now focused on redesigning the means of analysis, as the human eye is unable to accurately assign numerical values to perceived variations in colour [2], [49]. As such, current research has shown few attempts at cost effective opto-mechanical smart-phone attachments [50].

*Confirmed Quality*

To confirm the quality of the results being obtained by the FTK, deionized water is used to generate a blank TSI, confirming that arsenic is not present. As stated prior, the presence of arsenic impurities in the reagents may be determined this way. A FTKs proper functionality can further be assured by forming a set of standardized arsenic solutions, for each of the specified concentrations for which the kits chart has been built [11].

The rate for arsenic evolution is strongly dependent on the agitation that is experienced by the reagents in the reaction vessel [11]. It is suggested that the performance of the test should incorporate information on the reaction temperature, exposure time of the strips, and the lighting conditions. In terms of the reaction time, although manufacturers suggest a total of 20 minutes, an investigation showed that an increase in time allows further arsine to evolve and increase the

intensity of the samples. One example of this compared results obtained from the Hach EZ FTK, here the reaction time was doubled and the accuracy raised to 88 % [51].

In all cases, the acidity of the solution being studied has a considerable effect on the colour intensity and droplets that are formed in the reaction vessel. It must therefore be kept at a constant level to prevent droplets from damaging the colour-complex and to standardize the correlated range of colour [15].

The temperature is also essential to consider, as it will affect the speed of the FTK reaction. Most set standards are taken at room temperature (20 °C), yet developing countries such as Bangladesh generally experience temperatures around 35 °C, invalidating the test and its provided colour charts. Given these conditions, it would be preferable to either adapt the kits or the means of analysis [15], [45]. It would be ideal for the calibration chart to be formed at the time of the analysis or to incorporate these factors through a database of expected calibrations.

In essence, quantitative analysis of the FTK has not been practical, owing to difficulty in handling very small samples with accuracy and precision [49]. To improve upon this, both the apparatus used to take the images and the means of analyzing images must be enhanced. Considerations must be made to prevent inflections/damage to the colour-complex while furthermore providing precise control for a reproducible capture setting. The occurrence of false positives and false negatives while running a FTK have been examined by Kinniburgh and Kosmus [11], stating the frequency of these occurrences related to the precision involved in the measurements. Here a false-positive result occurs when the colour intensity used to predict the concentration is believed to be greater than its actual value. Although it is not detrimental to health, poor quantitative performance of a FTK is still an issue that must be dealt with as it results in associated costs for well treatment and prevent optimal use of water sources. Conversely, for the case when a false-negative result occurs, it can prove to be detrimental to human health if a high concentration is believed to be acceptable for consumption [11]. Finally, the deviation that is caused in the formation of the coloured-complex within the indicator goes undetected with the camera [15].

## 2.3 Colourimetric Analysis for Arsenic Detection

As has been pointed out, digitally imaging the TSI's coloured-complex holds many benefits. In terms of the digital image analysis (DIA), there are many approaches that may be taken to study colour. Currently DIA can be flexibly implemented for a variety of applications. When an image is digitized, it becomes possible to enhance various features of the image through filtering techniques [12]. This allows for several parameters to be measured at a time, such as area, shapes and colour intensities. With commercial software readily available to end users, such as MATLAB, it has become possible to employ a more tailored analysis, fit for a specific task.

While the FTK generally requires the TSI to be analyzed within minutes of the reaction, this analysis may be approached at a later convenience through imaging the TSI. DIA provides a means for placing more emphasis on generating TSIs, lowering time spent on-site, removing the overhead expense associated with testing facilities, and guaranteeing a reliable result without the need for in-depth technical expertise [11], [12].

Through the controlled capture of digital imaging, it becomes possible to collect much larger datasets and obtain statistically significant results. Here the colour intensities have been collected and translated to a finite number of sample positions (x, y), referred to as pixels. These intensities have furthermore been quantized to a finite number of levels, typically 256. These intensity levels range from 0 to 255 [52]. Therefore, quantification will be improved as more pixels are allocated to analyze the colour-complex, formed by the arsenic.

The literature has shown that calibration curves based on pixel intensities can be generated from the colourimetric analysis of a FTK's TSI, to predict the concentration for a given sample. This calibration method only depends upon the reagents that have been selected and the means of which the images have been taken. It can furthermore be made portable by using a variety of devices, sought for improved quantification. This would include hand-held and flat-bed scanners [45], [53], Charged Coupled Device (CCD) arrays, video cameras, digital cameras, and digital colour analyzers [7], [23], [49], [54] – [56].

### *2.3.1 Colour Space Analysis*

A colour space defines a specific way in which to organize colour. Here the organization depends on the method used in capturing the colour representation. As such, colour space may be random and subjective. With even ambient light affecting the digitization of colours, the settings must be well controlled and reproducible. Existing technology for colour detection with arsenic FTKs is cumbersome, lacking a user-friendly interface, and most techniques do not properly control the light [57]. Present research seeks to alleviate these issues for a variety of colourimetric tests, with my research focused on arsenic FTKs. A colour space gamut is the precise distribution of multiple channels of the colour in which a portion of the entire colour space is represented. This can be seen in Figure 6 below, where the gray region signifies the entire range of possible chromaticities, or colours. This region is defined by the hue, or y, and the intensity/chrominance, or x, that make up visible colour. The inner region here is a model used to define a portion of the colour space. Further definition of the colour space breakdown and these terms is provided in the following section.

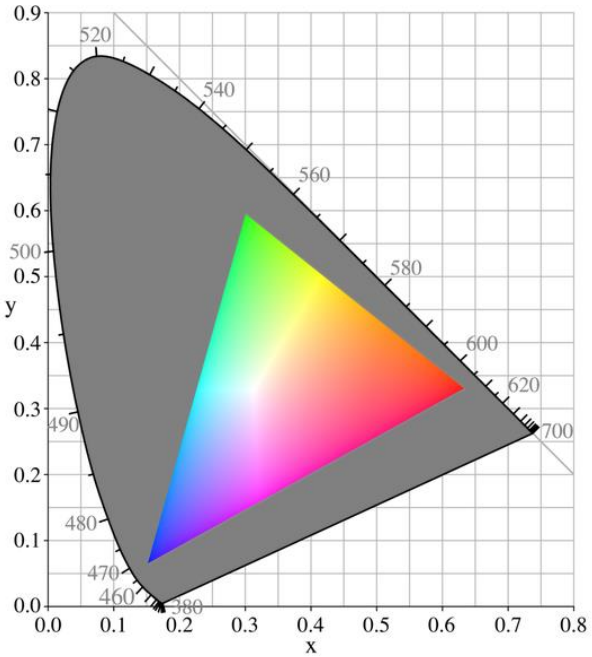


*Figure 6: Colour Space Gamut, inner coloured regions defines a colour model* [58].

*2.3.2 Colour Models*

The gamut, or colour model, can be defined in reference to the colour space through a variety of means, depending on how the space is to be organized. As such, a variety of colour models have been developed, attempting to provide an optimal abstract mathematical model that is reliant upon tuples and the properties that have been used to represent a range of colour in the gamut. As Figure 7 shows, model generation and interpretations are variable. Generally, five colour models are relied upon. In the following section, two essential models are explained, while the other three may be found in 7.2.1 of the Appendix.


*Figure 7: Breakdown of the colour space (or gamut), into a smaller range by a mathematical colour model where one of these possible models may be used to define the means for image analysis.*

*RGB Colour Model*

The RGB (red, green, and blue channels) model relies on an additive approach, in which all the colours in the gamut can be represented through the linear combination of the three additive primary colours, as seen in Figure 8 [52]. This combination is important in defining a scale for each of the proportions needed for generating a complete range of the present colours, serving as a reference for many other color models. Generally the standard RGB (sRGB) is used with most electronic applications, serving as a foundation that can be built upon. The RGB model is itself an absolute colour space; this means it is defined without reference to external factors and the difference in colours is solely based on the metrics used [57]. As such, input devices, such as scanners and cameras, generally rely upon this model to calculate a numerical representation of the intensity [23]. Notably, the RGB model has been applied for the derivation of an absorbance function for arsenic quantification in 2002 by Kompany-Zareh et al. [45], [49].

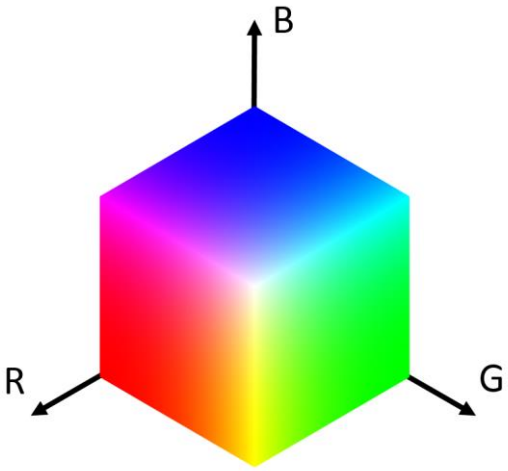


*Figure 8: The RGB model* [58].

*YCbCr Colour Model*

This colour model is based around a discrete encoding of the three channels that make up the RGB colour model. As illustrated in Figure 9, the YCbCr colour model encompasses a larger degree of colour space combinations, expanding upon the scope of the RGB model. While beneficial as a means of quantification it is generally not relied upon as technology cannot display these with existing displays. Here, the model focuses on the brightness of an image, based off weighted sum gamma-compressed corrected RGB, generally referred to as the luminance "Y". The other two channels are known as "Chroma Cb" and "Chroma Cr". These two channels are based on the chrominance, the quality of colour as determined by the hue and the purity. Generally this model is used for video applications given its discrete nature.

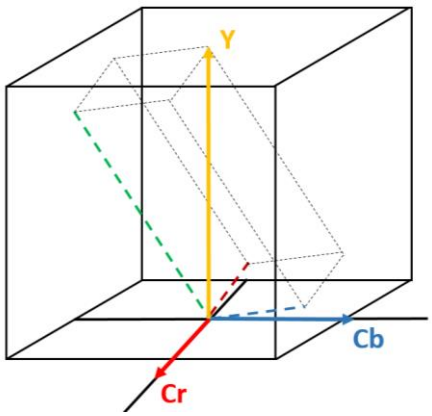


*Figure 9: The YCbCr model, the inner rectangle accounts for the limited range of the RGB model. Three lines of the rectangle are coloured to indicate the R,G,B vectors* [58].

### *2.3.4 Colour Space Transformations*

Digital images are produced initially within the RGB colour model. To analyze these within a variety of other colour models, they must first be normalized. The normalization of the RGB Model relies upon the characteristics of the original colour space [59]. The colour model YCbCr is derived from the sRGB colour space, where the channels are defined by the variables [Y,Cb,Cr] and [R,G,B]. Equations for the transformation are provided in 7.3.3 of the Appendix.

### *2.3.5 Segmentation and Object Recognition*

With the image adapted for analysis in YCbCr, the features of interest can now be extracted. To do this, a crude binary image can be produced to find dominant regions in the image. These regions would serve as reference points for the analysis. This binary image is generated by setting an intensity threshold, intensities above the threshold are made white while those below are made black.

From here the defined regions may be further classified from the binary image by looking at how the pixels are connected to each other. This allows the user to determine which groups of pixels are connected by intensity, thus allowing the location for each object. Once the dimension of an object has been determined through tracing its group of pixels, they may be cropped from the original image. This allows for the collection of an image for each of the reference areas and one for the test strip indicator's region of interest (ROI). These results are shown in the methodology and appendices sections.

### *2.3.6 Initial Reference Confirmation, Image Texture & Analysis*

Colourimetric analysis may be used to confirm repeatability and relation to previously calibrated tests, which is especially useful towards making accurate judgments for the research being performed here. To do this, the standard deviation, signal-to-noise ratio (SNR), and peak signal-to-noise ratio (PSNR) are determined across the image.

As image enhancements are made, the chromacity that defines an image will change with each algorithm perturbing the colour in its own way. As the objective is to ultimately improve the accuracy of the colourimetric quantification, slight disturbances in chromacity are found to be acceptable, especially with each image being affected in the same manner, nullifying any negative effects.

### *2.3.7 Colour Grading System*

To improve the consistency of a colour grading system, images captured in the RGB colour space are generally converted to a more appropriate colour model, such as YCbCr. After this is accomplished, image processing, such as segmentation, must be performed to obtain the desired objective that will be studied. At this point an image may be analyzed to form a means for representing an indexed grading system.

Here, the multiple channels that form a colour model (for example the R, G, and B channels) are simultaneously used in the classification of each colour grading threshold; a number of issues become apparent:

1. Non-contiguous regions
2. Non intuitive adjustments to thresholds
3. Unwanted complexity

To deal with these concerns, the performed analysis may be tuned for a specific purpose, for a specific application, or used with a specific apparatus. Through the literature the general practice for capturing the colour intensities has involved using existing software such as Adobe Photoshop graphics editor, Igor Pro v. 3.13 (Wavemetrics, Eugene, OR), MINITAB 14, Colours, or MATLAB to obtain details for the quantification [12], [15], [49], [60].

Calibrations are commonly constructed through plotting one colour channel against the concentration [45]. In terms of colourimetric analysis for arsenic, many approaches have been taken to achieve this goal. Salman et al. described an additive computation of the RGB colour density [56].The grayscale approach has been shown through research performed by both Bannur et al. [61] and by Johnson [45]. Abrazheev et al. [15] has also made it possible to determine

arsenic by a function analogous to absorbance. Use of software such as Microsoft Excel for statistical calculations, modeling and optimization have been common place. Modeling by polynomial fitting has been used to reduce multiple channels down to a one-dimensional solution and Artificial Neural Networks (ANNs), specifically multi-layer feed forward network, used as a decisive comparator to parametric techniques [49].

## 2.4 Knowledge Gap & Opportunity for Innovation

Despite the improvements that have been made towards the colourimetric detection of arsenic, it is still far from quantitative. Chemicals currently used in the detection, while still based on the generation of volatile arsine gas, have not drastically changed as they perform adequately in the generation of colour. Even if nontoxic reagents become readily available, a means for quantitative analysis must still be developed to streamline and standardize the detection of arsenic. An opportunity exists to create standardized quantitative analysis through both hardware and software innovations.

### *2.4.1 Hardware Opportunity*

In terms of the hardware, a better sense of control must be gained over handling and optically imaging samples. An apparatus that controls both the placement of samples and light conditions during image capture allows for reproducibility. To do this, larger devices such as office scanners or a wide variety of opto-mechanical attachments for smartphones may prove beneficial. While older scanner technology is adequate for handling samples, literature projects that smartphone attachments may hold the greatest advantages [62], [63]. With the number of phone users increasing daily, there has been a growing opportunity to develop these devices and their associated sensing technologies [64]. In terms of imaging, smartphones now contain cameras in which the mega-pixel count is projected to double every two years [64], providing better means of image resolution. With many smartphone users, it also becomes possible to easily spread the field-portable technology. As the indicator on a test strip is small, there are limitations in the imaging resolution that may possibly be resolved through the addition of macroscopic lenses in attachable

hardware [65]. Additionally, the improving computational abilities allow for more complexity in the numerical analysis that may be performed on the phone [14], [66].[14][14][14][14][14]

### *2.4.2 Software Opportunity*

In terms of the software incorporated for the quantitative analysis, it has been shown that a variety of approaches are possible, although not yet well defined for arsenic. There is a common need by users for simplicity in performing any analysis. While it may be simple to use the existing commercial software, like Adobe Photoshop and Microsoft Excel, breaking down an image and analyzing it should be confined to an exact protocol, with minimal human interference. The means of collecting a specific set of pixels within an image should place more emphasis on removing interpretation by the operator through automatic procedure [10], [67]. Cropped sizes, shapes and positions should be identical in making quantitative comparisons plausible. Software used for modeling and optimizing the correlated concentrations should be simplified by means of better control, discarding any manual procedures still maintained. Additionally, the literature has shown that a variety of colour models may be used as the basis for collecting a dataset. While the best colour model to use, for the colourimetric analysis, is subjective, the focus is placed on quantifying chromaticity [54]. If software is to serve its purpose in the field, it should be developed in parallel with the hardware that will define its use. While this may be ignorable for other realms, here it is essential for handling the specific and miniscule indicator on a FTK's test strip. Further normalization of datasets is useful in overcoming discrepancies caused by the imaging apparatus. Results of the experiments should be produced with linearity from one test to the next for datasets to be practical.

### *2.4.3 Other Initiatives*

#### *Microfluidics Applications*

Microfluidics is best described as a multidisciplinary field, evolving from microstructure technology for use with minuscule volumes of solution [68]. The ability to manipulate volumes inside micro-channels has become a very appealing method in the production of accurate analysis. Unlike current laboratory-scale technology, microfluidic devices provide an improved level of

control, lower reagent requirement and costs involved in both fabrication and disposal [69]. As these devices can conveniently be placed towards the detection and determination of many organic and inorganic compounds, they should serve well in the diagnostic interests of metalloids like arsenic.

It was found that recent development of microfluidic gas-liquid interfaces have shown promise, thus it may be possible to incorporate the existing Gutzeit method in these devices [70]. To enable liquid-gas interfaces in the microfluidic setting, interactions such as capillary forces and the surface chemistry of aqueous solutions have been utilized [71]. Simple microfluidic liquid-gas interfaces have been achieved through the application of hydrophobic–hydrophilic boundaries, as illustrated in Figure 10 [70]. Use of these boundaries are presented through the works of Greenwood and coworkers [71], [72], in which the analytical analysis has further shown their significance in handling gaseous samples. Further details is provided in the 7.5 of the Appendix.

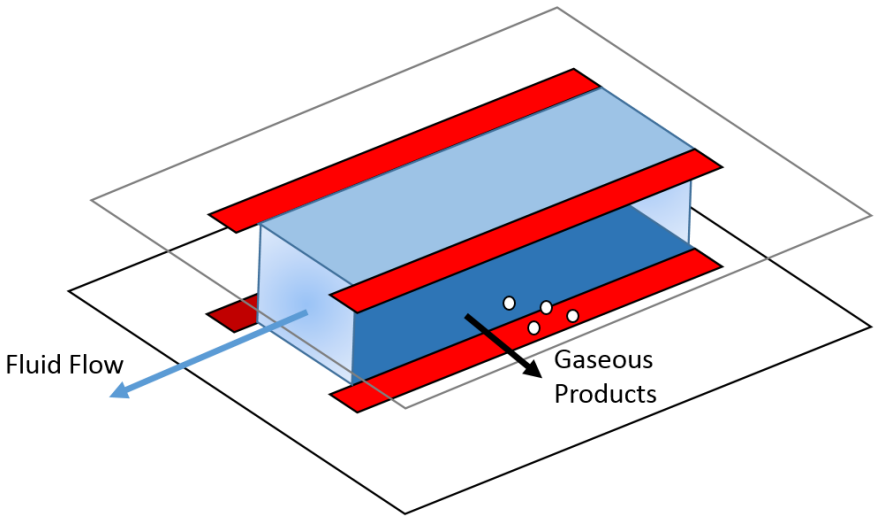


*Figure 10: Liquid-gas interface, in which the hydrophobic polymers (red) set restrictions on the fluid (blue) flow, only allowing gaseous products to leave, adapted from* [70].

*Probes and Indicators*

In addition to microfluidic applications, the probes and indicators may prove greater use down the road. Currently, very few probes, fluorescent or colourimetric, have been generated to target arsenic. The application of fluorescent probes directly to aqueous solutions or through arrangement

with microbial populations has become a growing area of research, with significant quantification, but as with microfluidics it still requires further advancement to become marketable technology [3]. One fluorescent probe, known as "ArsenoFluorl", has shown promise towards the detection of organic arsenite [73]. In terms of colourimetric probes, molybdate shows promise, through its production of a blue colour-complex [74].

Relevant towards the existing indicators in FTK, paper-based analytical devices (PADs) have shown promise towards the development of simple gaseous diagnostics. Although the use of paper analytics in microfluidic devices is currently limited, they do serve the needs of various diagnostic tools [69]. They have been shown already to assist in the detection of metal concentrations (Fe, Cu, Ni and Cr) present in industrial fumes, as illustrated in Figure 11 [75]. Just like the existing test strip indicators, their incorporation may serve in a variety of detection processes, for both the aqueous and gaseous phases.

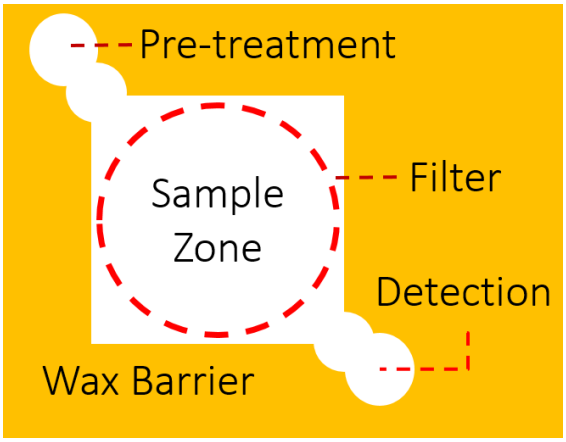


*Figure 11: Paper-based Analytic Device schematic, A filter is placed in the sample zone for metal collection from fumes. Reagents passed in through the pre-treatment zone. Collected material is flown to detection zone for colourimetric analysis* [75].

## 2.5 Chapter Summary

Although the conversion of arsenic to the gaseous phase is more toxic, it simplifies detection requirements. This conversion removes many sources of error created by the presence of other chemicals, especially phosphates. An increased level of control over the Gutzeit method would in itself be a drastic improvement over existing diagnostic tool performance. Given the reliance on

current testing methodology and commercial products, such as the paper-based test strips, a favorable progression towards global market acceptance can be anticipated.

The improved quantification by evaluating the formed colour-complexes is now a focal point. Currently, considerable room has been left for misclassifications, as colourimetric results can be variably affected by interfering species, solution turbidity, temperature, handling of produced samples, and visually evaluating colour with the naked eye or by limited digital analysis. A reliance on the user must be replaced by an impartial measure, one which advances the protocol for analysis through means of handling the samples and quantifying them digitally.

# Chapter Three

# 3. Benchmark Technologies

## 3.1 Methodology

Before a portable system for arsenic classification could be developed, a quantitative point of reference had to be set. With the goal of detecting arsenic concentrations below the WHO threshold, an appropriate benchmark was chosen. Here, arsenic was studied in the liquid state, affecting both water and biological sources. Figure 12 shows that a variety of techniques, such as extraction, may be used to improve the sample before detection is even performed. As the means of detection for both benchmark and FPT are to be defined, ideal sample solutions will be relied upon.

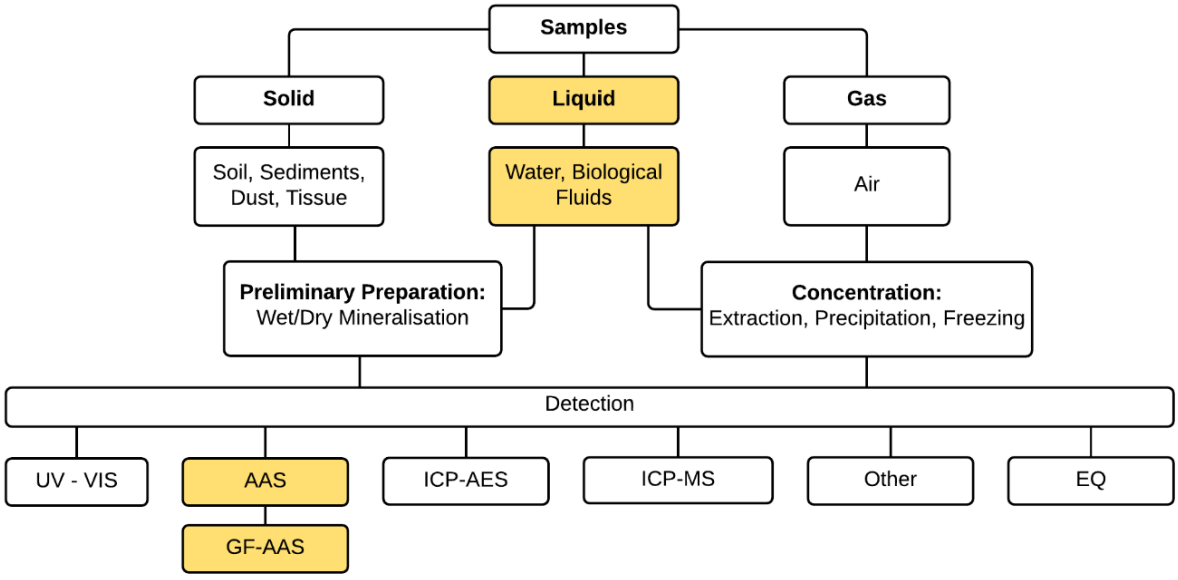


*Figure 12: Various arsenic speciation analysis in environmental samples, highlighted regions specify the chosen methods. Ideal liquid water samples were used with a variation of atomic absorption spectroscopy to perform the detection* [76].

### *3.1.1 Solution Generation*

Before using any of the technologies, a set of standard solutions had to be formed, shown in Figure 13. In general, the use of benchmark technologies generally require the addition of acid. This

allows samples to be maintained for longer periods of time. The desire to correlate results of the benchmark with FPTs led to the initial dilution of a standard 1,000 mg/L As(V) stock solution (Fluka Analytic 39436) in 2 % nitric acid (J.T. Baker 9601-1, 69-70 %). As testing was dependant on the FPT, stock solution concentrations generated were based off a chosen kit's concentrations gradations (specifically 0, 5, 10, 20, 30, 40, 50, 60, 80, 100, 150, 200, 250, 300, 400, and 500 µg/L). The protocol for the generation of these stock solutions has been placed in 7.3.2 of the Appendix.

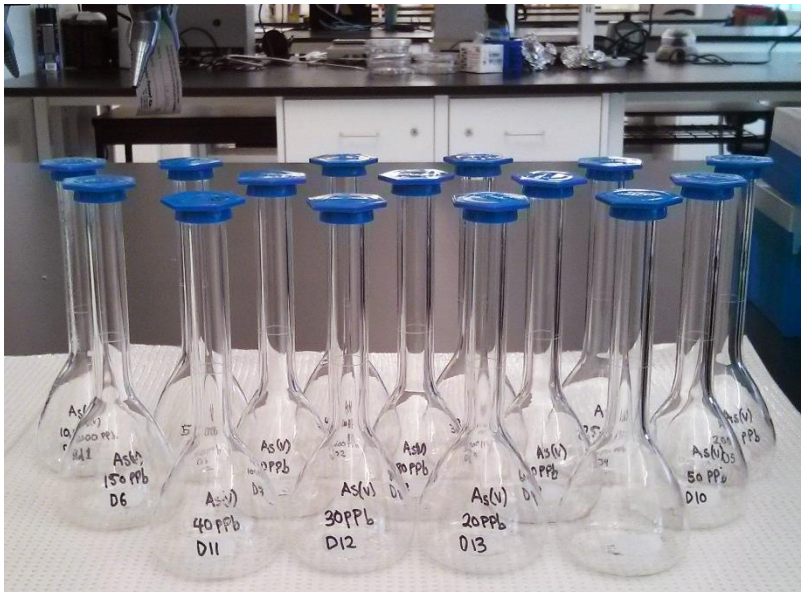


*Figure 13: Production of standard solutions for each of the chosen arsenic concentrations.*

Relying on this protocol, a stock solution of nitric acid was fabricated with deionized water, such that it could be used in the dilutions of the arsenic. Both nitric acid and arsenic dilutions are provided in 7.3.2 of the Appendix (Table 9, Table 12, and

Table 13).

### *3.1.2 Technology Interference Factors*

Before both benchmark and field-portable technology results could be collected, initial testing of the stock solutions were made. Concerns in the literature about acid and matrix interference were to be confirmed. Effects of the acid were found to be detrimental to the chosen branch of FPT. Here the FTK relies upon the release of arsenic from solution as a gaseous product. Through analysis of the incorporated acid we showed that the arsenic cannot be released efficiently, as the FTK TSIs did not consistently match the expected outcome, further illustrated by Figure 14. In the presence of nitric acid, the chemical reaction explained in the literature review could not reduce the arsenic to arsine gas. As this was the case, there was little to no arsine released for the reaction with the impregnated test strips. Although 2 % nitric acid is generally used with the benchmark technologies, such as atomic absorption spectroscopy, this would not be possible for the FTK. While other acids are suggested to be less detrimental, they were avoided altogether to maintain ideal test conditions. As such, stock solution would be produced without the incorporation of acid, remain viable within the imposed 24 hour time period.

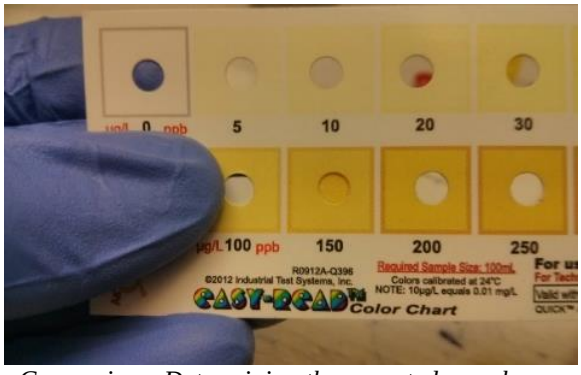


*Figure 14: Colour Comparison. Determining the expected sample concentration with the provided colour chart. Here samples are placed behind the chart and visually matched using the cut out holes.*

Standard solutions were prepared for correlation with use of Arsenic (V) Standard for ICP 1,000 mg/L As(V) in $H_2O$, produced by Sigma-Aldrich. These standard solutions of arsenic were prepared in triple deionized water, to maintain ideal conditions, and generated in bulk to allow for the simultaneous production of FPT and benchmark results. Table 4 and Table 5 are provided for

the initial dilutions of the stock solution, performed to maintain the accuracy of the dilutions ranging from 0 to 500 µg/L.

Table 4: Arsenic (V) Major Dilutions in $H_20$ - Fluka Analytical

| Sample # | Concentration (µg/L) | Desired Sample Volume (mL) | Amount of Stock Solution (mL) |
|---|---|---|---|
| Stock Solution | 1,000,000.00 | - | - |
| Dilution Std1 | 10,000.00 | 100.00 | 0.99 |
| Dilution Std2 | 500.00 | 100.00 | 5.00 |

Table 5: Arsenic (V) Standards for the FTK in $H_20$ - Fluka Analytical

| | Sample # | Concentration (µg/L) | Desired Sample Volume (mL) | Amount of Stock Solution (mL) |
|---|---|---|---|---|
| | Stock Solution | 1,000,000.00 | - | - |
| | Std1 | 10,000 | 100 | 0.999 |
| | Std2 | 500 | 100 | 5 |
| **Std1** | Dilution 1 | 500 | 100 | 5 |
| | Dilution 2 | 400 | 100 | 4 |
| | Dilution 3 | 300 | 100 | 3 |
| | Dilution 4 | 250 | 100 | 2.5 |
| | Dilution 5 | 200 | 100 | 2 |
| | Dilution 6 | 150 | 100 | 1.5 |
| | Dilution 7 | 100 | 100 | 1 |
| **Std2** | Dilution 8 | 80 | 100 | 16 |
| | Dilution 9 | 60 | 100 | 12 |
| | Dilution 10 | 50 | 100 | 10 |
| | Dilution 11 | 40 | 100 | 8 |
| | Dilution 12 | 30 | 100 | 6 |
| | Dilution 13 | 20 | 100 | 4 |
| | Dilution 14 | 10 | 100 | 2 |
| | Dilution 15 | 5 | 100 | 1 |

In addition to the removal of acid, matrix interference was also analyzed. This analysis holds little importance while relying on ideal laboratory conditions. As such, it can be stated that just like the presence of acid, other interfering chemicals prevent the release of arsine gas for FTK detection.

Further details may be found in section 7.4.1 of the Appendix. Essentially, all sample solutions were produced and analyzed within 24 hours with FTK TSIs simultaneously generated alongside the benchmark technologies' calibration curve.

While a variety of benchmark technologies may be used as the gold standard and correlated to the FPT, results were narrowed down to two analytical techniques. The two initial measures were HG-AAS and ICP-MS. While the two techniques are perfect for defining samples below the WHO threshold, access to the equipment was limited on Ryerson University's campus. As such, GF-AAS was chosen for analysis of solution samples. With a detection limit at around 20 µg/L and a relative standard deviation of 5 %, GF-AAS was still within a tolerable level. Other researchers have also used GF-AAS to quantify arsenic concentration [11].

### *3.1.3 Graphite Furnace-Atomic Absorption Spectroscopy*

In GF-AAS, a sample is injected into the atomization chamber where it is vaporized. The lamp emits resonance radiation, in tune with the element of interest, which passes through the vaporized sample. When the sample absorbs the radiation being passed through the flame, it does not reach the detector, allowing an element's presence to be quantified. The system protocol for GF-AAS has been provided in 7.3.2 of the Appendix. Through the use of GF-AAS, calibration curves were fabricated by sampling the standard arsenic solutions at 17.5 µL.

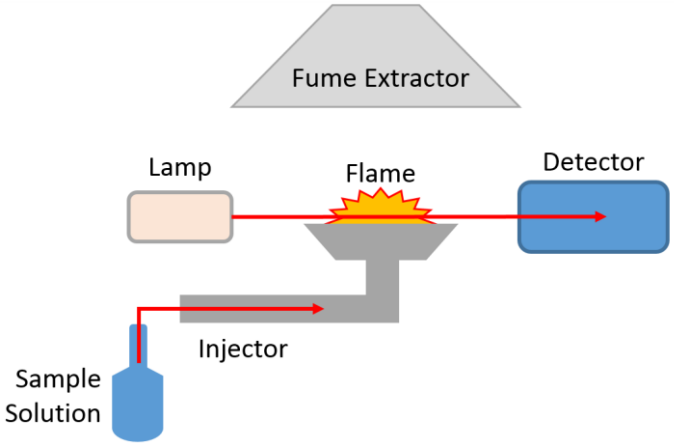


*Figure* 15*: The GF-AAS system, the sample is injected into the atomization chamber where it is vaporized. The lamp emits resonance radiation that passes through the vaporized source and gets detected through the absorption that is witnessed. Arsenic's peak wavelength is 193.7 nm.*

Technical difficulties in handling the equipment led to collaboration with the University of Toronto's Scarborough TRACE Centre, in the production of precise calibrations. As stated by the literature review, these benchmark technologies are fickle, similar to the field portable technologies, requiring a high level of maintenance and control for proper functionality and precise detection.

## 3.2 Results for the Benchmark Technologies

The following graphs, Figure 16 and Figure 17, were generated using GF-AAS. Each point on the graphs was generated through resampling a solution three times. Generated points of the GF-AAS curve were required to maintain a relative standard deviation (RSD) below 5 %. Any sample beyond this tolerance or believed to be compromised was omitted and resampled by the technician. Further confirmation of these results was obtained through plotting the points of the generated stock solutions with samples generated in house by the TRACE Centre.

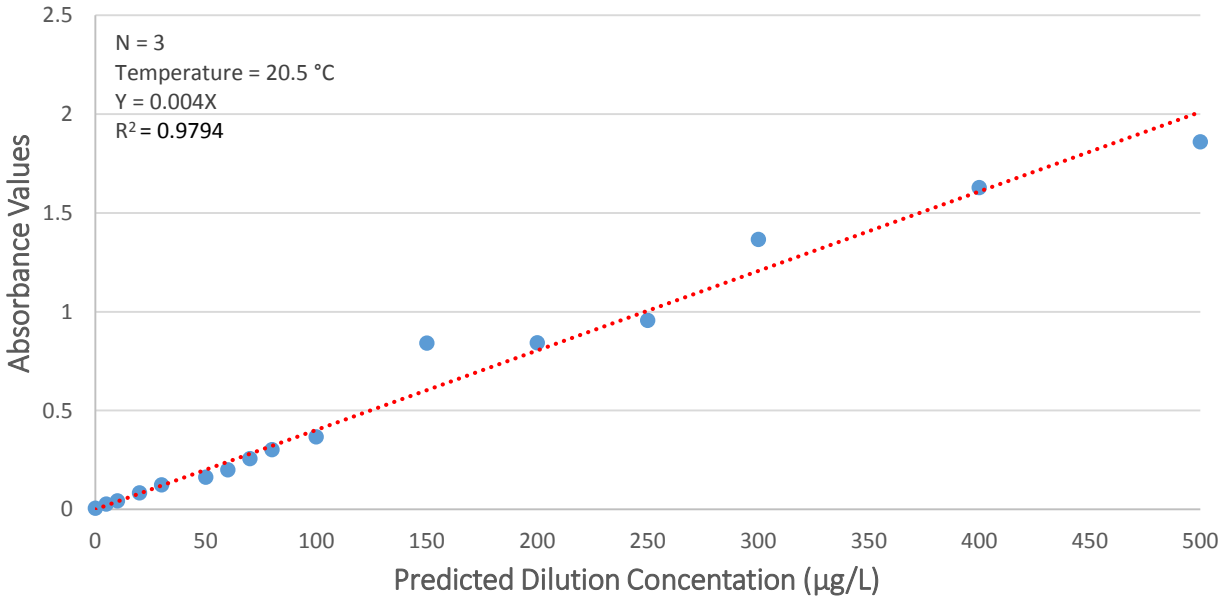


*Figure 16: Comparison of the solution GF-AAS absorbance values and prepared solutions*

The absorbance values of the GF-AAS, shown in Figure 16, were converted to concentrations using Beer's Law, illustrated by Figure 17. The generated results follow a linear trend, steadily

increasing with the increasing concentration. Here, stock solution standards should be within close range when fabricating a curve with GF-AAS. Concentrations used here jump through a large range resulting in some deviations. Concentrations above 100 µg/L were generated through a second curve, resulting in the wider deviations when the resulting datasets were merged. While this graphical deviation is apparent, it is a negligible concern, as it was formed through the association of the two collected datasets and the $R^2$ for each graph is exceptionally high. Given the $R^2$ factor is a static measure of how close the data holds to the fitted line, this demonstrates the trend accounts for almost 100 % of the variability. As the colour chart used by the selected FTK requires this range of concentrations, it was only suiting to use its specifically generated colours, especially through the initial testing.

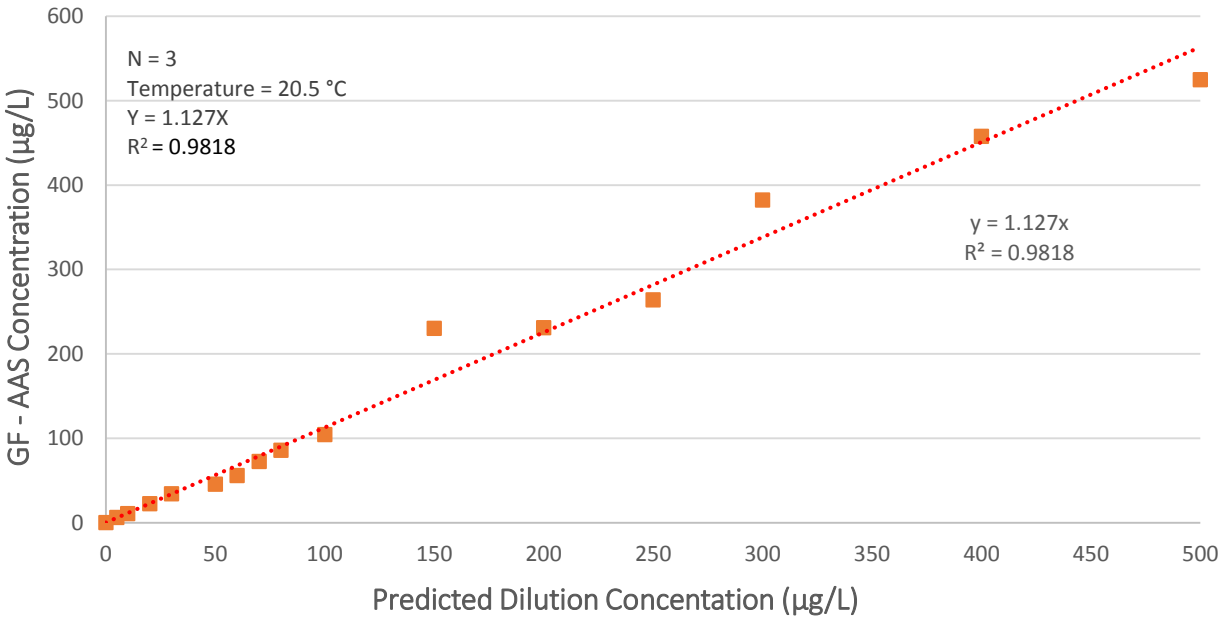


*Figure 17: Comparison of the solution concentration, as defined by GF-AAS and prepared solutions*

Obtaining these results posed a difficult task for technicians without the appropriate equipment at hand. As stated in the methodology, these results were generated over a variety of attempts. While GF-AAS is the benchmark technology for testing, these results are nevertheless important in the generation of a quantitative analysis for the FPT. Ambiguities in the results existed during the generation of these results that may have been caused by the equipment used, modifiers incorporated, presence of acid, and the difference between concentrations in the chosen range. Through maintaining a RSD of 5 % and a controlled setting for sample generation, these are

negligible. Looking at the linear trend line for the GF-AAS Concentration vs. Stock solutions, it can be seen that the gradient, or slope, is close to a value of 1. This suggests an almost constant rate of change, the ideal linear result.

## 3.3 Chapter Summary

Through this chapter, graphite furnace-atomic absorption spectroscopy was chosen as the benchmark technology to classify the concentrations for the produced arsenic solution standards. While a variety of benchmarks exist, as previously indicated by Figure 12, GF-AAS was suited to the existing requirements. Here it was shown that even a benchmark may suffer difficulties for proper quantification, with a strong reliance on system maintenance and proficient technical staff. Through controlled production of standard solutions and the generation of Figure 17's empirical results, it was made possible to compare a benchmark with the portable image analysis of a FTK.

# Chapter Four

# 4. Field Portable Technology

This chapter focuses on the chosen field portable technology. The methodology used to prepare for the colourimetric analysis, in Chapter 5, is defined. The development of an improved apparatus and means of capture will also be discussed.

## 4.1 Field Test Kit (FTK) Performance

The Quick™ Arsenic FTK was obtained to perform experiments. This kit is designed to detect arsenic in the 0 to 500 µg/L concentration range. While it is important to improve detection around the 10 µg/L threshold, this is of less concern here. In the research conducted, the aim was to quantify the TSIs by colourimetric analysis. The instructions for the chosen FTK were followed, with minimal changes being made to the protocol. This general protocol for the Quick™ Arsenic FTK has been placed in 7.3.2 of the Appendix.

## 4.2 Test Strip Indicator (TSI) Generation

Following the protocol for the FTK, provided in 7.3.2 of the Appendix, the typical analysis was performed with slight modifications from the literature. The time of the reaction was increased from 10 to 20 minutes, the temperature of the solution and the room were both monitored throughout the tests, and samples were given a drying period to prevent the loss of the impregnated arsenic through physical contact or movement. During the measurement, a significant amount of hydrogen gas is evolved, as shown in Figure 18.

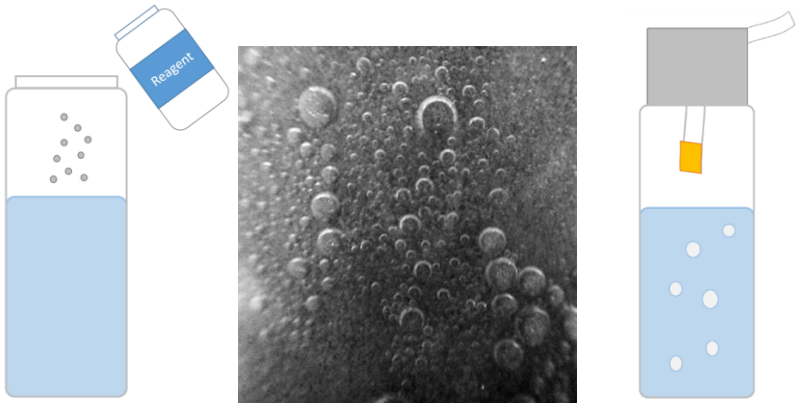


(a) (b) (c)

*Figure 18: Performing the Gutzeit Method. (a) Adding reagents leads to the (b) generation of hydrogen gas that releases the present arsenic (c) forming the coloured complex.*

When bubbles burst at the surface, aerosol droplets can be ejected onto the mercuric bromide sensing surface of the TSI, giving rise to uneven colouration. Therefore, three replicates were made for each experimental measurement. After completion, samples were kept within a labeled petri dish, indicating the batches date of production. Stock solution samples and TSIs were repeatedly made and tested to increase the level of precision before producing the final samples for analysis and correlation in Chapter 5. Through this process, stock solutions were generated, as detailed in Chapter 3. Once the FTK reactions were run, TSIs were handled according to the protocol placed in 7.3.2 of the Appendix. Through maintaining these procedures, both stock solutions and TSIs were kept within an ideal setting for production.

## 4.3 Digital Imaging Equipment

In Chapter 5, results were generated using reflectance. While transmittance may be used to measure the flux, it is more practical for existing kits to rely upon the light reflected back, used in photography. While TSIs can be modified to allow transmission through the impregnated surface, it is not conveniently used by the wide variety of field kits in use. To obtain digital images for the colourimetric analysis, two cameras were put to use: the digital single-lens reflex (DSLR) and a smartphone with macro lens attachment (SML). These devices can be seen in Figure 19 and Figure 20. The digital images taken by these devices are compared and contrasted in Chapter 5 for their use in the field. Both of these imaging devices were placed inside of the imaging apparatus, illustrated below in Figure 21, to hold the camera in a specific arrangement. In maintaining the

light conditions and camera settings, it was possible to produce consistent results between the various tests.

*Figure 19: DSLR Camera D90 with VR 85mm f/3.5G lens attachment*


(a) (b)

*Figure 20: The SML consisted of both (a) Nexus 4 Smartphone with 8 MP camera and (b) a macro lens attachment*

After completion of the drying period, the test strips were placed into the imaging apparatus so that multiple digital images may be taken of the impregnated medium, using both cameras. These images were later transferred into MATLAB to perform the analysis. Further imaging was performed on the next day, to capture the variations after the initial exposure. Through use of these devices, a protocol was standardized, as found in 7.3.2 of the Appendix.

Using the protocol, images were initially generated using the colour chart provided by the Quick Test ™ kits. These images served as both a theoretical model and a testing ground for the design parameters, before generating actual images with the TSIs. While these reference colour charts are generated for visual comparison, in the field, it is possible to digitize it as a calibration curve for immediate analysis. Images were taken with a Nikon D90 camera with an 85 mm lens operating at a vertical/horizontal resolution of 300 dpi and 24 Bit depth.

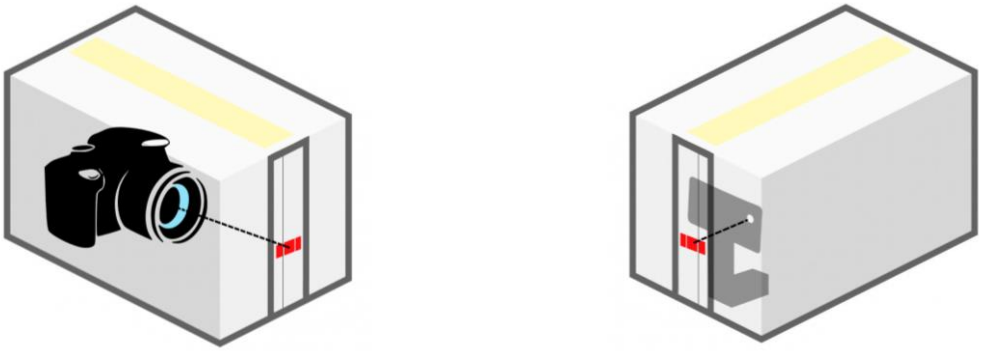

(a) (b)

*Figure 21: Imaging apparatus for (a) DSLR Camera and (a) Smartphone with macro lens attachment, mounted to align the images captured for the desired test strip indicator and references.*

To prevent deviations such as image misalignment or shaking while improving the repeatability of image capture, each test strip was secured within guiding lines and an adaptive sampling protocol was incorporated in the algorithm. The imaging apparatus removed ambient lighting, caused by the environments, and replaced it with a controlled fluorescent light source. The method of securement additionally allowed for light conditions to be judged, both for the replicate images and between the various samples. To do this, two black reference squares were placed on either side of the sample, as shown in Figure 22, allowing software to judge the light variation across each sample.

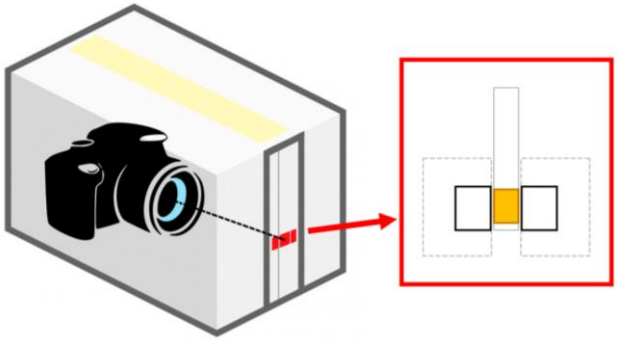

*Figure 22: Methods of interest for arsenic detection.*

### *4.3.1 Calculation of the Macro Lens Ratio*

A lens' focal length is the distance from the center of the lens to the point where the rays of light converge in a focal point. Setting the macro lens attachment to the precise focal length allows for the optimal image capture, but given that the Depth of Field (DOF) is reduced, a limited area is in focus. Here, self-shading becomes an issue, as it becomes difficult to light the region of interest.

To confirm the magnification being used in this setting, specifications for the lens were taken, as shown in Table 6, to calculate the magnification as shown in 7.4.3 of the Appendix. The magnification was confirmed to be within the 1:5 ratio of super Macro.

Table 6: The macro lens

| **Description** | **Value** |
|---|---|
| Elements | 1 |
| Shot distance | 10 - 23mm |
| Dimensions | 15.8 mm x 6.5 mm, 13.06 mm x 9.38 mm |
| Magnification ratio | 1:5 |

*4.3.2 Variation of the Imaging Apparatus*

Through the progression of defining the imaging apparatus, a solid model has been formed for in-field application. The initial imaging apparatus, as shown in Figure 23, was used as a means to define the necessary dimensions and components that would be incorporated in this device. It was also used for comparative purposes between the images produced by both the DSLR and SML cameras.

Further simplifications of this apparatus have shown promise towards in-field application. The optical arrangement proved to be beneficial in obtaining both a reference and the sample at once. Further work has been done to improve the apparatus layout and analyze its optical properties for use with SMLs.

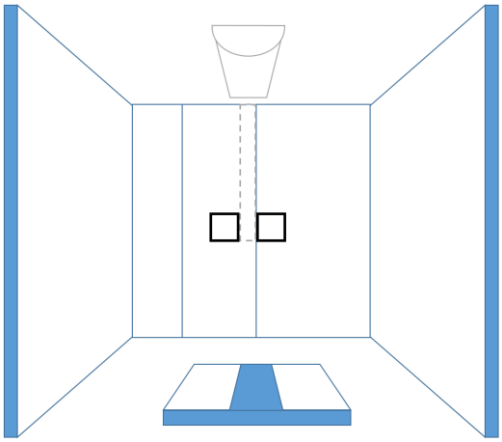

*Figure 23: The imaging apparatus used to control and maintain the image capture of various test strips, the black squares served as the reference regions for measuring the light deviation. Dashed lines were used to confirm the strip was placed in the desired alignment. The camera was mounted to prevent its movement.*

While the initial apparatus made comparison possible, the end goal is to design an apparatus solely for smartphone use, as to maintain small size and reduce associated costs while remaining quantitative. In an initial attempt, a model was printed with acrylonitrile butadiene styrene (ABS) plastic filament, as shown in Figure 24. Here the design was based around three components, an insert, the box and a layer to attach the smartphone and macro lens. The insert was made to hold TSIs while allowing them to be raised or lowered for the camera with a block of the plastic. The box was made to restrict background light and contain its own light source. This initial model was not optimal as the material let light in and restricting sample placement would improve capture with the macro lens.

*Figure 24: The first attempt at a 3D-printed imaging apparatus for in field use.*

The model was redesigned, as seen below in Figure 25. Here the general parameters of the previous design were maintained while improvements were made for handling the samples, providing a diffused light source and the means of smart phone placement. Control over the exact distance between macro lens and TSI made imaging samples far more quantitative. A ridge was placed on the apparatus to maintain the placement of the smartphone with macro lens. This smartphone ridge could be modified and printed specifically for a variety of current phones, as the goal would be to make the apparatus universal.

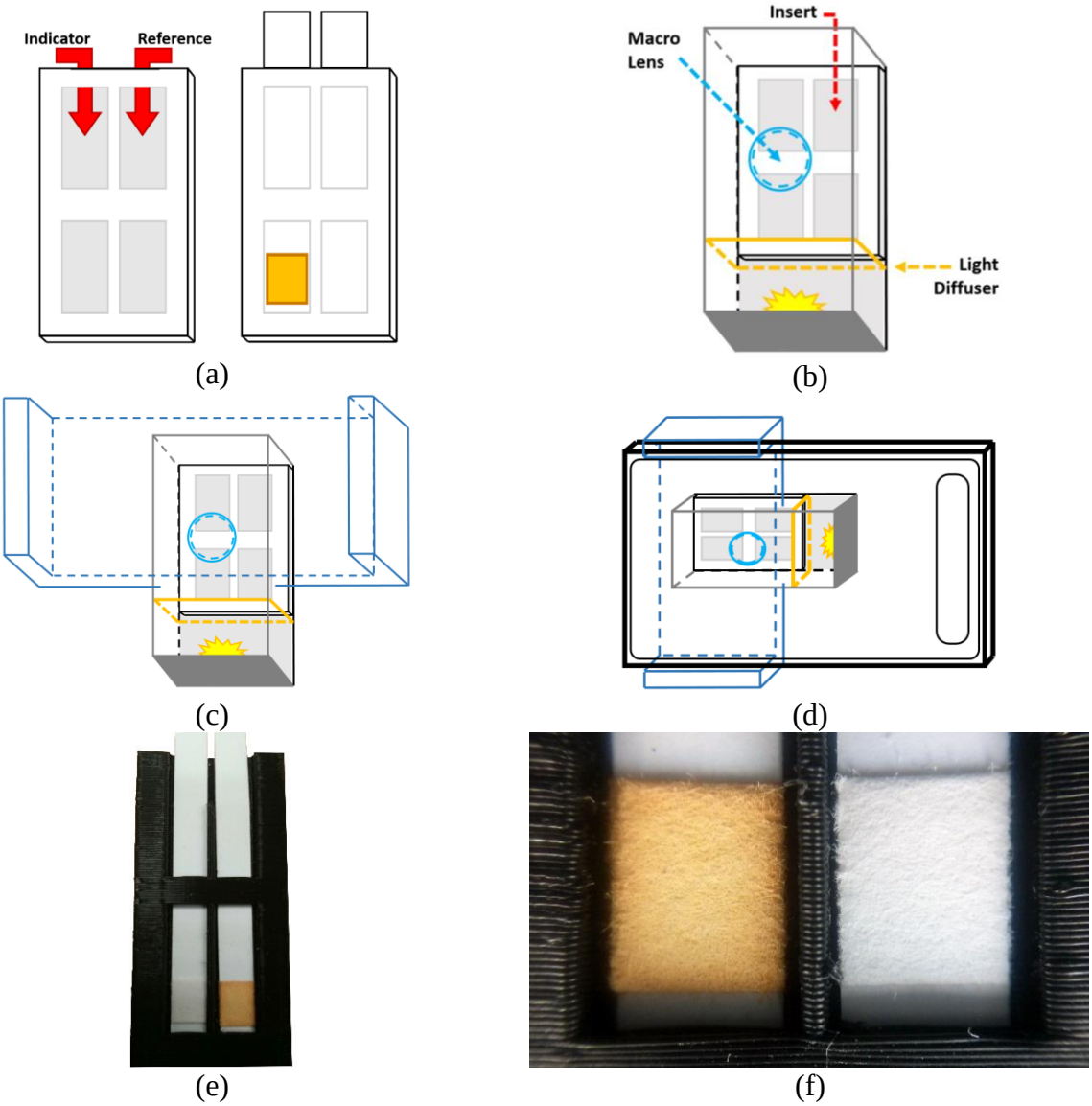


*Figure 25: Modifications to the in-field imaging apparatus. (a) Shows the insert which allows the user to control the placement of both a reference and test strip in the apparatus. (b) Illustrates the general image apparatus layout with control of the lighting and macro lens placement for optimal image capture. (c and d) Illustrate the final component needed to attach the apparatus and Smartphone together. The printed models (e) TSI insert tray and (f) imaged samples with the macro lens.*

## 4.3 Imaging Methodology

Image analysis for the SML holds promise towards the development of FPTs. The overall goal would be to perform the image capture with SML, tag it with essential details and send it to a database. From here the collected data could be processed in a controlled setting, thus allowing for both quick responses and long-term trend-line production, as shown by Figure 26.

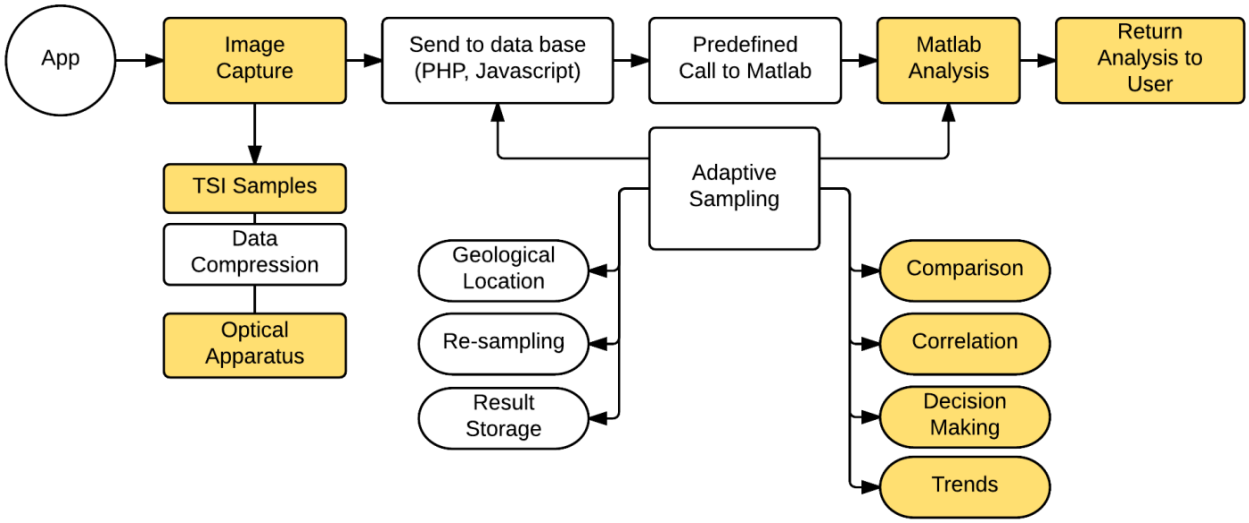


*Figure 26: Optical analysis through use of the SML, highlighted regions specify areas worked upon. Images of the TSI's were initially captured by the optical apparatus. From here MATLAB adaptively compares, correlates and develops a prediction to inform the user. The additional components must be incorporated to be more user friendly.*

The FTK images were processed using defined routines, built in MATLAB. While there are various routes that may be taken to process the images, a general outline was followed, as shown in Figure 27 and described below. Further details of the calculations incorporated in this analysis may be found in 7.3.3 of the Appendix.

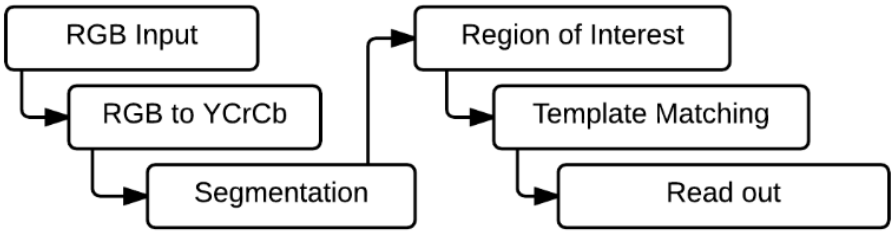


*Figure 27: Basic Image Analysis Outline.*

As shown below in Figure 28, image files were opened from their source folder through the programming environment. Once each of the files was opened and read into memory for a specific concentration of colour, the images were first masked to determine the location of two reference areas and the coloured region of interest (ROI).

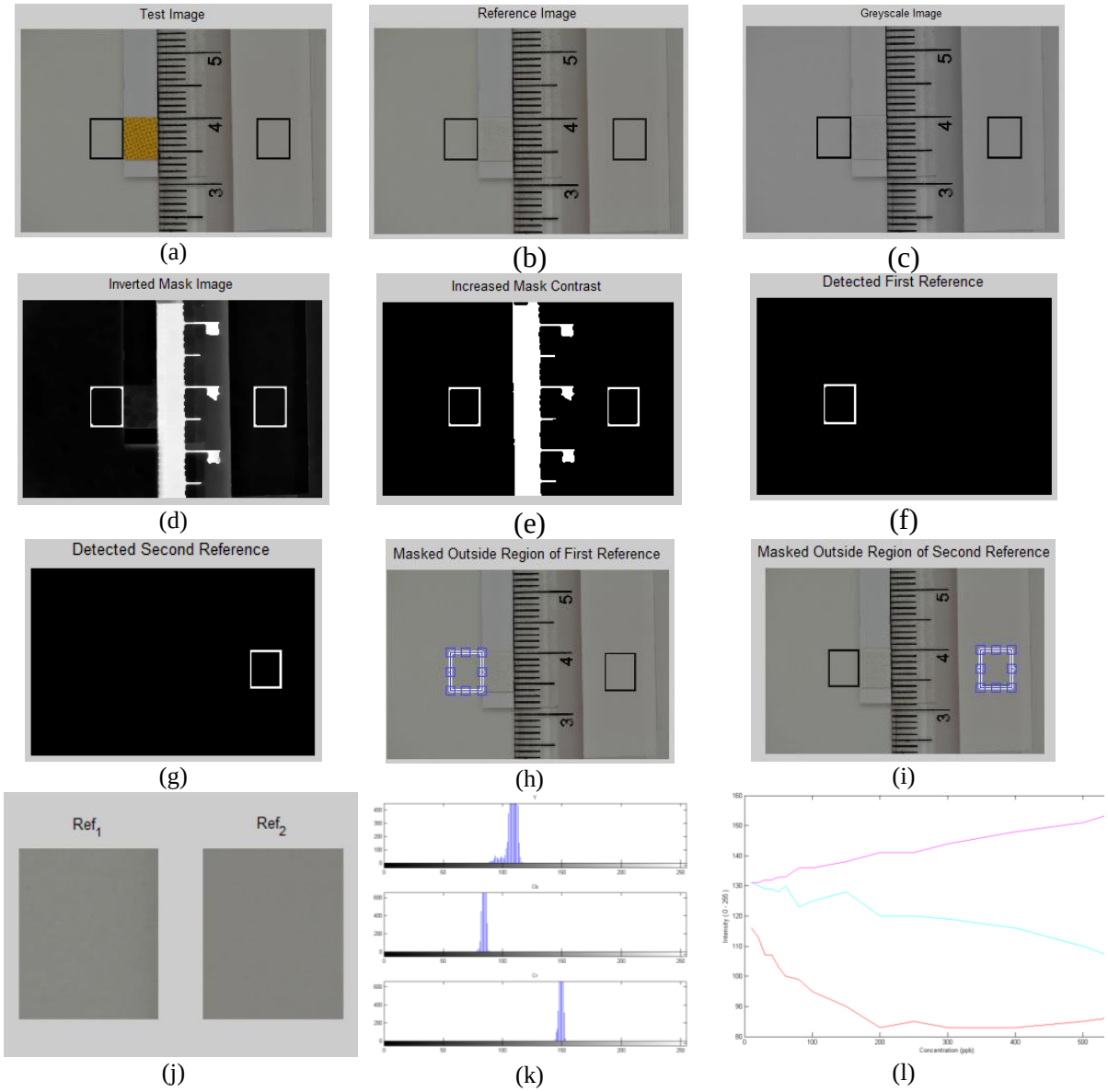


*Figure 28: Segmentation Process, the images, shown above, illustrate the segmentation process that was used. The test image (a) is first compared to the reference image for overall quality. From here the image is made into a binary mask (through c, d, and e). Connected regions are located and the two references areas found. Dimensions of the references are taken to crop them out of the original image. These locations are also used to locate the region of interest (ROI) before finally returning the three regions for analysis (j). Following this procedure histograms have been generated for each of the arsenic standard solutions (k) and their peak intensities combined (l)*

From here, a segmented image was broken down using a binary mask, Figure 28(c, d, e) to determine how many features exist, this should result in a total of three when imaged correctly, making the miscategorization of the pixels obvious and correctable. The binary mask converted the image to black and white, with the RGB channels containing a value of either 1 or 0. To

determine the number of features present a function was incorporated to look at each pixel and determined from its neighboring pixels whether or not it was part of a feature, defining their boundaries with a pixel value of 0 constituting the background.

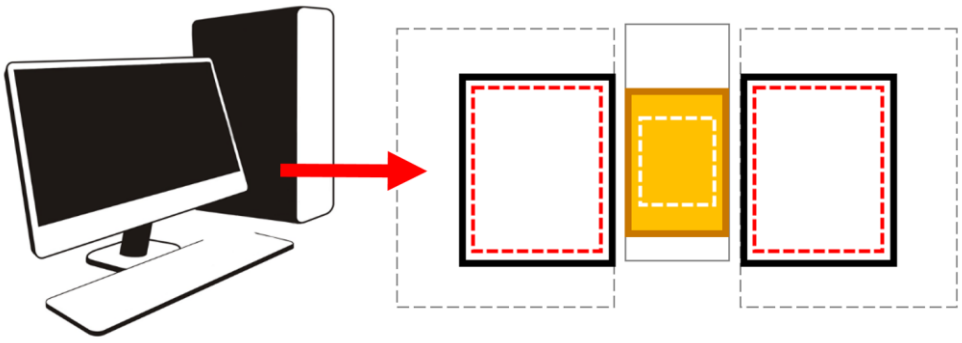

*Figure 29: Computer software is used to confirm the selected ROI and quantify it.*

When the three regions are registered, the original image will be displayed in a window along with predefined boundaries, as shown by Figure 28(h, j) and Figure 29. Here the user will be asked to confirm the selection was made correctly before proceeding to crop out each of the features. If the number of features exceeds expectation, the outcome will be flagged for the user to adjust accordingly. The predefined boundaries are used to consistently select the same number of pixels for comparison purposes. After these steps, each of the cropped out sub-images are now redefined. To analyze these images within the YCbCr colour model, the RGB values must first be normalized. The normalization relies upon the characteristics of the original colour space. Equations for the normalization are provided in the 7.3.3 of the Appendix to generate the YCbCr values, derived from the sRGB colour space [59].

Before handling the ROI, the light deviation between the two reference areas of the original image are captured for the blank image in the calibration set. Three images are taken when analyzing one FTK TSI, allowing an algorithm to confirm the capture settings are consistent. The light deviation is therefore also compared among the three images using the luminance channel of the YCbCr colour model.

With the light deviation across the image to be consistent, a calibration curve for the colour range must be created. The above segmentation process will be repeated for each concentration in the

FTK range. The ROI is collected for each image and an algorithm is performed upon them. Here a ROI image will be adjusted by both median and average filters to remove artifacts caused by the test strip texture. As this process is consistent across each of the images, it does not pose a loss but instead helps to remove the variation in defining a specific intensity for each of the colour models channels.

Colourimetric analysis may be used to confirm repeatability and relate to previously calibrated tests, which is especially useful towards making accurate judgments for the research being performed here. Equations provided in 7.3.3 of the Appendix were used to calculate mean square error; the mean and the signal-to-noise ratio. The peak signal-to-noise ratio was also calculated with the division of the maximum power of the signal, in the case of an image this would be the maximum pixel intensity of 255, and the mean squared error, calculated along the x and y axes that define the pixels of an image [77]. The variance of the image was also calculated along the rows and columns for each [78]. Finally, a measure of the randomness across the image and the estimate of the variance and its corresponding bias, the mean square error was found through multiplication of the variance values along the rows and columns [78].

Once the images have been adjusted and analyzed they are split into the separate grayscale channels for luminance and chrominance measurement. The histogram for each of these channels is retrieved, as shown in Figure 28(k). Here a summation of the pixel intensities multiplied by the corresponding number of pixels is used to generate the points of the calibration, as shown in Figure 28(l) and 7.4.1 of the Appendix.

The resulting values of the channels are stored into separate arrays to form a dataset. With the datasets for each channel obtained, the maximum and minimum values may be collected. These allow each of the datasets to be normalized for the intensity range, 0 to 255. The normalized datasets are combined and averaged to obtain the final YCbCr Calibration Curve with associated error bars, obtained from the standard deviation values.

Generation of the calibration curve must be performed before a random sample concentration can be analyzed. To do this, an appropriate polynomial equation is generated for each of the present

curves in the obtained calibration. Here the calibration is additionally split into three concentration ranges to produce better polynomial fittings. In this way, the stored calibration, deviations, and maximum/minimum values are used to predict where a new sample will fit. The general segmentation and determination of the channel values for the ROI are set. The calibration values are used to normalize the new values into its range.

Further improvements were made before the well-defined sets were taken. The codes produced and additional calibration sets may be found in the Appendix. The overall process that has been just discussed can be further illustrated by Figure 51 in section 7.3.1 of the Appendix.

## 4.4 Chapter Summary

This chapter has provided the methodology and advancement of the image capture for field portable technology. Developing a basis for imaging in the field, where it needs to go and a means to do so requires further definition. Image capture was also contrasted for both the digital single-lens reflex (DSLR) camera and smartphone with a macro lens (SML) attachment, which is used in the following chapter for correlation with the graphite furnace-atomic absorption spectroscopy. Focus is placed on describing the development of novel algorithms that are used for a tailored analysis of the TSIs.

# Chapter Five

# 5. Image Analysis with Field Portable Technology

## 5.1 Calibration Results

The following are the results used in the generation of the calibration curve for colourimetric analysis with the chosen FTK. Colour-complexes were formed for the set concentrations, specified in Chapter 3's methodology. Images for each of the experiments were acquired under the same conditions, it is noted that this was one of the reasons the smartphones light source was not optimal. The DSLR camera was set to macro mode and the focus kept consistent. To maintain the background lighting, the fluorescent imaging apparatus, discussed in the previous chapter, was used. The influence of different lighting conditions were initially reviewed, indicating it would be possible to obtain tabled values for the various settings, with slight changes in signal strength and white balance. While various light sources and settings were possible the parameters settled upon are listed in 7.4.2 of the Appendix.

Here the chosen FTK's colour chart has been used only in the initial creation of a theoretical model before moving onto actual samples as shown in 7.4.1 of the Appendix. The generated colours for each specific concentration were used to form the overall colour range of a calibration curve. Results have been provided in 7.4.1 of the Appendix for the generated calibrations, produced in parallel with the GF-AAS. Table 7 has been used to provide basic details on the FTK reactions. Tests were performed within the FTK's reaction vessel from low to high concentration, with the reaction vessels cleaned and dried between performed sets. This was done to minimize the chance that the TSIs would read the presence of arsenic incorrectly.

As stated in Table 7, after all reagents had been added the reaction was set for a total of 20 minutes. As discussed in the literature review and methodology sections, it was found that an extended reaction time would be beneficial for colour-complex formation. As discussed in Section 5.2,

initial tests showed samples were more likely to vary in intensity for a period of time after removal from the reaction vessels.

Table 7: Field test variables held constant

| Parameter | Measure |
|---|---|
| Reaction Time | 20 min |
| Room Temperature | 20.5 ◦C |
| Temperature in Solution | 19.0 ◦C |

As stated in the literature review, it was essential for the solution temperature and room temperature to be incorporated; both were maintained and recorded throughout the experiments. This is to be maintained across all calibration curves for comparative measure.

Finally, the test strips' drying interval was set for 60 minutes, recorded and maintained. This was essential to alleviate issues caused by the moisture. As initial tests had shown, moist samples easily fragmented through physical contact. Droplet formation on the surface also posed an issue in surface variations. Both of these issues were significant to image capture and sample analysis, as the produced colour-complexes are significantly small even without artifacts affecting SNR. Although initial tests followed the FTK's suggestion of immediate analysis to capture the test strips initial heightened intensity, the process had to be altered if quantitative analysis was to be made possible.

While a test strips indicator was found to have the most intense colour right after the reaction completion, making it optimal for the visual approach, the capture of digital images makes it easily ignorable. For the FTK being used in this analysis, the lower concentrations already do not generate a highly intense colour. While this has been a discussed problem, the literature has stated new kits are adapted to amplify the colour at specific concentrations, specifically the lower range needed. In addition to this, it can be seen through the calibration curve of Figure 30 that there is far less of an issue than expected.

Figure 56 in 7.4.3 of the Appendix has been provided to show the intermediate graphics results gained through the MATLAB analysis. As stated in the methodology, images of the test strip

indicator were cropped for the desired regions of interest and the histogram for their associated channel intensities taken. Here two datasets have been provided for the summation of these intensities multiplied by their pixel count. This method was found effective in capturing the various concentrations as the present histogram intensities, in a given channel, are affected differently for the range of chromacity.

To obtain the calibration, resulting curves were normalized using the maximum and minimum intensities present among the two datasets. With the images normalized to remove discrepancies, the results could now be averaged to obtain a fitting curve with further indication of the standard deviation, captured by the combination of two datasets taken from a total of 6 images per concentration. Figure 30 illustrates the calibration curve with a confidence interval of 95 %. Here "Y" is the luminance, "Cb" is the Chroma Cb and "Cr" is Chroma Cr. The results were to be found within very close proximity to the suspected fitted line. This should still be considered when predicting sample location, showing that the multiple curves may be of use. While the confidence intervals for each point of the Chroma Cr channel are smaller than those of Chroma Cb, it could suggests that the Chroma Cr is not responsible for capturing the colour that is present on the TSIs. Here the larger deviations of Chroma Cb may therefore be expected, as it is focused on the applicable yellow intensities.

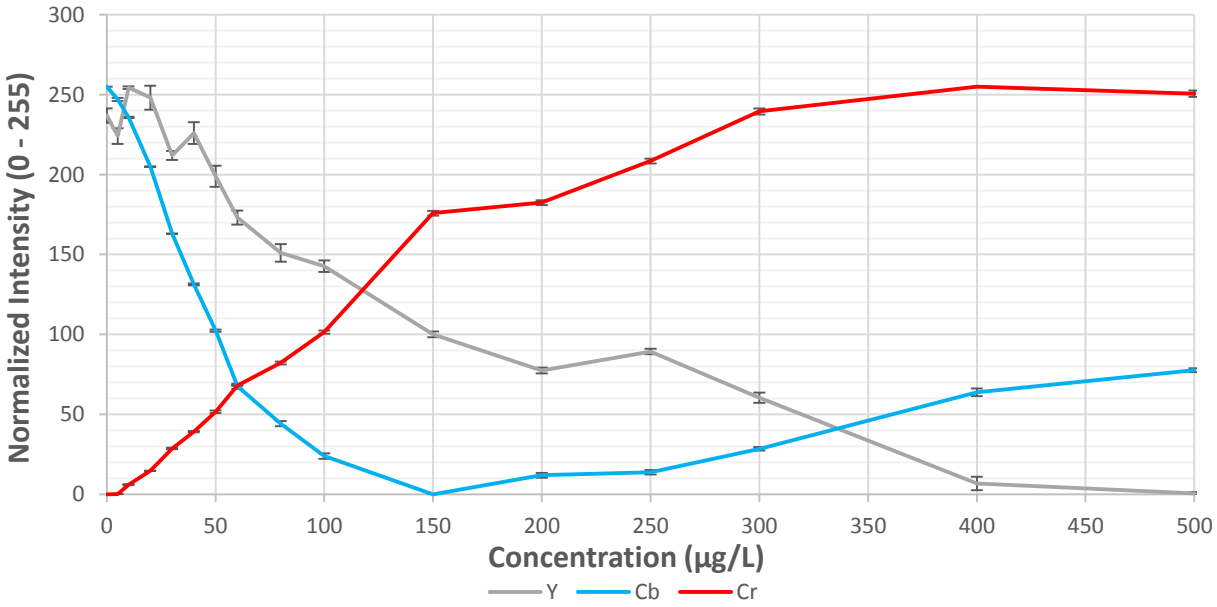


*Figure 30: Calibration curve with 95 % confidence interval, for which the expected range of intensities are represented.*

Using the acquired dataset, a further set could now be taken, incorporating the calibration into the actual prediction of further concentrations. The additional set of images was taken alongside calibration sets CS10, and CS11, which were correlated with the GF-AAS. The additional code, produced in MATLAB, incorporates the final mean calibration curve in predicting where a new image is best fit onto the calibration. In this iteration, the code predictions were based on an averaging of the points of intersection, between the predicted images Y, Cb and Cr channel intensities and the calibration curves. The predicted image was normalized, using the calibration curves' generated max and minimum intensities, to fit the curve.

Below, Figure 31 provides a comparison of the predicted concentrations for both the generated images and the GF-AAS. In the legend "CS#" stands for the calibration set that was used and "linear (Avg)" indicates the line of best fit. Here, even in its simplest prediction format the generated comparison is highly linear, especially for the lower concentrations, which are found to overlap quite thoroughly. Again, the $R^2$ value is reasonably high in accounting for the plotted variability. These initial prediction results are already consistent and comparable to the gold-standard results of the GF-AAS. It is noted that image predictions for the higher concentrations vary, given the averaging that was used in the prediction code. To further prove the comparable quantitative capabilities of the image analysis to the GF-AAS, the prediction code was be adapted to match each of the separate chromacities and an average of the two.

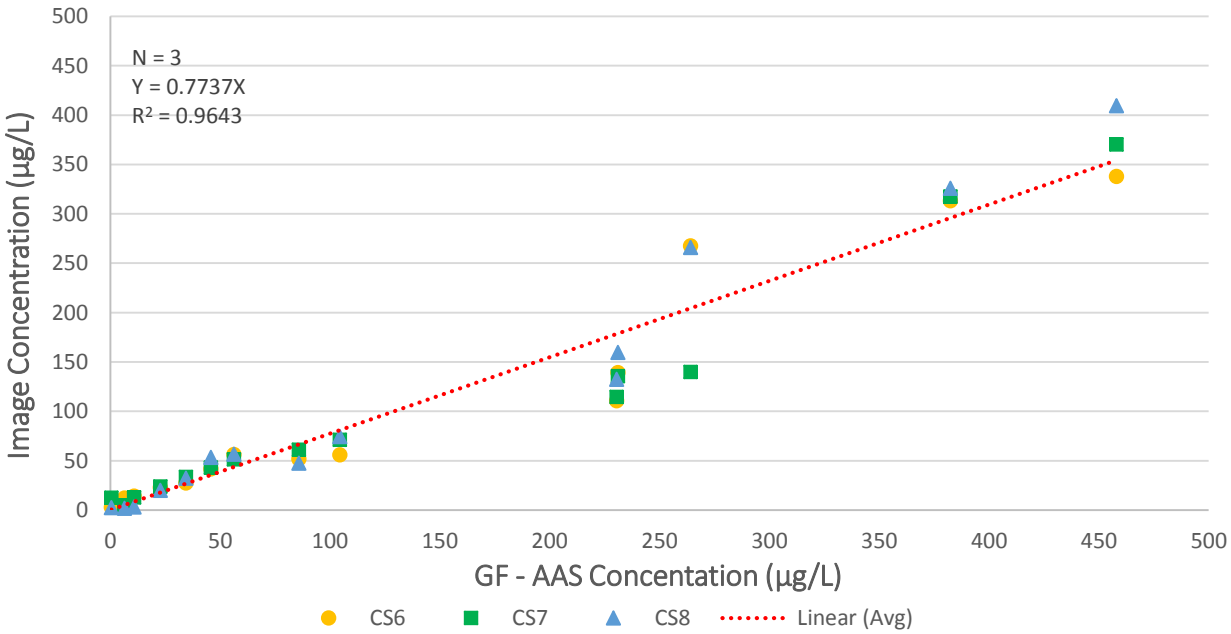


*Figure 31: DSLR image predictions, an average of three channels (Y, Cb and Cr).*

Although each of the image channels play a role in classifying pixel intensities, excluding the supposed luminescence could improve the analysis, as the focus here is on measuring the colour (CbCr), not the associated light deviations (Y). Looking at Figure 56 in 7.4.1 of the Appendix, the calibration curves clearly show that the channel for luminance is associated with the greatest variations, especially at lower colour intensities, where most of the light has been reflected, not absorbed by the coloured surface.

For Figure 31 to Figure 34, it can be said with certainty that the colourimetric analysis of the field test kit can be performed digitally, removing user interferences, but it is required that very strict protocol with a high level of control be put in place. The effective advancement of the in-field qualitative test to one of a quantitative nature is achievable. The initial prediction attempt, Figure 31, using an average of the three channels, shows that while the luminance, or Y channel, is part of the overall image, it has to be separated as it is used to handle deviations associated with the lighting and not the actual generated colour, resulting in a confidence of only 73%.

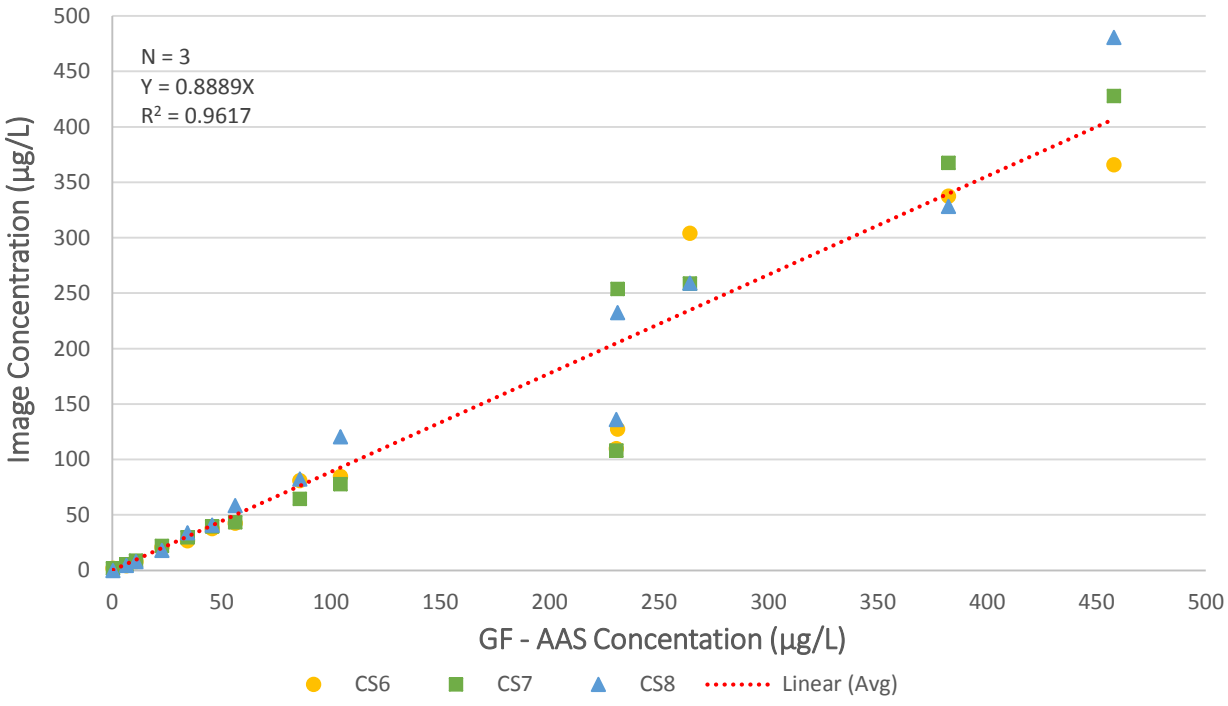


*Figure 32: DSLR image prediction, Chroma Cb channel.*

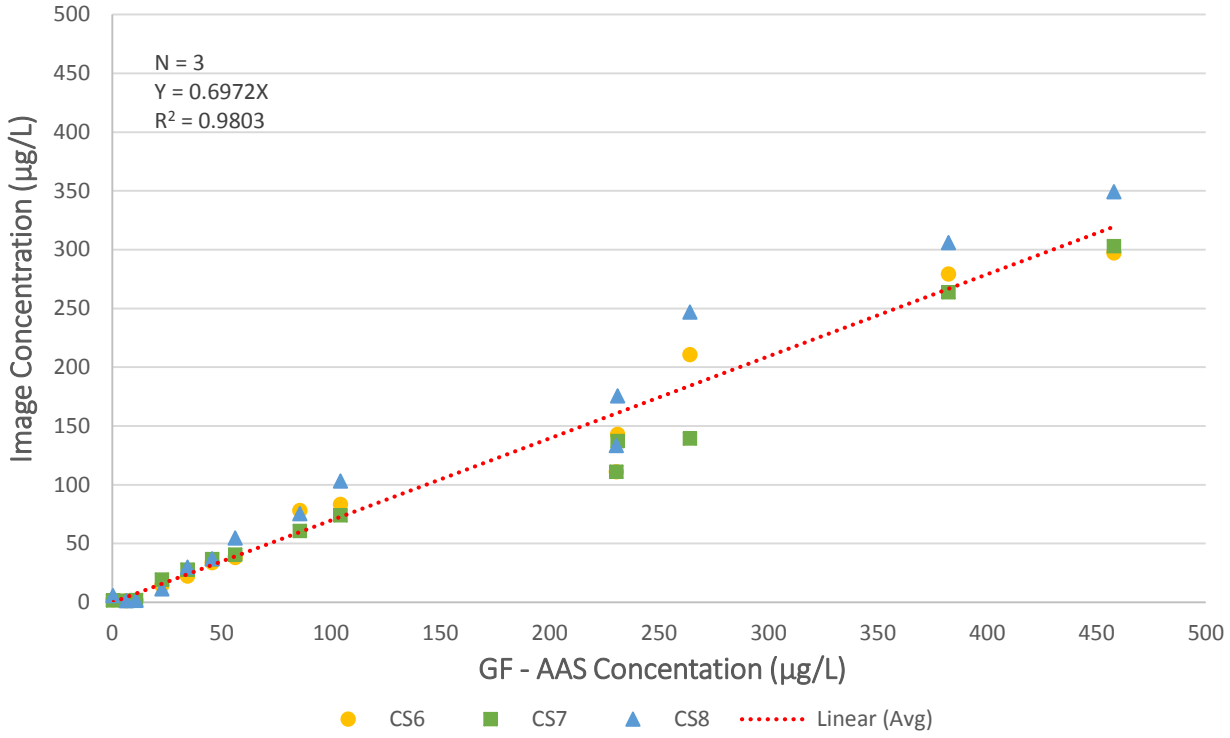


*Figure 33: DSLR image prediction, Chroma Cr channel.*

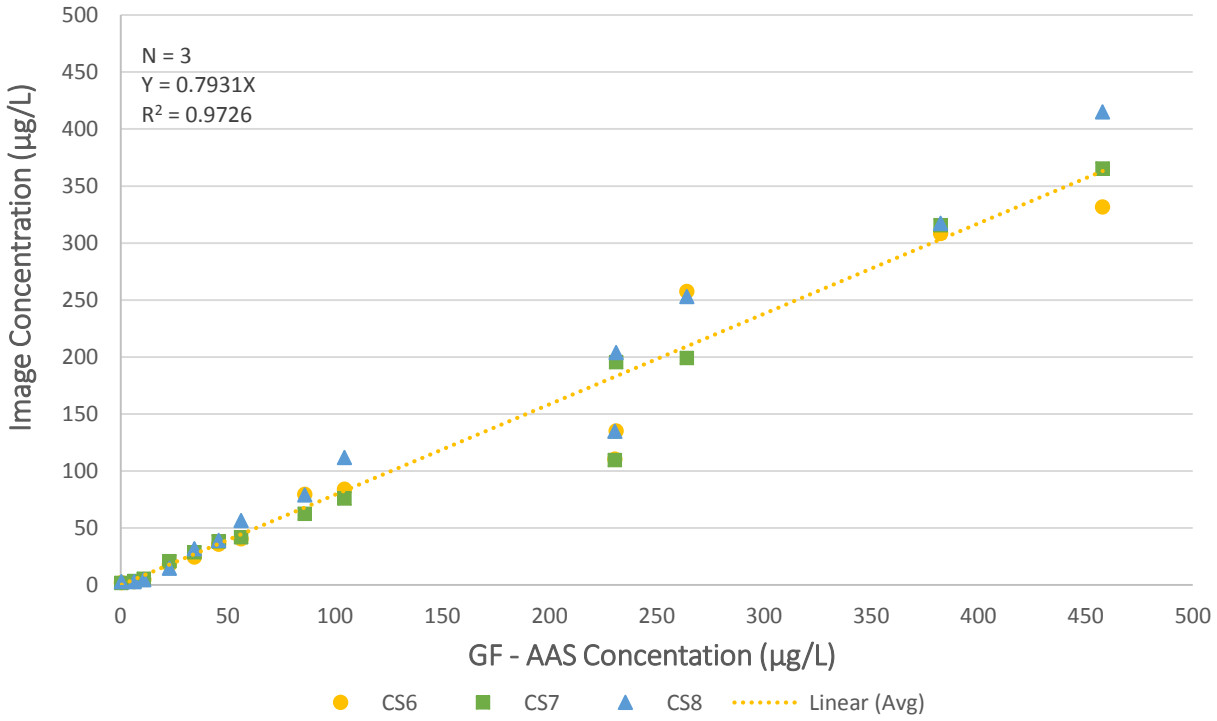


*Figure 34: DSLR image prediction, average of the Chroma Cb and Cr channels.*

In Figure 32, the response of Chroma Cb produces a slope that differs from a perfectly linear response by an approximate value of 0.89, or 11 %, with a reasonable R-squared value of 96 %.

In Figure 33, the generated slope for Chroma Cr is found to be off by approximately 31 % with a higher R-squared value of 98 %. Finally, through averaging both the value of Chroma Cb and Cr, as seen in Figure 34, it was possible to obtain a linear result within the tolerance, a confidence of 79 % with a reasonable $R^2$ value of 97 %.

Alone, Chroma Cb is prone to producing multiple intercepts, as the calibration curve it produces bends back, while for Chroma Cr the response is more linear, making it easy to assume the prediction is with the calibration curves error bar tolerance, set by the calculated deviations. While Chroma Cr possess the more simplified means of prediction its confidence is not adequate for colour at the lower concentrations. It appears that the best option may come through considering both the Chroma channels results, without averaging the two. As both are separate components of the same image, both defining the presence of colour, it makes sense that the combination of these two would result in a better prediction of the overall chromacity but as the colour generated for low concentrations is yellow the Chroma Cb channel best represents the generated colour-complex's.

Chroma Cr should have more success in quantifying the higher concentrations, as it deals with red vs. cyan, while Chroma Cb handles the faint yellow intensities well, yellow vs. blue. As the test strips colour range goes from a faint yellow to a dark orange/red, both Chroma Cb and Cr are essentially needed. The best result would therefore be obtained through the use of Chroma Cr to define the initial predicted location along the calibration curve, then to finalize the resulting colour prediction through the value associated with Chroma Cb.

## 5.2 Comparing the Image Intensity Variation

Taking into consideration that the intensity of a sample is stated to vary over time, images were captured for concentrations of 50, 100 and 500 µg/L over an extended period of time. Results for 50 µg/L have been provided in Figure 35 below, while graphs for the other two concentrations have been placed in 7.4.1 of the Appendix. Running them through the code developed in MATLAB, it was possible to view how time affects the samples. Test strips were maintained

within petri dishes to maintain their quality and prevent them from being subjected to external environmental factors between each imaging period.

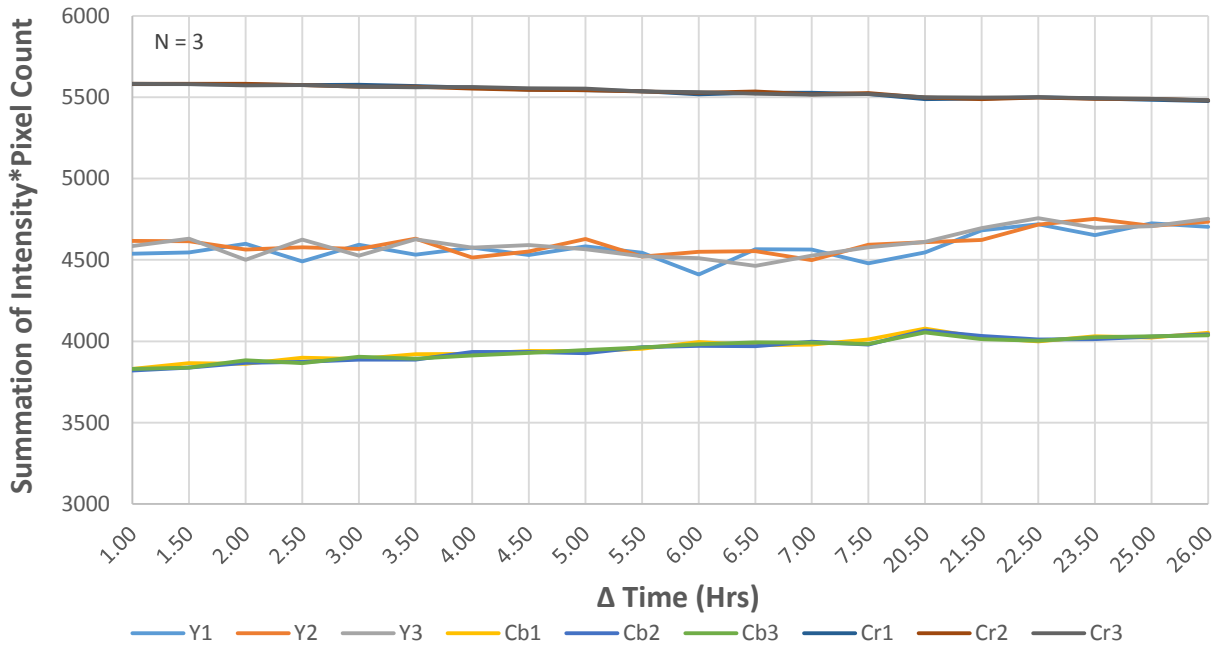


*Figure 35: Variation in the image intensity over a period of time, for a 50 µg/L sample.*

At each of the sampling times, three images were taken for each of the given concentrations. Placing the images into the associated MATLAB code, graphs were generated by a summation of the histograms pixel intensity multiplied with the pixel counts, as done to achieve each of the calibration curves. Here it is shown that for each of the three channels that compose the YCbCr model, there is a slight linear increase over the 24 hour period. This effect, although it appears minimal, must be taken into account, especially as samples were imaged during this phase. After longer periods of time, oxidized samples will still maintain colour but the intensity is lowered, as shown in Figure 36. As samples of the various concentrations will still differ in the degree of colour at this later point, it may indicate that the remaining arsenic has bonded strongly or permeated deep into the paper indicator, making it hard to escape.

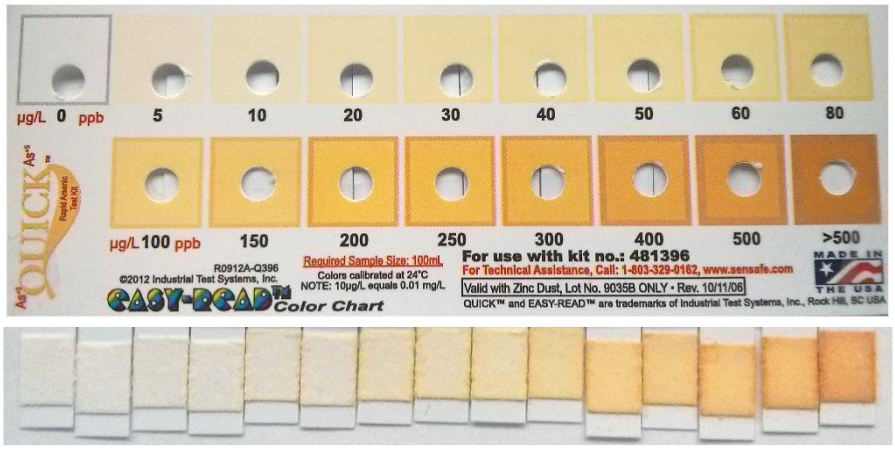


*Figure 36: Aged samples, faded but still may be quantified six months after production.*

Here the first images were taken an hour after the reaction, as defined through the protocol. Though the variation in this period would show the greatest spike it has not been included as it is already been shown that a drying period is essential to prevent greater errors.

Over the following 24 hours, the samples maintained in a petri dish slowly fade in colour, caused by oxidation. Through these graphs, it could be practical for a simple linear model to be built, allowing for the production of a correction factor for samples that will be predicted against the image calibration curve, once a period of time has passed. As the activities of a single technician tasked with visiting many locations in a single working day are further affected by an increased reaction time, imaging the sample and having a correction factor could alleviate the need for multiple individuals to perform the task.

In Figure 35 above and Figure 59 and Figure 60 in 7.4.1 of the Appendix, it was noticed that at 21 hours an artifact occurred for both of the lower sample concentrations, associated with the chromacity. The defect was barely noticeable in the highest concentration, 500 µg/L. While this artifact is ignorable, as it departs in the image samplings that follows, it illustrates that lower concentrations, in which the generated colour-complex is significantly less intense, require better control over the imaging to prevent the signal from merging with the reference.

## 5.3 Smartphone Charge-Couple-Device Lens with Macro Attachment

In order to study the influence of the smartphones camera, the DSLR imaging apparatus with a fluorescent light box was used. Following the guidelines set out in the methodology that define the digital image capture and analysis, the smartphone results were analyzed. Here the purpose was to apply the developed process, used by the DSLR camera, to illustrate the SMLs capability in providing an adequate quantitative analysis.

The produced graphs mimic those of the previous section very thoroughly. Figure 37 shows the production of a calibration curve that closely resembles the previous, although slight deviations are made apparent. In comparison, the Smartphone has shown difficulty capturing the same deviations of the luminance, which is in essence not an issue but one to do with the possible change in light caused by the capture settings associated with the camera. Overall the two generated curves could be adequately overlaid. In essence, the use of a common calibration curve in the field would require a set image apparatus and optical setting, although as both the results of the DSLR and Smartphone are adequate, building each their own specific calibration would not be of any challenge.

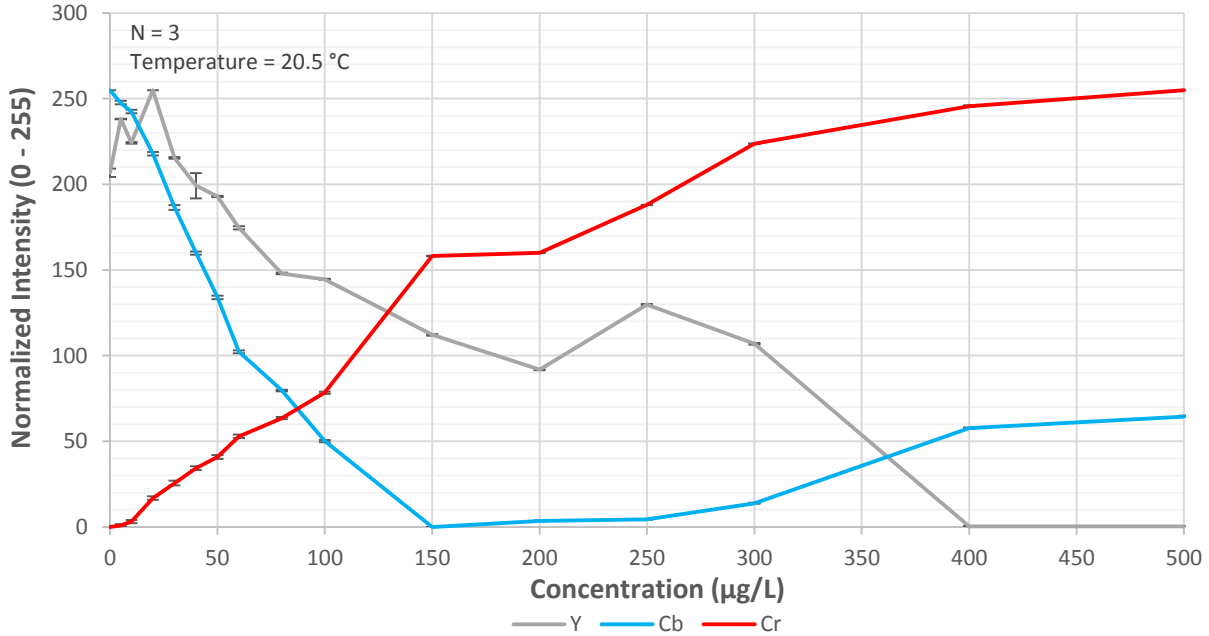


*Figure 37: The SML dataset is further reduced to indicate a 95% confidence interval, for which the expected intensities with be represented.*

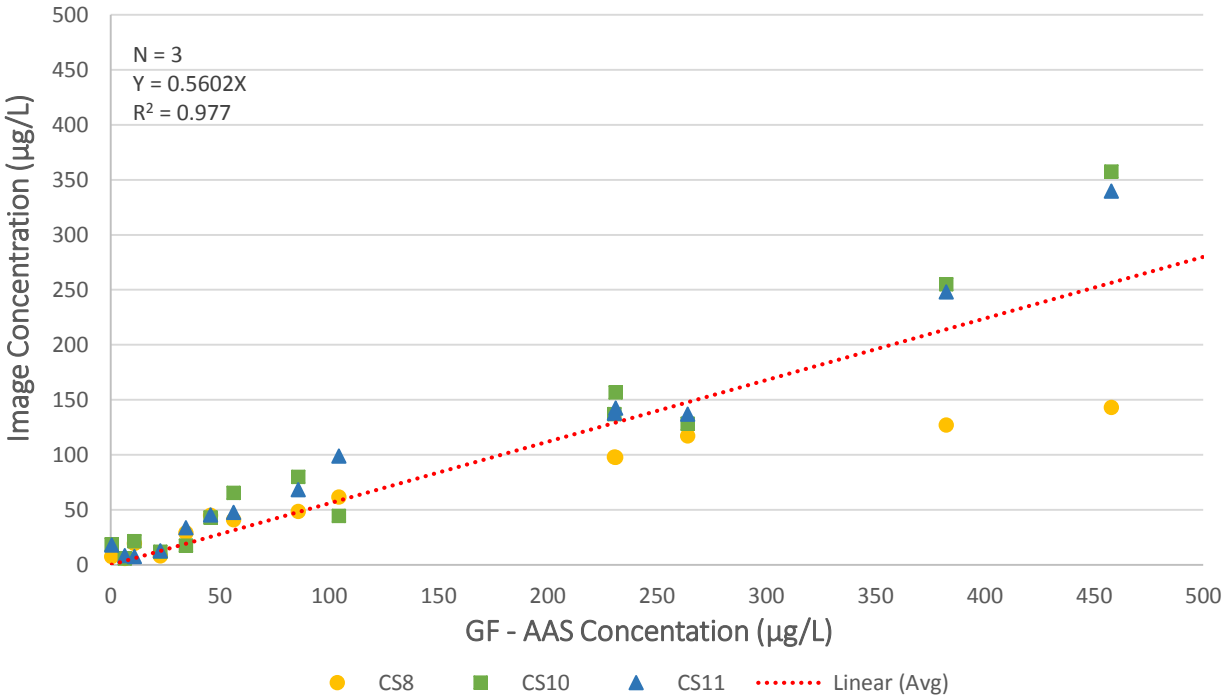


*Figure 38: SML image prediction, average of the three channels.*

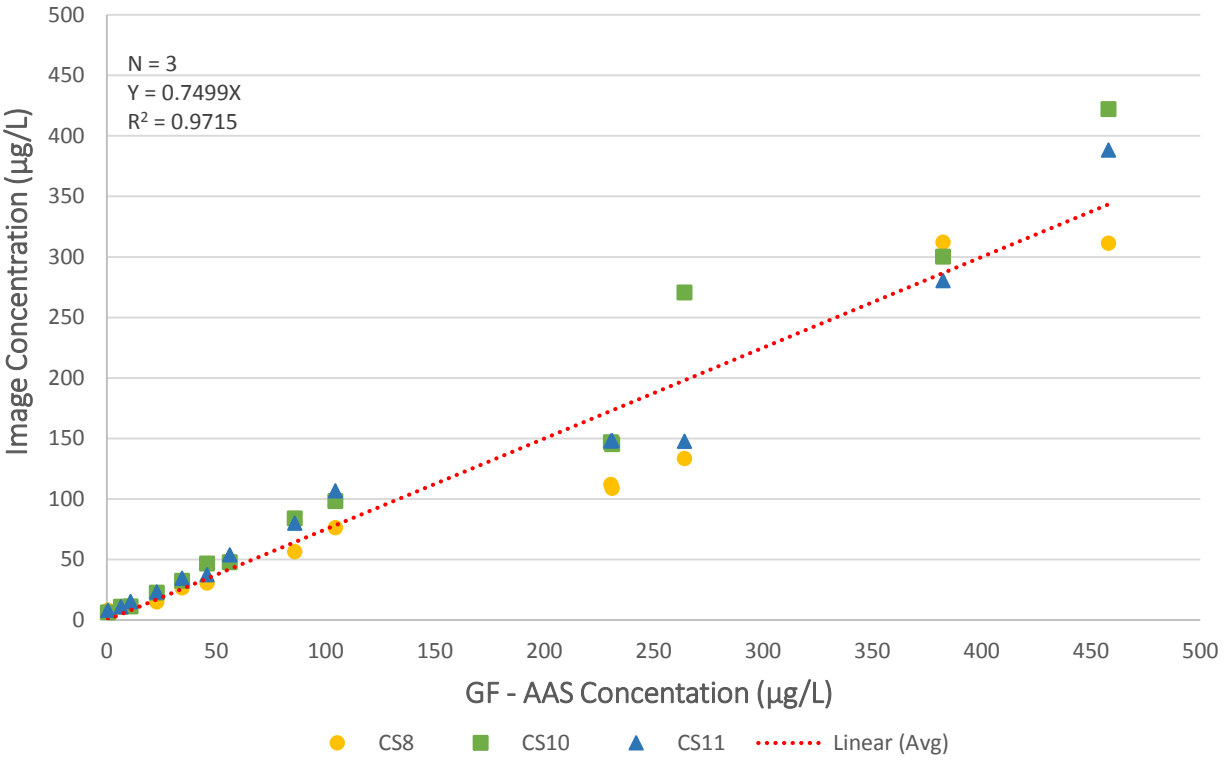


*Figure 39: SML image prediction, Chroma Cb channel.*

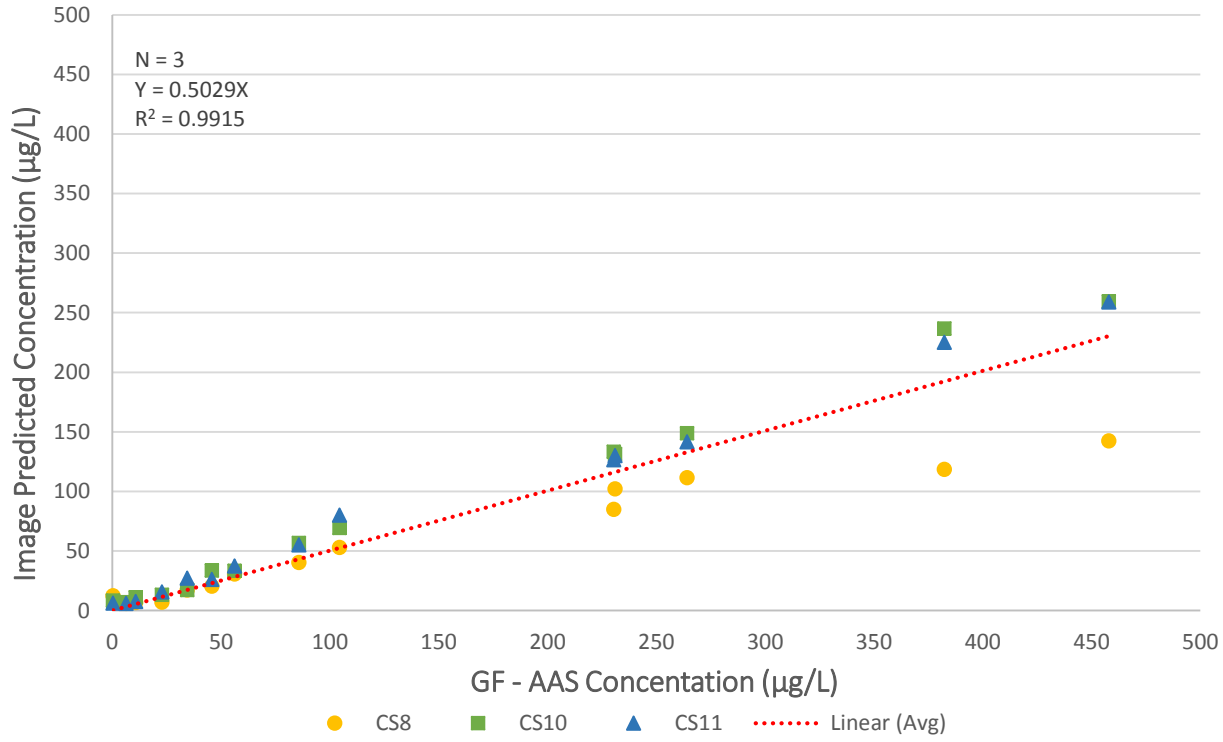


*Figure 40: SML image prediction, Chroma Cr channel.*

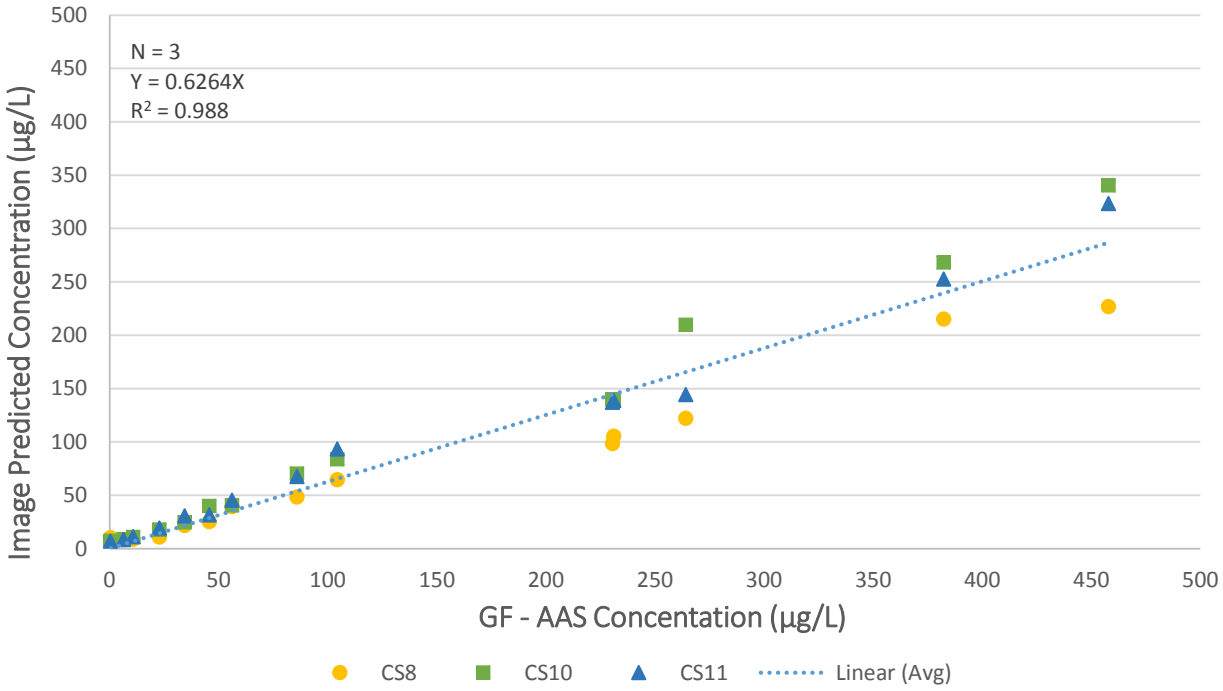


*Figure 41: Predictions of the concentration by SML, average of the Chroma Cb and Cr channels.*

In terms of the concentration predictions, for the SML vs. GF-AAS, it is again shown that the prediction, based on averaging the intersections with the calibration curve, provides a moderately

linear result with an exceptional handle on the variability, as seen by the high $R^2$ values. As shown through the previous section, the ambiguities that exist in the linearity should also decrease through the use of the Chroma Cr channel, to locate the general position, and the Chroma Cb to define the actual concentration, with its associated confidence of 75%. It can be explicitly stated that the results of the SML are again well correlated with the chosen gold standard, GF-AAS.

In comparing the generated calibration curves to those of the DSLR, it should be noted that while the number of pixels used to define the region of interest has stayed constant, the image size has not. As such, there is a suggested discrepancy between the regions of the image that are being compared here. This apparent issue will be discussed more thoroughly in the following section.

## 5.4 Comparing the Image Capture Methods

Here the results for the DSLR and Smartphone, with attached macro lens, have been overlaid to display the deviations between the two calibrations, as seen in Figure 42 to Figure 44. Viewing the DSLR camera as a benchmark in optical technology, the Smartphones shortcomings can be better defined. Diverse uses are made possible for a DSLR camera through its interchangeable lenses and adjustable apertures, enabling greater control over a variety of image settings. The sensor array of a DSLR camera has a greater number of elemental pixels that contribute to the final image, equating to higher sensitivity to available light and chance for increased pixel resolution. A dedicated light meter in the body also automatically provides accurate exposure while, in comparison, the dynamic range is several stops wider than what smartphones provide. A Smartphone platform is relatively limited in what it can optically achieve with its CCD camera. Still, the number of light sensitive pixels in a smartphone camera CCDs tends to increase every year, increasing the image quality and shrinking the image quality gap between the DSLR and smartphone cameras. While DSLR cameras are still far more capable devices, smartphones have become the tool of choice. Convenience aside, use within a defined set of parameters lowers their apparent limitations, as seen through the results above. Markers for Figure 42 to Figure 44 indicate the YCbCr Channel being compared for both DSLR and SML generated intensities. It can be seen for each of the graphs, specifically those of the chrominance channels, that the compared normalized intensities are slightly shifted from each other with the produced curves, following a

considerably parallel path. Using the DSLR as the point of reference, for standards on image capture, the smartphone can be shown to efficiently capture the higher colour intensities while it only adequately captures the lower intensities, given the deviation in producing a parallel curve. Separate calibrations for each chosen device should be captured to confirm the device lies within expected parameters, specifically for the lower concentration range that is of interest.

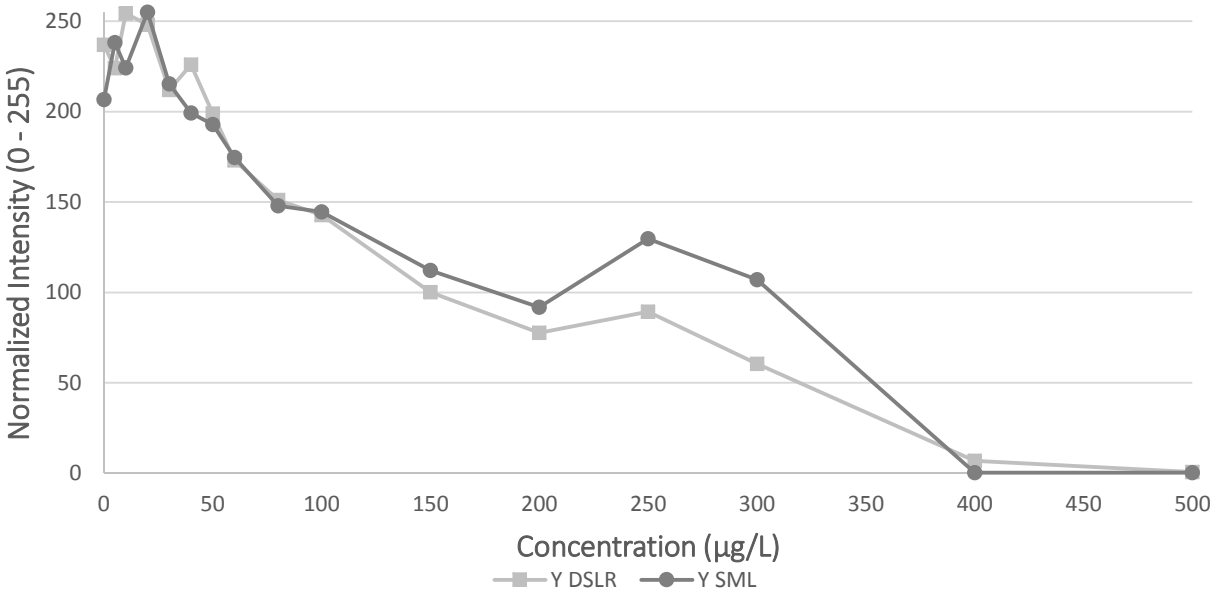


*Figure 42: Comparison of the DSLR and SML for the Luminance Y channel.*

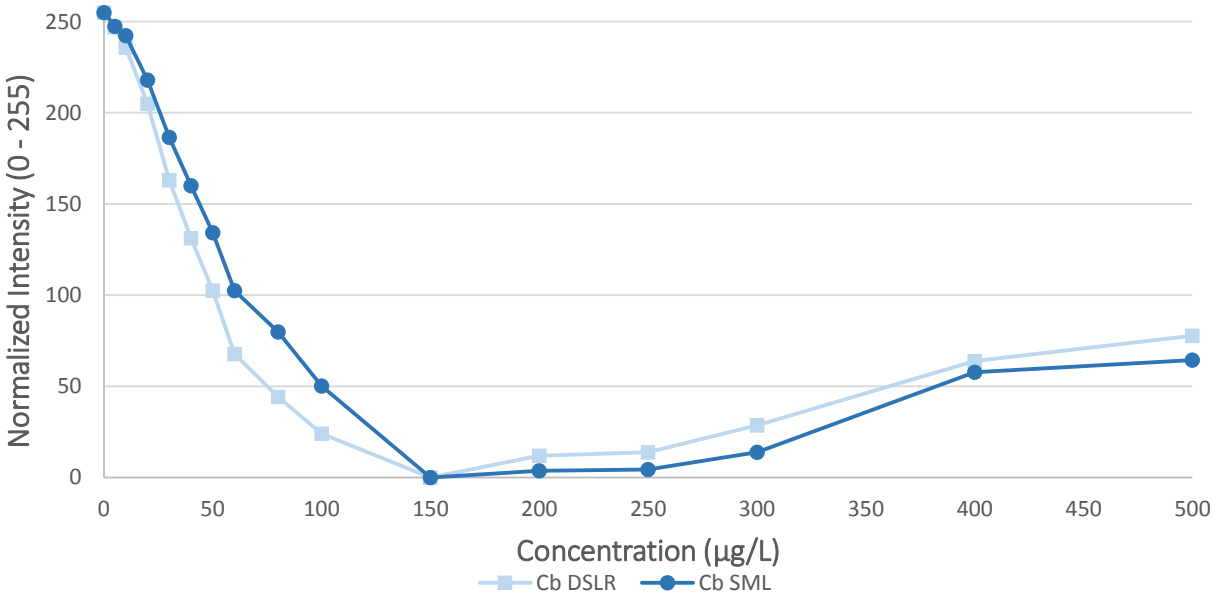


*Figure 43: Comparison of the DSLR and SML for the Chroma Cb channel.*

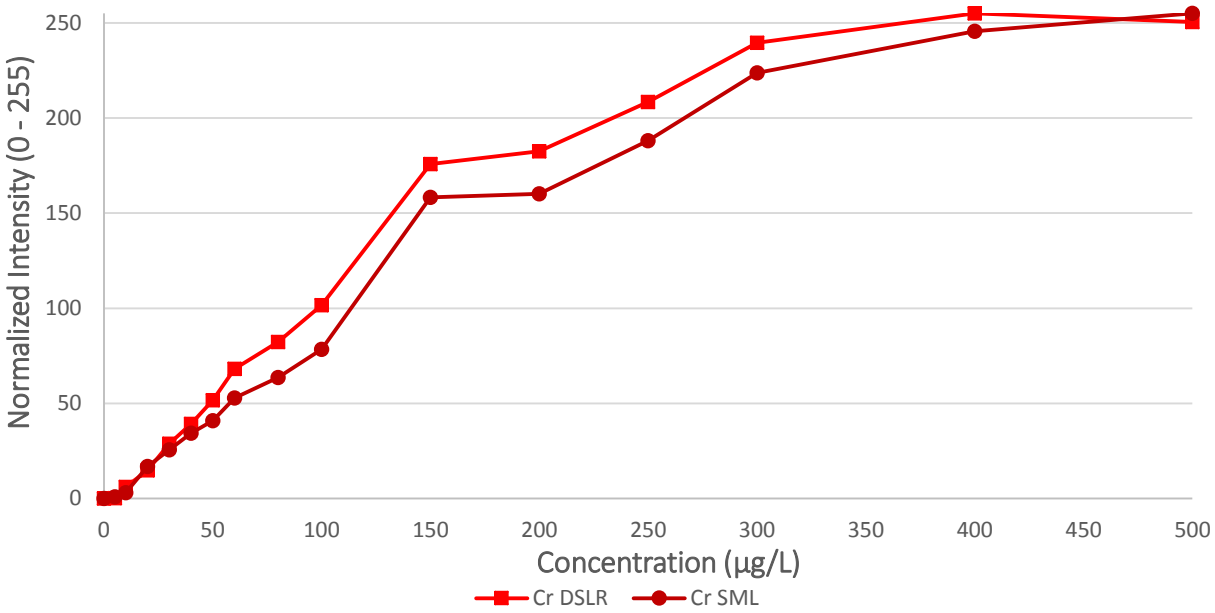


*Figure 44: Comparison of the DSLR and SML for the Chroma Cr channel.*

## 5.5 Comparing Variations of the Region of Interest (ROI)

As previously mentioned, the cropped ROI was defined by a specific size. This in turn had an effect when switching to the analysis of smartphone samples. Here the number of pixels that composed the image was far less than that of the DSLR, as such the ROI considered far more of the test strips indicator. To compare these two settings, the image set, taken by the DSLR camera, was analyzed a second time, with the crop size decreased to a half, as shown in Figure 45. Through this process, not only was it possible to confirm the effects were made negligible through the averaging and normalizing the result, but it was also possible to gain insight on the "coffee ring" effect. The surrounding border of the indicator, with its large exposed surface area, is generally of higher colour intensity than the inner region. For this reason, the effect of including this perimeter in the results, as shown in Figure 46, is beneficial in raising the associated calibration intensity for the lower concentrations. In comparing Figure 46 and Figure 47, for lower concentrations, the included perimeter shifted the intensities for each concentration. Looking at a concentration of 50 µg/L for the Chroma Cr channel, expected to account for red colour intensities, the shift in intensity may be solely based on the coffee ring providing higher intensities that do not match with the colour of the inner region. For the same concentration of the Chroma Cb channel, the shift is drastic, from 100 to around 200 µg/L without the perimeter.

In essence, it is shown that the region of the test strip selected for comparison must be obtained with exactly the same parameters and within the same portion of the test strip. Test strips images that deviate by defects to the indicator surface or through the inclusion of the outer perimeter should not be included. While captured images may be filtered, to limit the impact of defects, a sole reliance on this is not suitable as the filtering must remain consistent across all the images. Maintaining the protocols for image capture and processing effectively minimize many of the common errors that can occur.

The perimeter or "coffee Ring" could not be effectively analyzed on its own as it accounts for a very small portion of the image, with few associated pixels. As such, its small size poses a higher chance of misclassification, especially as the edges of an indicator are associated with far more defects. Analyzing the entirety of the indicator could in essence be said to incorporate irrelevant data, producing a lower signal-to-noise ratio.

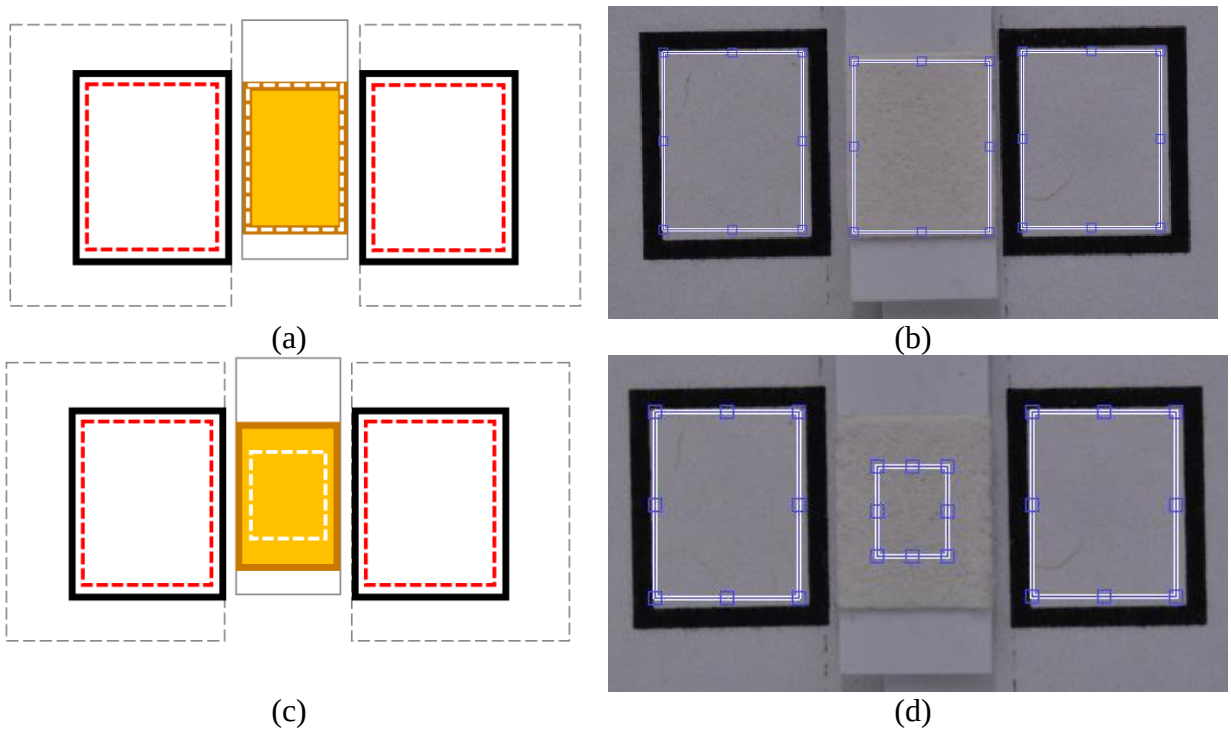


*Figure 45: The above images are used to show how the ROI may be defined, (a, b) illustrate the inclusion of the entire space whereas (c, d) only display the central region (without the "coffee ring" effect).*

As the end goal here is to associate one set concentration to a supposed position in the colour range, it would be optimal to exclude this region of uncertainty and focus only on the inner region, removing the vast deviations and expected sample defects from the analysis. In any case, the analysis of a sample must follow the same protocol and perform the analysis on a consistent manner, as even a slight change in the defined region of interest shows a change in the shape of the generated curves.

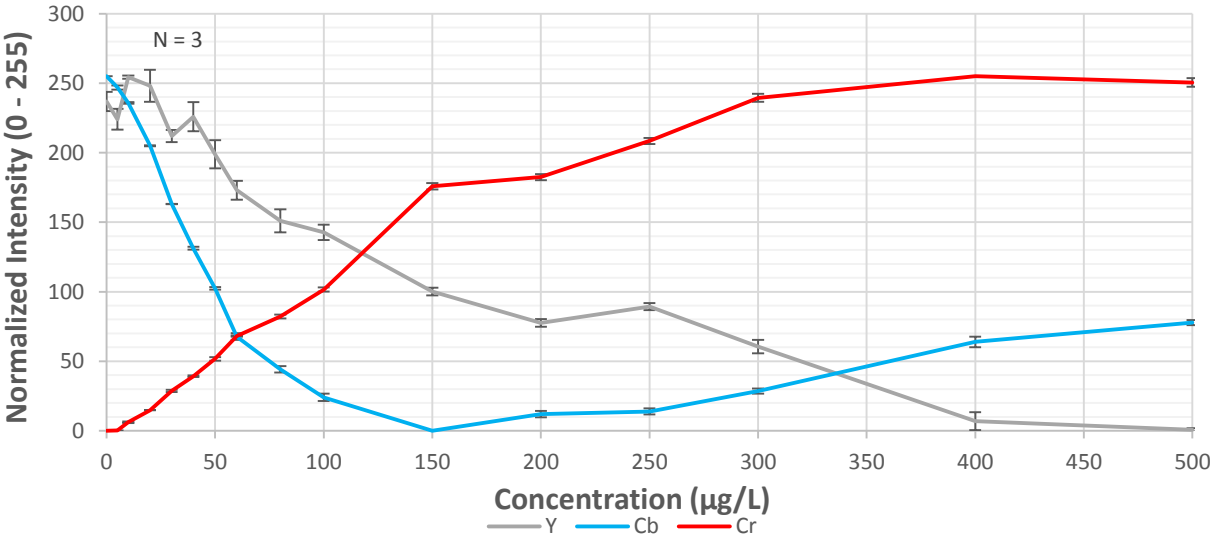


*Figure 46: The calibration curve, using the entire cropped region.*

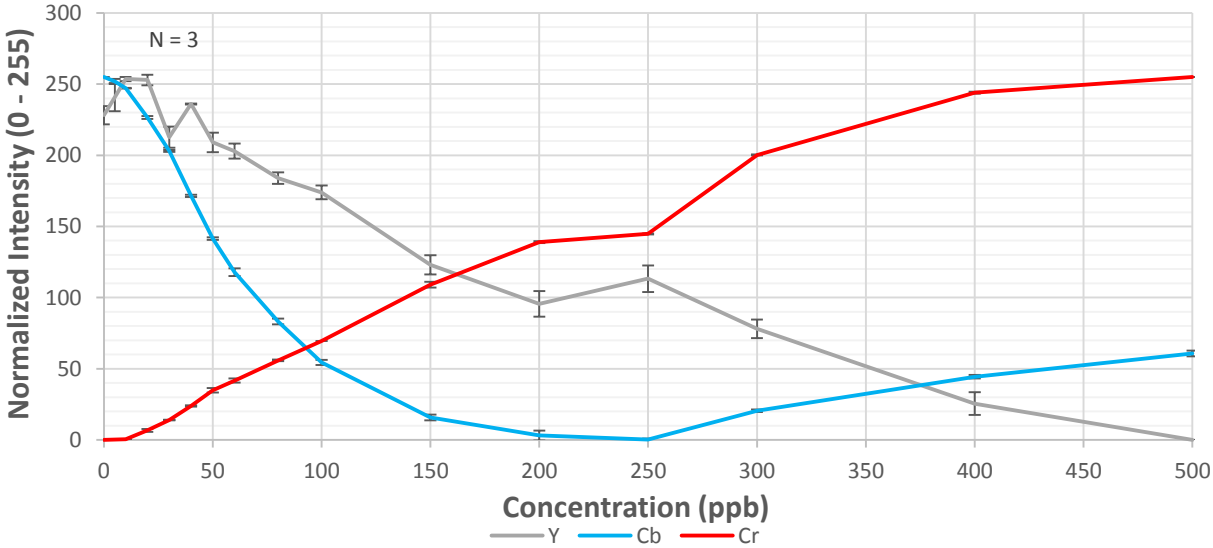


*Figure 47: The calibration curve, using 50% of the original cropped region.*

## 5.6 Chapter Summary

For each of the image predictions plotted against the results of the GF-AAS, it was shown that a linear regression was well suited. As it minimizes the distance between the fitted line and all of the data points, the expectation was that the trends would illustrate a close relation between the two measures. Table 8 has been provided to show all of the linear fitted prefactors and R-squared values. As previously mentioned, Chroma Cb was found to have the best linear fitting, for both the DSLR and the SML results, emphasizing its sensitivity and correlation with the benchmark. The R-squared factor has also been included in Table 8, for each of the image prediction graphs, as it is a static measure of how close the data holds to the fitted line. As shown, for all cases it is above 95%, demonstrating that the model can account for almost all the variability of the response data. As this factor can explain the total variance that occurs, it should be expected that the Chroma Cb has the lowest $R^2$ values, in comparison to the other combinations, as the Chroma Cb channel is built to effectively register the colours generated by the TSIs. Without prior consideration of the Chroma Cr channel in generating the Chroma Cb predictions the variability would increase further. This measure may be improved through placing further restraints to the image processing algorithm and means of image acquisition. As such, when the field test kit is run and results are imaged to form a calibration curve both the room temperature and smartphone specifications should be recorded. This is essential as FTKs are defined to function within a specific temperature range, yet are used in a variety of settings. With various smartphones on the market knowledge of a specific devices performance could be essential in maintaining a quantitative state for the calibration curves.

Table 8: Summary of image prediction, 0 – 500 µg/L

| **Channel Combination** | **Linear Prediction** | | **$R^2$** | |
|---|---|---|---|---|
| | **DSLR** | **SML** | **DSLR** | **SML** |
| Cb | 0.89 | 0.75 | 0.962 | 0.971 |
| Cr | 0.70 | 0.50 | 0.980 | 0.991 |
| CbCr | 0.79 | 0.63 | 0.973 | 0.988 |
| YCbCr | 0.77 | 0.56 | 0.964 | 0.977 |

# Chapter Six

# 6. Conclusions

## 6.1 Overview

Through investigating the use of colourimetric analysis in the characterization of arsenic, its quantification is shown to be possible. Tuning this process will make existing FTKs more flexible, beyond the current limitations in the field. Further development will lead to a clearer understanding of the various colourimetric responses and improve upon the means of analysis. Greater control of the image acquisition will make it possible to prevent variation in the incident illumination while raising the achievable colourimetric accuracy, with the goal of reducing the deviation to within a tolerance of 5 % from the current 15 to 35 %, as stated in the first chapter.

### *6.1.1 Benchmark Technology*

As the results of Chapter 3 show, benchmark technologies provide a highly defined means of quantitative analysis in comparison to most in-field technologies. This is generally achieved through accounting for the various technical issues that could limit performance. Here, GF-AAS was shown to provide adequate results. The apparent deviation would have been detrimental without the resampling that was performed by the technician. While GF-AAS may analyze arsenic, it suffers with a cut-off frequency that is close to arsenic's measurable wavelength. As discussed and illustrated through Figure 12 of Chapter 3, there are a variety of benchmark technologies used to test for arsenic. The system chosen for this analysis depends on numerous factors. This very specific need for the quantification has drastically improved the accuracy of laboratory analyses, as long as proper equipment is available.

Field portable technologies have yet to make drastic adjustments, but many make use of preconditioned samples. As shown through the results, it is possible to closely match the expected outcomes of current transmittance FPTs being used.

In addition, while the benchmark technology adjustments rely upon the need for a well-trained technician, the FPTs seek to be less biased and user-dependant. In comparison to generic laboratory software, such as ImageJ, the use of associated apparati and algorithms for processing the data remove the typical user biases these software provide, thus reducing various deviations including variations in ambient lighting, sample placement and angle of capture.

Precision of benchmark technologies, as FPTs, should be established for a range of AAS concentrations and duplicated though regeneration of calibration curves. As stated in the literature review, a significant number of misclassifications are possible as arsenic concentrations in well water vary with time. Unlike the benchmarks, FTKs allow for consistent testing of a location, providing a higher level of knowledge on the present state, preventing long-term effects of such misclassification with laboratory technology.

### *6.1.2 Field Portable Technology for Quantification*

Developing countries, such as Bangladesh, are in need of FPTs for water testing. While various methods of detection exist it is generally a toss between reflectance and transmittance, the former being chosen, for quantifying the result. While transmittance has been applied for arsenic detection through various technologies, like the Arsenator® and GF-AAS, analysis requires specific conditions. For transmittance FPT, a measure of the lost energy is accounted for, detecting the change in light that passes through a medium. TSIs used in FTKs generally place the indicator on a plastic strip for handling. This backing would need to be removed to allow the light transmittance through the indicator. While removal of this plastic strip is not drastic, it does pose an issue to how samples are to be handled. Without this barrier, light can pass through samples moderately but may suffer at higher concentrations. For a dark colour-complex or a thicker indicator filter, depending on the chemicals used, light is more readily absorbed, causing issues with quantification. An additional concern to take into account here is the effects absorbed light may have on the samples, as molecules begin to interact with each other effecting chemical composition. If the light source fails to give off wavelengths evenly, it will experience similar issues of reflectance. An additional consideration here is the challenge to keep the FPT reliable but with minimal expense, which smartphones allow for. While transmittance has been claimed to

be the more effective means of quantification, it is still more common to rely upon visual analysis. Finally, while SML imaging can be adapted for a variety of additional sample analyses, including geographic trends, it has been impractical for standalone transmittance technologies.

### *6.1.3 Image Analysis*

With control over sample acquisition, the generated calibrations have been split into the luminance and chrominance channels of the chosen YCbCr colour model. Generating images, one for each concentration, and determining the deviations between them, helps to define a consistent process. Through analyzing the separate channels, it was shown that the luminance channel may be used as a means to confirm that images fall within expected lighting conditions before any further effort is placed on analyzing the acquired image. This removes error in the performed image capture, which would leave the result in a more semi-quantitative state.

Results suggest that one channel of the YCbCr colour model alone will not be sufficient in predicting a given TSIs concentration. Although the Chroma Cr channel is shown to have a linear result when handling the increasing concentration of the coloured TSIs, it alone is not suited for the range of colour that is produced. Chroma Cb, as stated in Chapter 4, is suited to handling the low concentration yellow colour-complex while Chroma Cr handles the red hues. As this is the case, polynomial fitting of both Chroma channels is necessary. More emphasis is placed upon Chroma Cb, as the analysis of low concentrations is the focus of arsenic FTKs. Further simplification of this two dimensional problem may be obtained through merging the chrominance channels into a one dimensional solution.

## 6.2 Recommendations

For FTKs to provide a means of quantitative measure, the literature and results of this thesis have posed a number of recommendations:

### *6.2.1 Field Portable Technology*

- Additional Marco lenses could be incorporated into the imaging apparatus, such that a greater majority of the pixels can be used to classify the ROI using a smartphone.
- Using the existing platform, sample generation will be worked upon for the creation of PAD inserts to replace existing FTKs.
- Gaseous generation in microfluidic platforms will be performed, as discussed in the Appendix, to use hydrophobic barriers as a means for containing the liquid in channel while releasing the generated gaseous product into a chamber with the µPAD.
- PADs may be split into smaller segments as to provide more surface area, intensifying generated colour and providing a means of comparison. Instead of averaging the TSIs region of interest, the goal will be to show a level of confidence between the dots.
- Detection of arsenic in solution may also be made practical through the use of colourimetric or fluorescent probes, replacing the need for gaseous generation.
- Besides the initial production of a robust model, an investigation of the economic feasibility for developing countries must be performed.
- An investigation on the efficiency of the in-field device must also be made to prove its quantitative nature, over existing semi-quantitative methods.
- Further analysis should be performed to study the effects time has on the coloured TSIs. Producing a trend with the SML could allow for a time adaptive analysis of the TSI samples.

### *6.2.2 Analysis through Software*

- An investigation should also be made on the application of field portable technology with an incorporated microfluidic chip for colourimetric reactions, as they have yet to appear in a variety of settings but hold much possibility.
- The analysis for the image prediction code must be advanced through implementing the upper and lower bounds of a predicted sample.
- The polynomial fitting used, although effective, showed that ranges must be overlapped. As the point of intersection may occur at these cut-offs, there is a chance for error in the prediction.

- Although the “Coffee Ring” effect does provide higher intensities, and error has been shown to be minimalized through taking an average of all the pixels associated with the TSI, it comes at a price. Generated TSI samples experience most of their fragmentation around their boundaries. As such, they not only provide the most intense colour to analyze but a high level of associated noise. Sampling this “Coffee Ring” alone is not recommended; sampling the entire region and determining an average has been shown to function well but sampling and averaging the TSI’s middle section would provide the most consistent, given its reduced noise content.
- The normalization of a sample could be performed using a more developed maximum and minimum intensity, as a couple normalized results fell outside of the appropriate range. This may in part be due to the light deviations, showing the importance of defining the light deviation at the start.
- If the colour model (YCbCr) is to be continually used in analysis,
    - The Luminance channel should be used only to define the light deviation across samples before further definition. After confirming samples fall within predicted light settings it may be ignored. The luminance plays an essential role in the consistency of the quantification of the chrominance. As it accounts for a portion of the acquired image it should be considered; without this the test results are semi-quantitative at best.
    - The Chrominance Cr channel may be used as an initial test to predict where along the calibration a test strip will best fit. It will also serve as a means to define the higher concentrations, as it is better at defining orange/red colour.
    - From here the Chrominance Cb channel would be used to define sample concentration, as the concentrations of interest produce yellow hues.
- Match predicted samples within the calibration curves upper and lower error bars,
    - As the predicted samples channel values are generated by the mean of three synchronously captured images it could be possible to intersect the image with the calibration curve and its upper and lower deviation bounds.

*6.2.3 Correlation to the Benchmark Standard*

- The generated GF-AAS curve should be replaced, once it becomes time to build a database of calibration curves. Sample solutions should also be analyzed with ICP-MS, given its ability to quantify much lower concentrations.
- Generated test strips should be sampled over an extended period of time to further show how the relationship changes. Samples that were stored over 6 months have continued to display a moderate level of colour indicating that the sample colour may stabilize.
- Simple generation of an application to link the smartphones camera to a database will allow the collection of images and specifications (temperature/location, etc.) in the production of long term trends (displaying seasonal changes ...etc.) and calibrations that may be used more effectively.
- Beer's Law should be used on FTK results to generate absorbance values/curve for comparison to benchmark technology.
- Nanoparticles could be produced using the sought out method, as described in the Appendix. Generated particles would be used to create ratio for shrinking volume size and increasing present concentration of Arsenic, allowing easier detection with more intense colour.
- This algorithm and cellphone apparatus should be passed over to other colourimetric analysis for a variety of substances that can currently generate a colour-complex and could be suiting to adapt a database for quantities over qualitative results.
- Although the stock solutions were correlated between the GF-AAS and FPT it was realized that a second method more suitable could be incorporated. The use of Energy Dispersive X-ray Spectroscopy, or EDS, was chosen as a means for analysis of the FPTs impregnated TSIs. This technology provides a means for comparing the various technologies' ability to classify the TSI. While this serves as a better comparison of the technologies, it has yet to be incorporated. EDS would not only help to better quantify the TSIs coloured-complex, but additionally capture three points across the impregnated surface, allowing variations across the surface to be studied as TSIs are prone to form the intense boundary colour, known as the "coffee ring" effect. This could serve great importance towards how the existing colourimetric calibrations are generated from an image.

## 6.3 Author's Contributions

The author's contribution can be summarized as follows:

- Development of a rigorous algorithm, for Chapter 5 of this thesis, used to increase the accuracy of quantifying a test strip indicator while minimizing the involvement of FTK users.
- Developed an imaging apparatus as both an initial model for the in-field portable model and to serve as the testing grounds for comparing and evaluating images captured.
- A platform has been designed for the reflectance detection of arsenic TSIs. An attachment to the phone is composed of three parts:
    1. The insert, allowing both a generated TSI and reference blank TSI to be inserted;
    2. The main body, encasing the light source, light diffuser, macro lens attachment and holder attachment allowing for optimal magnification and imaging;
    3. The connector, this may vary in shape from one phone to the next as it allows for the optimal placement of the main body with the smartphones' camera.
- Three studies were performed on the prediction code; using the existing framework the code was modified, as explained through Chapter 5, to establish an increase in the certainty for the predicted outcome.
- A study was performed on the chromaticity of aging samples.
- A study was performed on the TSI's ROI, to determine the effects caused by the outer ring.
- Further analysis of the use of the enrichment has been provided in 7.5 of the Appendix. Here the literature and research has been prepared to delve into the use of NPs that may effectively reduce a solution volume with low arsenic presence so that its concentration may be increased. This will allow for analysis of much lower sample solutions through current microfluidic means.

# 7. Appendix

## 7.1 Initiatives

### *7.1.1 Long-Term*

The long-term objective of this proposed research will be the commercial development and global acceptance of a comprehensive microfluidic platform for the colourimetric analysis of arsenic. To achieve this goal, platform development will follow practises coined by the term "ASSURRED", in which an end product is Affordable, Sensitive, Specific, User-friendly, Rapid and Robust, Equipment-free and Deliverable [10]. In terms of application, it is projected that the use of other diagnostic tools will significantly decrease or be replaced entirely through a transition period, as the platform will alleviate the need for human interaction, lower reagent consumption and provide a level of control never before witnessed in use of the Gutzeit method.

### *7.1.2 Short-Term*

In the production of this platform, a number of short-term goals will be achieved, answering the questions that remain in the literature. The short-term goals will include:

1. Theoretical development of the platform, in which the selection of material layers and modeling will be performed to decide the most appropriate arrangement.
2. Experimental development, in which the theoretical models will be incorporated to produce physical products that allow for the amendment of theoretical interpretations in incorporating chemical interactions on various layers.
3. Finding ways to amplify the detection limits, in which pre-concentration in both the aqueous and gaseous phases will be tested to determine which is the most effective and simple direction. The combination of the two methods may be used if they both hold significance towards the detection of lower limits.

4. Incorporation of additional equipment, in which the requirements for optical probes, correlation tables and necessary software will be analyzed. This will hold useful towards the development of other microfluidic systems.
5. Testing, in which a final model will be inserted into the field for testing purposes and determination of further application improvement.

## 7.2 Literature Excerpts

### *7.2.1 Figures*

*LAB Colour Model*

The LAB colour mode, illustrated by Figure 48, is based off of a colour-opponent space. This model has been designed to approximately mimic the human visual system. Colour-opponent space works on the idea that it is more efficient to record the difference between opposing channels. Thus the model is designed around three channels, the luminance "L", red vs. green "A", and blue vs. yellow "B". Unlike RGB, this model does not depend upon the devices being used to capture an image, as most rely on RGB [57].

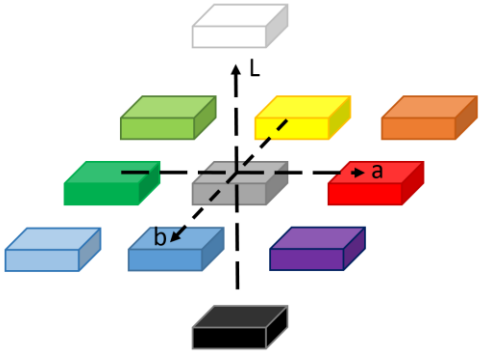


*Figure 48: The LAB model* [58].

*HSV Colour Model*

This model, as illustrated in Figure 49, was produced to improve upon the defined relationship of the RGB colour model. Here the model is defined by hue, saturation and value. The hue (H) is a numerical representation of the colour, which is derived from the three primary colours but without

the presence of white/black to lighten/darken an image. It ranges from 0 to 360 degrees, with each degree referring to a colour. The hue is further segmented for specific computations each 60 degrees. The saturation (S) is based on the intensity of the colour, the degree to which a single channel dominates the light intensity distribution. Finally the value (v) is a measure of the brightness ranging from black to white. Unlike RGB, this model is not absolute and does not necessarily have to be contiguous; the hue introduces visible discontinuities. HSV has additional issues with separating the hue and saturation, as the models channels have overlapped regions [23], [57].

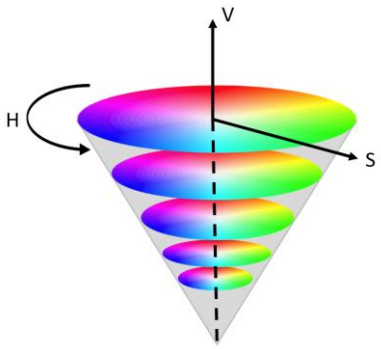


*Figure 49: The HSV colour model* [58].

*CMYK Colour Model*

Finally, the CMYK colour model is based on a subtractive approach. CMYK assumes that the background of an image is white and subtracts an assumed brightness from the background. Force colours channels are subtracted from: cyan "C", magenta "M", yellow "Y", and black "B". Black has been added along with the three colours (CMY) because they do not produce a fully saturated image on their own. This colour model is generally used in printing technologies [57].

*Comparable Means of Quantification*

As shown in Figure 50(a), arsenic has been compared for analysis by both Hydride Generation-Atomic Absorption Spectroscopy and Inductively Coupled Plasma-Mass Spectrometry. Looking at each of the points in the graph, it is apparent that there is significant disagreement between the plotted concentrations of arsenic. While a trend line has been plotted, the present variation is

concerning. In Figure 50(b) the field portable technology for arsenic detection, the Arsenator®, has been plotted against the two showing an adequate level of correlation.

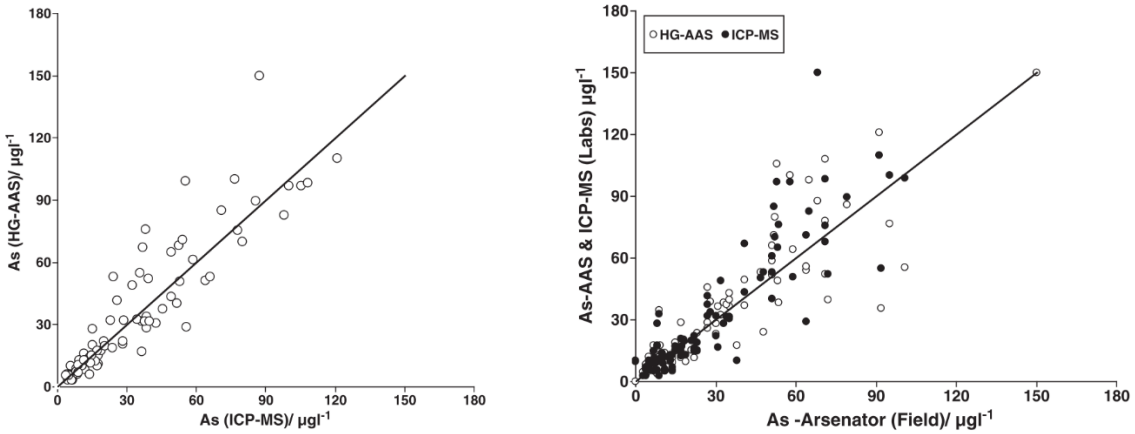


*Figure 50: (a) Comparison of the HG-AAS with ICP-MS for the determination of arsenic concentrations. (b) Comparison of the Arsenator® with AAS and ICP-MS, adapted from* [11].

## 7.3 Methodology

### *7.3.1 Figures*

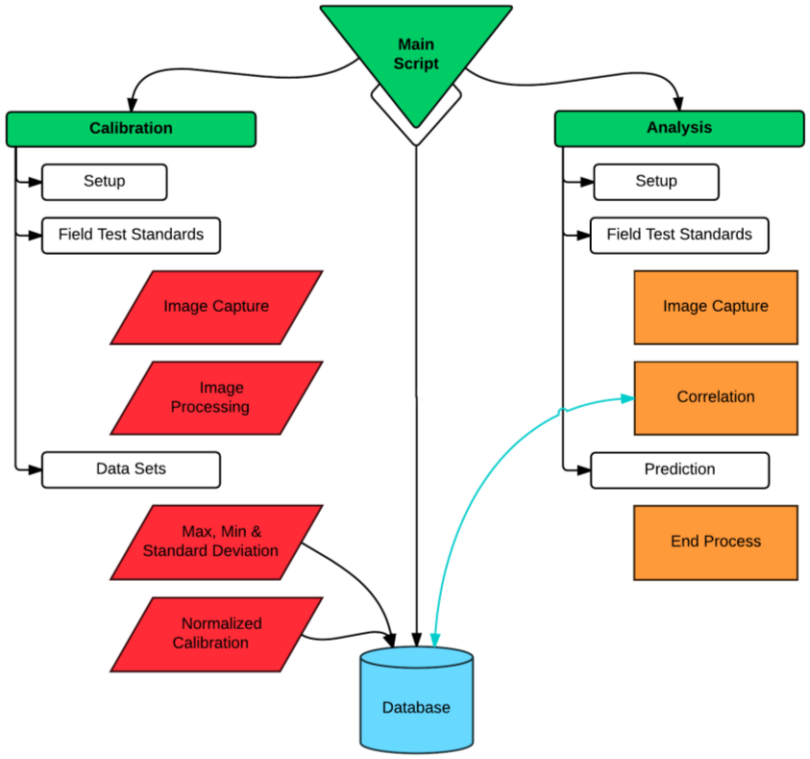


*Figure 51: Outline for the FTK Calibration/Prediction*

*7.3.2 Tables*

The following tables have been provided to state the developed protocols and desired settings in the production of the experimental results.

Table 9: Stock Solution Protocol

| Step # | Description |
|---|---|
| 1. | Measure 250 mL ± 5 % deionized water with a graduated beaker |
| 2. | Transfer to Kimble Glass Jar |
| 3. | Calculate amount of stock solution needed to create the desired sample |
| 4. | Use Eppendorf Pipette with tip attachment to measure out solution |
| | a. Set pipette dial for required volume |
| | b. Submerged tip into solution |
| | c. Slowly release pressure on pump to ensure accurate measured collection |
| | d. Place pipette in container and release contents into solution |
| 5. | Replace cap and swirl solution |

Table 10: Protocol for the GF-AAS system

| Step # | Description |
|---|---|
| 1. | Turn on air compressor |
| 2. | Turn on acetylene tank |
| | o Must stay above 80 psi |
| 3. | Open "winlab32" software |
| 4. | First build a method "new method" |
| 5. | Select pre-programmed arsenic testing procedure |
| 6. | Set wavelength range |
| | o Monochrome lamp at 193.7 nm sends an optical beam to measure the absorption |
| 7. | Set "calib blank" to be 0 in the first column of table |
| 8. | Save method |
| 9. | Turn on flame |
| 10. | Perform a "Blank test" |
| 11. | Perform "Standards test" |
| | o 1,3,5,10 ppm (mg/L) calibrations |
| 12. | Sample gets sucked into the flame |
| 13. | Produces clear absorbance lines & atomic admission (Looks at one element at a time) |
| | o Results should be linear |
| | o Perform with actual sample |
| | o Results are displayed on the computer screen and on a printer printout |

Table 11: FTK protocol

| Step # | Description | Step # | Description |
|---|---|---|---|
| 1. | Add 100mL of sample solution to reaction bottle | 4. | Reagent 3 + White Spoon (Zinc)<br>o Add 3 scoops to bottle<br>o Shake for 15 seconds |
| 2. | Reagent 1 + Pink spoon (tartaric acid)<br>o Add 3 scoops and cap the bottle<br>o Shake for 15 seconds<br>o Let sit for 15 seconds | 5. | Testing:<br>o Change cap for insert<br>o Place mercuric bromide test strip<br>o Let sit for 30 minutes<br>▪ Hydrogen + Arsine gas will collect<br>▪ Arsine reacts with mercuric bromide<br>▪ Formation of mixed mercury halogens<br>o Remove test strip (Hydrogen gas may explode)<br>o Compare to colour chart |
| 3. | Reagent 2 and Red spoon (ferrous salts - reaction catalyst)<br>o Add 3 scoops to bottle<br>o Shake for 15 seconds<br>o Let sit for 2 minutes | | |

Table 12: Nitric Acid - J.T. Baker 9601-1, 69-70% 500mL

| Sample | Concentration (ppb) | Sample Volume Size (mL) | Amount (mL) |
|---|---|---|---|
| Start | 70% | 500 | |
| Dilution | 2% | 1000 | 28.57142857 |

Table 13: Arsenic Solution in Nitric Acid - Fluka Analytic 39436 - 250mL

| Sample | Concentration (ppb) | Sample Volume Size (mL) | Amount (mL) |
|---|---|---|---|
| Start | 1000000 | - | - |
| 1 | 10000 | 100 | *1 |
| 2 | 1000 | 200 | **20 |
| 3 | 500 | 200 | 10 |
| 4 | 400 | 200 | 8 |
| 5 | 300 | 200 | 6 |
| 5 | 250 | 200 | 5 |
| 6 | 200 | 200 | 4 |
| 7 | 150 | 200 | 3 |
| 8 | 100 | 200 | 20 |
| 9 | 80 | 200 | 16 |
| 10 | 60 | 200 | 12 |
| 11 | 50 | 200 | 10 |
| 12 | 40 | 200 | 8 |
| 13 | 30 | 200 | 6 |
| 14 | 20 | 200 | 4 |
| 15 | 10 | 200 | 2 |
| 16 | 5 | 200 | 1 |

*Solution is 998 mg/L +/- Std ~ 1000ppm (* Use for > 100ppb, ** Use for < 100 ppb)*

Table 14: Comparison of the present methods for arsenic detection, adapted from [79].

| Method | Reagent | MDL | Reaction Time |
|---|---|---|---|
| Merck Kit | Zinc, Hydrochloric Acid, Mercury Salt Chloride/Bromide | 0.01 mg/L | 10-30 min |
| Hach | Zinc, Sulfamic Acid, Mercury Salt | 0.01 mg/L | 10-30 min |

Table 15: DSLR Camera Settings

| Parameters | Description |
|---|---|
| Mode | Manual |
| Shutter Speed (Exposure Time) | 1/160 Sec |
| Aperture | f/8 |
| Exposure Comp. | 1 EV |
| Flash Comp. | 0 EV |
| Flexible Program | 0 Step(s) |
| Metering Mode | Matrix |
| ISO (Sensitivity) | 640 |
| White Balance | Fluorescent - White Fluorescent |
| Image Quality | NEF (RAW) + JPEG fine |
| Image Size | Large (4288*2848) |
| Release Mode | Continuous Low Speed - 4 Shots |
| Lens | VR 85mm f/3.5G |
| Picture Control | Standard |
| Colour space | sRGB |
| Active D-Lighting | Auto |
| High ISO NR | On (Normal) |

### *7.3.3 Equations*

*Generating Standard Solutions*

The following equations have been provided as they were used to generate the desired standard arsenic solutions used in the results.

Dilutions:

$$M_{initial}V_{initial} = M_{final}V_{final} \quad \text{Eq. 8}$$

Molarity:

$$M = \frac{\#\ \text{moles solute}}{\text{L of solution}} \quad \text{Eq. 9}$$

$$\#\ \text{moles solute} = (\text{solute g})\left(\frac{1\text{mol}}{\text{periodic table g}}\right) \quad \text{Eq. 10}$$

Percent Composition:

$$\frac{\text{mass of solute}}{\text{mass of solvent}} \text{x } 100\% \quad \text{Eq. 11}$$

The following Equations have been used in the coded algorithm to allow for an ideal classification of the TSIs.

*RGB Colour Model*

Digital images were produced initially within the RGB colour model. To analyze these within a variety of other colour models, they must first be normalized. The normalization of the RGB Model relies upon the characteristics of the original colour space [59].

$$r = \begin{cases} \left(\frac{R}{12.92}\right), & R \leq 0.04045 \\ \left(\frac{R + 0.055}{1.055}\right) * 2.4\,, & R > 0.04045 \end{cases} \quad \text{Eq. 12}$$

$$g = \begin{cases} \left(\frac{G}{12.92}\right), & G \leq 0.04045 \\ \left(\frac{G + 0.055}{1.055}\right) * 2.4\,, & G > 0.04045 \end{cases} \quad \text{Eq. 13}$$

$$b = \begin{cases} \left(\frac{B}{12.92}\right), & B \leq 0.04045 \\ \left(\frac{B + 0.055}{1.055}\right) * 2.4\,, & B > 0.04045 \end{cases} \quad \text{Eq. 14}$$

Where R, G and B are the values of the RGB model, and r, g, and b are the normalized values.

*Segmentation and Object Recognition*

Images were initially segmented using a binary mask to determine the location of the present regions of interest.

$$I(n) = \begin{cases} 0, & \min + D \leq I(t-1) \\ 1, & \min + D(n-1) > I(t-1) \end{cases} \quad \text{Eq. 15}$$

Where I is the binary image produced from threshold, D is the dynamic threshold.

To detect and retain the location of only the largest objects, white regions, in the binary image mask:

$$C_y = \sum_{r=1}^{N} P_{con}(m, n) \quad \text{Eq. 16}$$

Where m and n refers to the rows and columns, N is the total number of rows in the mask and $P_{con}$ refers to the approximate diameter of the object.

*Colour Space Transformations*

The colour model YCbCr is derived from the sRGB colour space, where the channels are defined by the variables [Y,Cb,Cr] and [R,G,B], as shown below:

$$Y' = k_r R' + (1 - k_r - k_b)G' + k_b * B \quad \text{Eq. 17}$$

$$C_b = \frac{\left(B' - Y'\right)}{2(1 - k_b)} \quad \text{Eq. 18}$$

$$C_r = \frac{\left(R' - Y'\right)}{2(1 - k_r)} \quad \text{Eq. 19}$$

Where $k_b$ and $k_r$ are defined by the RGB colour space, the symbol ($'$) is used to indicate gamma corrected and normalized (between 0 and 1) values are being used.

This conversion from RGB to YCbCr has been simplified as follows,

$$\begin{aligned} Y &= 0.299R + 0.587G + 0.114B \\ Cb &= 128 - 0.168736R - 0.331264G + 0.5B \\ Cr &= 128 + 0.5R - 0.418688G - 0.081312B \end{aligned} \quad \text{Eq. 20}$$

*Segmentation and Object Recognition*

With the image converted to analyze in YCbCr, the features of interest can now be extracted. To do this, a crude binary image can be produced to find dominant regions in the image. These regions would serve as reference points for the analysis. This binary image is generated by setting an

intensity threshold: intensities above the threshold are made white while those below are made black.

From here the defined regions may be further classified from the binary image by looking at how the pixels are connected to each other. This allows the user to determine which groups of pixels are connected by intensity, thus allowing the location for each object. Once the dimension of an object has been determined through tracing its group of pixels, the dimensions and crop it from the original image can be declared. This allows for the collection of images of the reference areas and an image for the located region of interest (ROI), the test strips read out.

*Initial Reference Confirmation, Image Texture & Analysis*

Colourimetric analysis may be used to confirm repeatability and relation to previously calibrated tests, which is especially useful towards making accurate judgments for the research being performed here. To do this the standard deviation, signal-to-noise ratio (SNR), and peak signal-to-noise ratio (PSNR) are determined across the image.

The mean intensity of the pixels in an image can be calculated as,

$$\mathrm{m} = \sum_{\mathrm{i}=0}^{\mathrm{L}-1} \mathrm{z_i p}(\mathrm{z_i}) \qquad \text{Eq. 21}$$

Where $z_i$ is the location of a single pixel p in the Cartesian plan of an image.

The mean calculation can also be stated as follows,

$$\mathrm{mean} = \frac{1}{\mathrm{MN}} \sum_{\mathrm{i}=1}^{\mathrm{M}} \sum_{\mathrm{j}=1}^{\mathrm{N}} (\mathrm{I}(\mathrm{i},\mathrm{j})) \qquad \text{Eq. 22}$$

Where I is the value of the element i, j in the matrix, and M and N refer to the number of rows and columns.

The standard deviation provides detail on the image contrast,

$$\sigma = \sqrt{\mu_2(z)} \qquad \text{Eq. 23}$$

Where $\mu_2$ is the second moment (variance of the pixels).

To obtain an images' relative intensity across the image,

$$R = 1 - \frac{1}{1 + \sigma^2} \quad \text{Eq. 24}$$

The skewness of the image histogram is provided by the third moment,

$$\mu_3 = \sum_{i=0}^{L-1} (z_i - m)^3 p(z_i) \quad \text{Eq. 25}$$

The uniformity across the image is obtained,

$$\mathrm{U} = \sum_{\mathrm{i}=0}^{\mathrm{L}-1} \mathrm{p}^2(\mathrm{z_i}) \quad \text{Eq. 26}$$

To measure the randomness across the image,

$$\mathrm{e} = -\sum_{\mathrm{i}=0}^{\mathrm{L}-1} \mathrm{p}(\mathrm{z_i}) \log_2 \mathrm{p}(\mathrm{z_i}) \quad \text{Eq. 27}$$

To estimate the variance and its' corresponding bias the mean squared error is found,

$$MSE = mean[Gi,j - Ti,j2] \quad \text{Eq. 28}$$

Where G is the reference image, and T is the test image.

Using the calculated mean squared error (2.23) and the mean equation (2.17) above to calculate a value for the signal power of the compressed image, the signal-to-noise ratio can be obtained using the following equation.

$$\mathrm{SNR} = 10 \log_{10} \left( \frac{\text{Signal Power}}{\mathrm{MSE}} \right) \quad \text{Eq. 29}$$

The peak signal-to-noise is calculated with the division of the maximum power of the signal; in the case of an image, this would be the maximum pixel intensity of 255, and the mean squared error, calculated along the x and y axes that define the pixels of an image [77].

$$\mathrm{MSE} = \frac{1}{\mathrm{MN}}\sum_{\mathrm{i}=1}^{\mathrm{M}}\sum_{\mathrm{j}=1}^{\mathrm{N}}\big(\mathrm{G}(\mathrm{i},\mathrm{j}) - \mathrm{F}(\mathrm{i},\mathrm{j})\big)^2 \qquad \text{Eq. 30}$$

Where: G is the original image, F is the final image.

$$\mathrm{PSNR} = 10\log_{10}\left(\frac{255^2}{\mathrm{MSE}}\right) \qquad \text{Eq. 31}$$

The variance of the image may be calculated along the rows and columns [78],

$$\mathrm{Variance} = \frac{1}{\mathrm{N}-1}\sum_{\mathrm{i}=1}^{\mathrm{N}}(\mathrm{G}(\mathrm{i}) - \mathrm{mean}(\mathrm{i})^2) \qquad \text{Eq. 32}$$

Where G is the image needed to obtain the variance along a given axis (i).

Finally, to find the covariance of the image the multiplication of the variances values along the rows and columns is performed a summation of the average [78].

$$\mathrm{Covariance} = \frac{1}{\mathrm{N}}\Big(\sum\big((\mathrm{G}(\mathrm{i}) - \mathrm{mean}(\mathrm{i})^2)\big)\big((\mathrm{G}(\mathrm{j}) - \mathrm{mean}(\mathrm{j})^2)\big)\Big) \qquad \text{Eq. 33}$$

## 7.4 Results

### *7.4.1 Figures*

*Matrix Interference*

Here the purpose of analyzing iron was to confirm what affect it had on the presence of arsenic in solution, an initial goal of collecting arsenic out of solution, as to concentrate it. Known as enrichment, the incorporation of varying concentrations of iron into a set arsenic concentration was shown to slowly absorb the present arsenic, preventing it from being released as arsine gas for

detection. This process is illustrated by Figure 52. Initial validation for the use of these nanoparticles in arsenic extraction was shown while proving a need for coatings to serve as a means of enrichment. Refer to 7.5 of the Appendix for further detail on nanoparticles and enrichment.

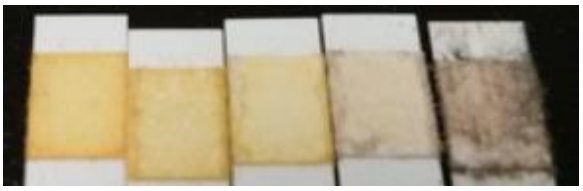

(a) (b) (c) (d) (e)

*Figure 52: Matrix interference for 100 μg/L arsenic solution. (a) Without interference it fits 100-150 μg/L range. (b) Addition of 0.05g of iron oxide is still in range, (c) 0.15g appears to fit the 80 μg/L range. (d) 0.3g appears to fit between 30-80 μg/L. (e)1g of iron oxide cannot be registered.*

*Theoretical Images*

The following images were generated to serve as an initial test for the generated algorithms before attempting to classify actual produced samples.


*Figure 53: Initial images of the theoretical colour chart, placed within the imaging box to capture for each of the provided calibration concentrations, shown beneath each image as CC_#, in µg/L (ppb).*

*Calibration Imaging Results*

Using the generated algorithms actual image sets were processed. Here intermediate graphs are provided, leading to the DSLR calibration curve with provided confidence intervals in Chapter 5.

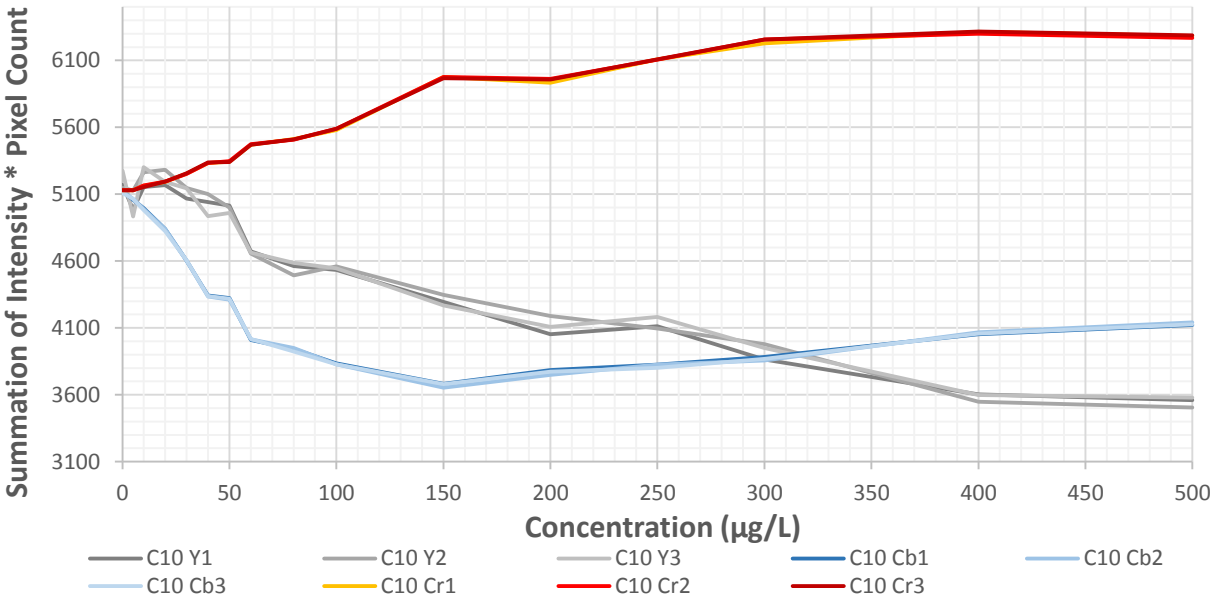


*Figure 54: Dataset from the 10th DSLR calibration made, results taken in combination with GF-AAS.*

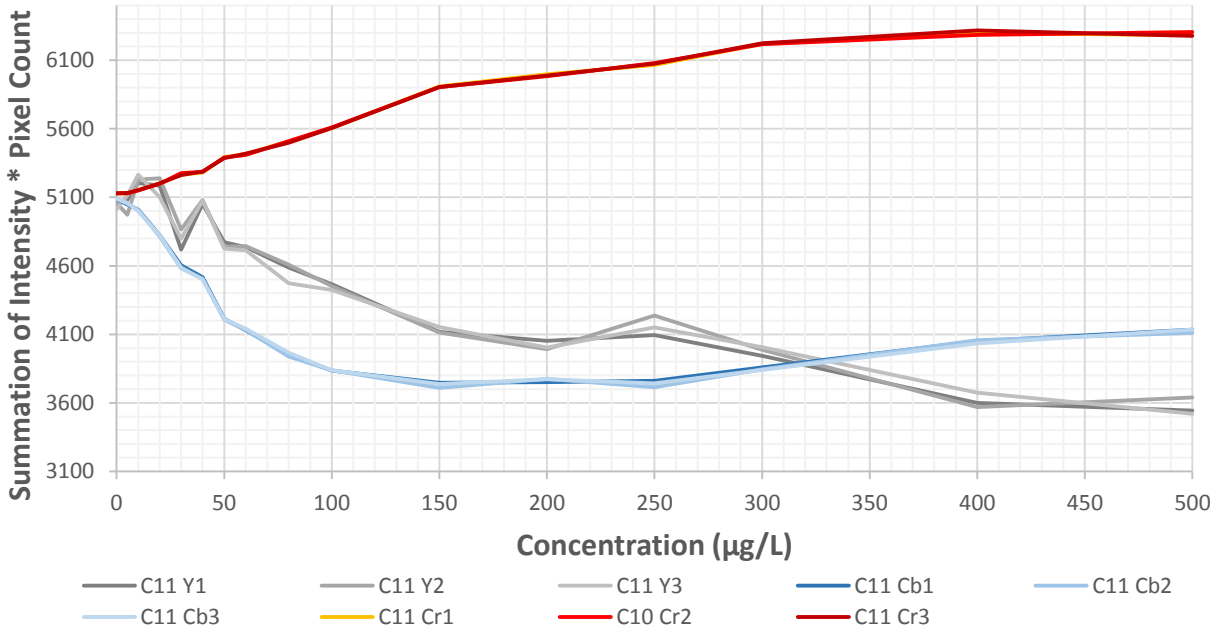


*Figure 55: Dataset from the 11th DSLR calibration made, results taken in combination with GF-AAS.*

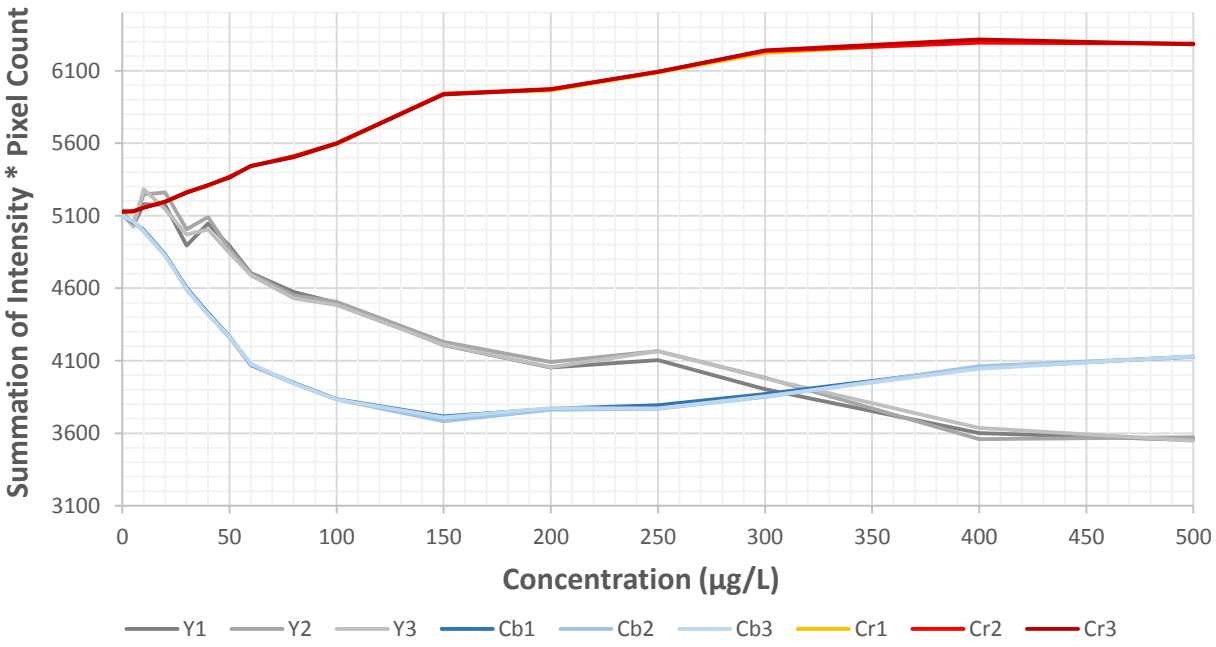


*Figure 56: Combing the two DSLR datasets 10th and 11th, results show good overlap.*

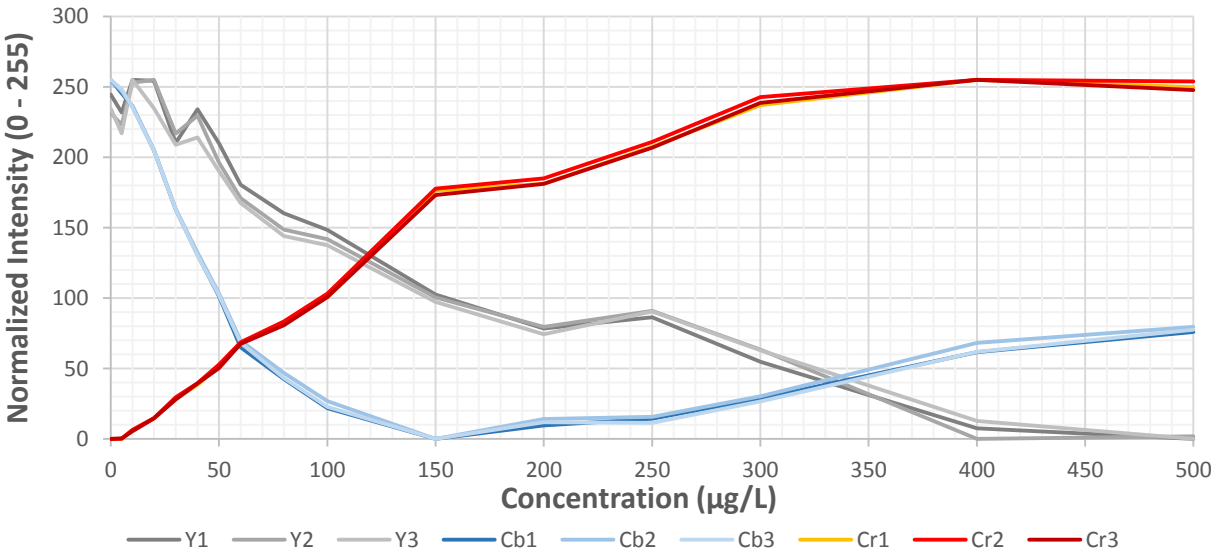


*Figure 57: The combined DSLR datasets are normalized within the general range colour variations (0 - 255).*

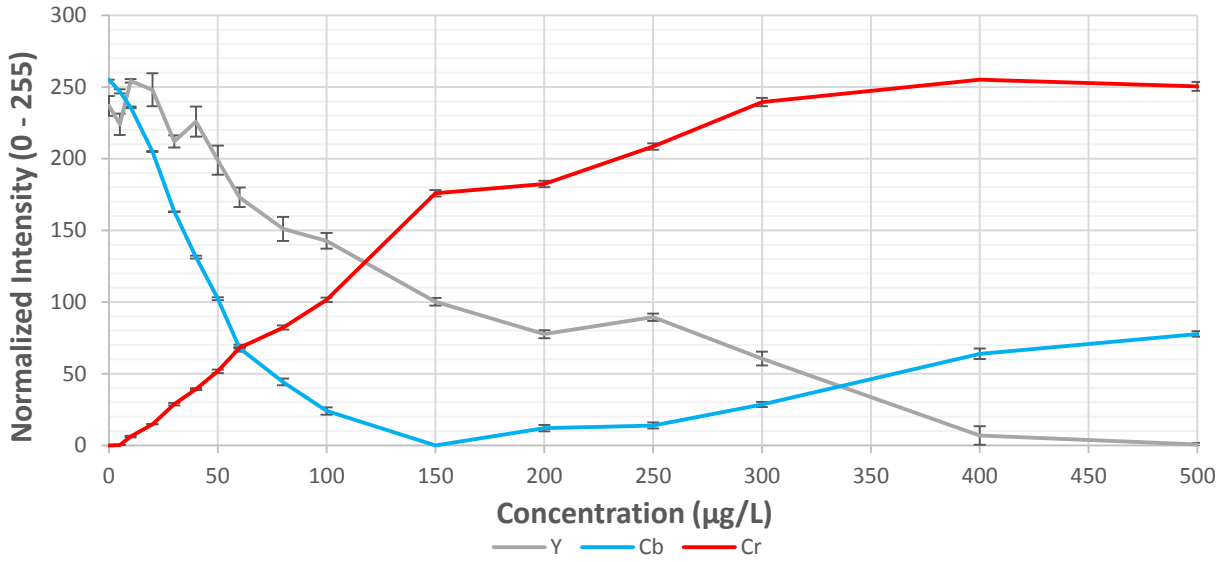


*Figure 58: The DSLR datasets are now reduced to the average values, with the expected deviations for each concentration.*

The following two graphs, Figure 59 and Figure 60, are provided for the 100 and 500 µg/L results of Chapter 5's section 5.2.

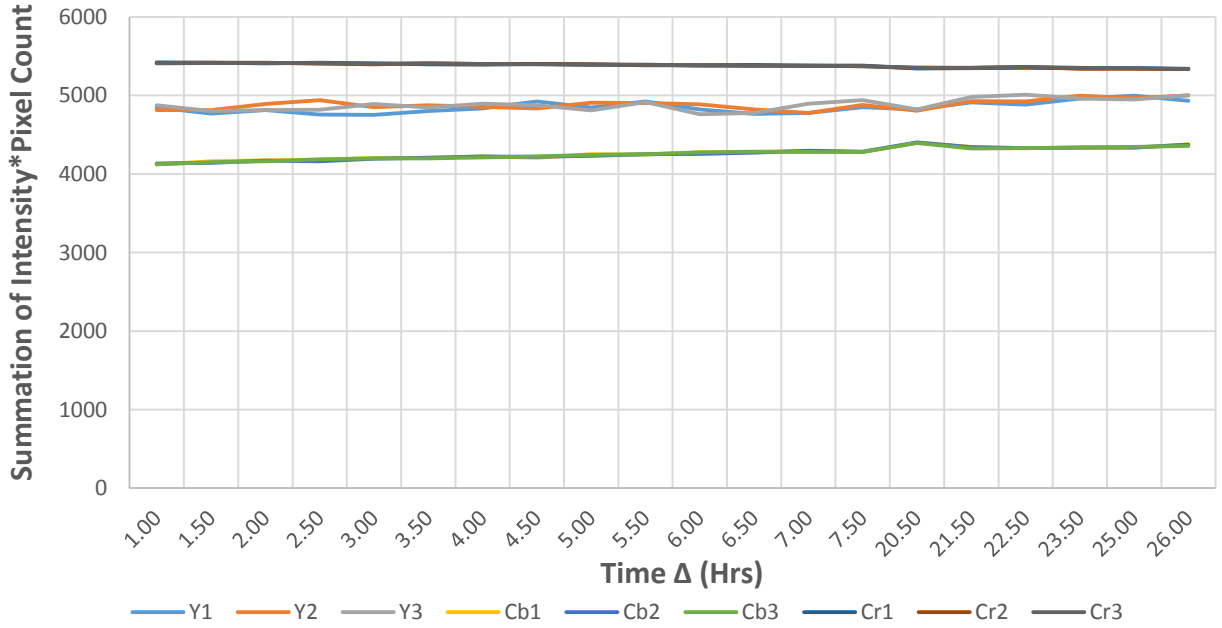


*Figure 59: Variation in the image intensity over a period of time, for a 100 µg/L sample.*

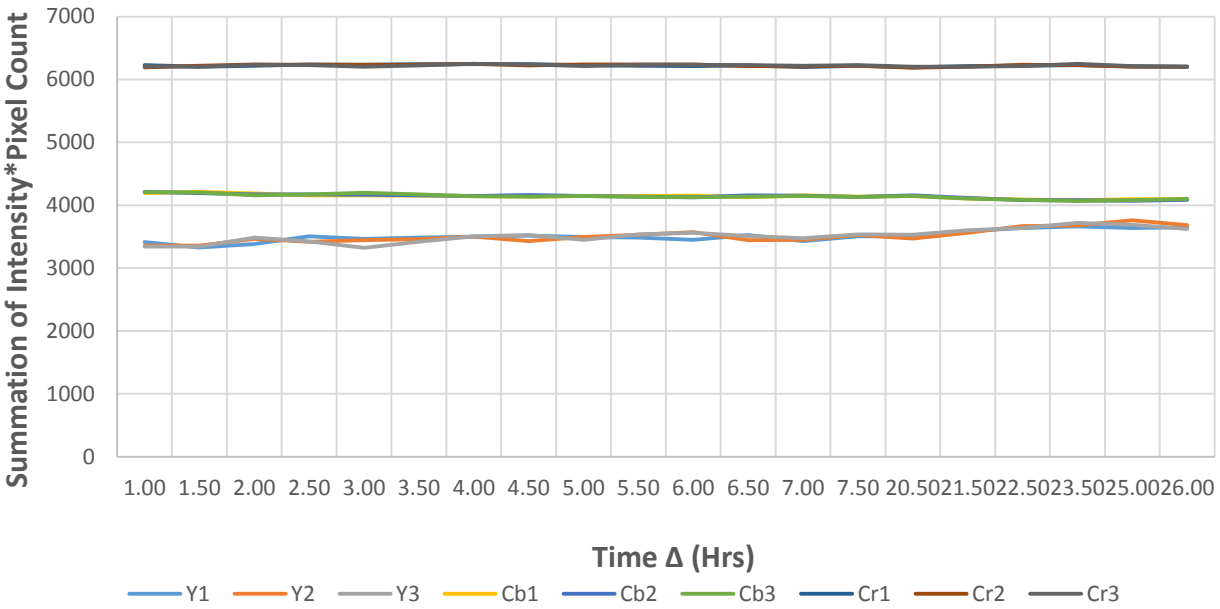


*Figure 60: Variation in the image intensity over a period of time, for a 500 µg/L sample.*

Using the generated algorithms actual image sets were processed for the SML. Here intermediate graphs are again provided, leading to the SML calibration curve with provided confidence intervals in Chapter 5.

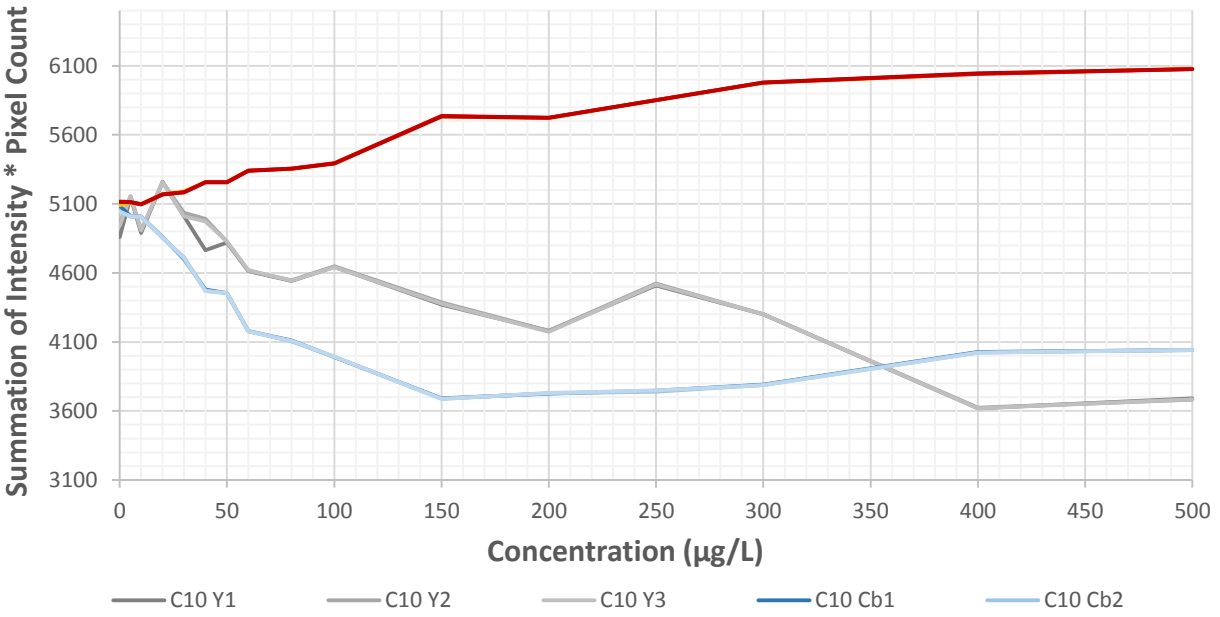


*Figure 61: Dataset from the 10th SML calibration made, results taken in combination with GF-AAS.*

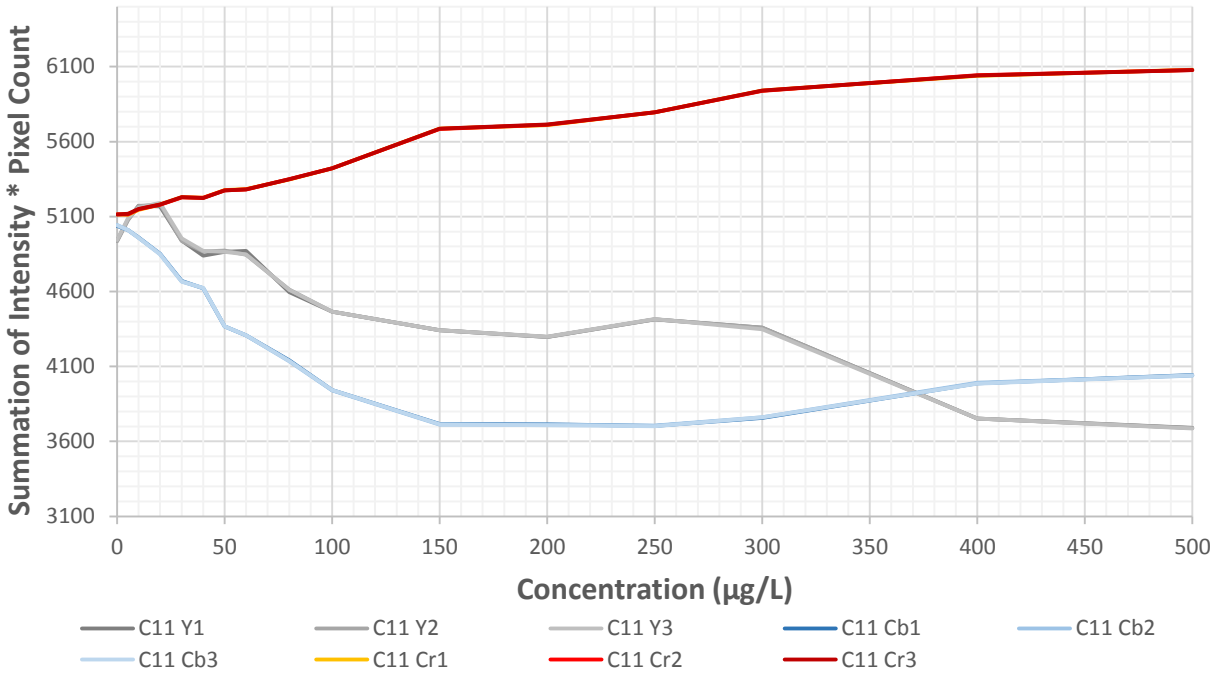


*Figure 62: Dataset from the 11th SML calibration made, results taken in combination with GF-AAS.*

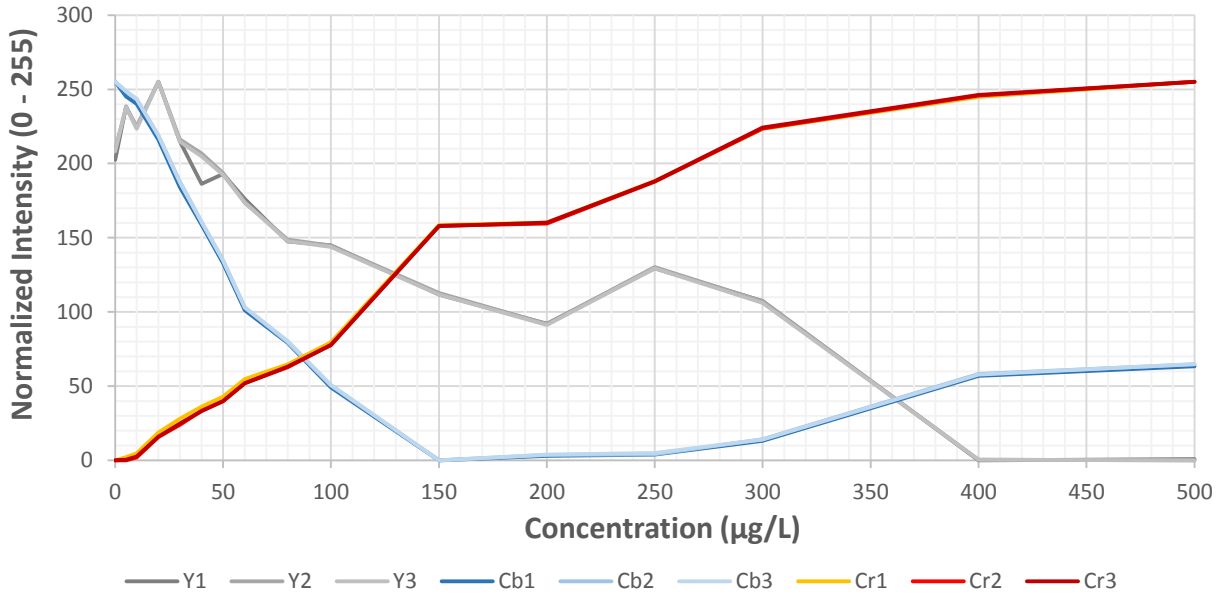


*Figure 63: The combined SML datasets are normalized within the general range colour variations (0 - 255).*

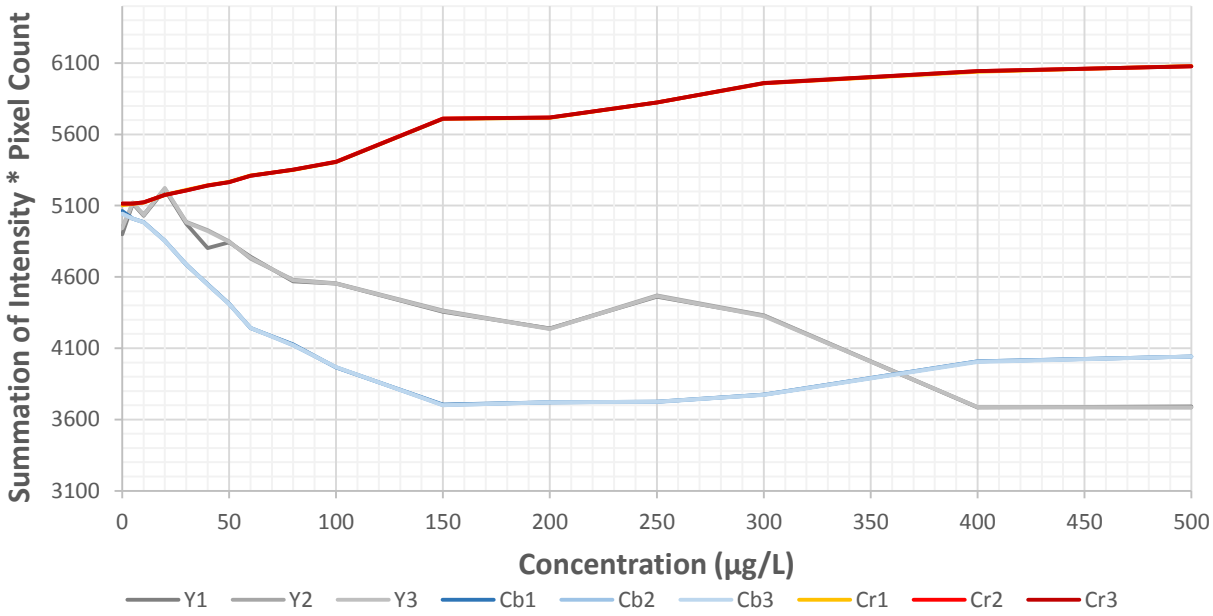


*Figure 64: Combing the two SML datasets 10 and 11, results show good overlap.*

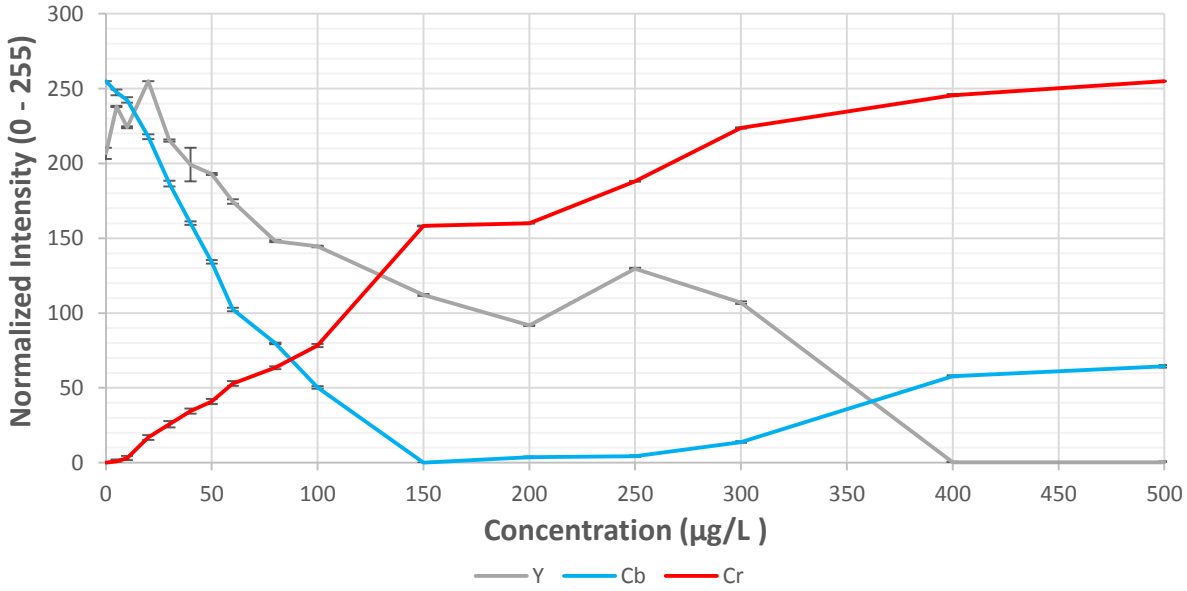


*Figure 65: The SML datasets are now reduced to the average values, with the expected deviations for each concentration.*

*7.4.2 Tables*

Table 16: Calibration set # 10

| Sample # | Sample Concentration | Reaction Completion | Day 1: Drying Time |
|---|---|---|---|
| 1 | 0 | 1:52 PM | 2:52 PM |
| 2 | 5 | 1:56 PM | 2:56 PM |
| 3 | 10 | 3:00 PM | 4:00 PM |
| 4 | 20 | 3:01 PM | 4:01 PM |
| 5 | 30 | 4:00 PM | 5:00 PM |
| 6 | 40 | 4:05 AM | 5:05 AM |
| 7 | 50 | 5:15 AM | 6:15 AM |
| 8 | 60 | 5:18 AM | 6:18 AM |
| 9 | 80 | 6:25 AM | 7:25 AM |
| 11 | 100 | 6:26 AM | 7:26 AM |
| 12 | 150 | 7:37 AM | 8:37 AM |
| 13 | 200 | 7:41 AM | 8:41 AM |
| 14 | 250 | 8:45 PM | 9:45 PM |
| 15 | 300 | 8:50 PM | 9:50 PM |
| 16 | 400 | 9:55 PM | 10:55 PM |
| 17 | 500 | 9:58 PM | 10:58 PM |

Table 17: Calibration set # 11

| Sample # | Sample Concentration | Reaction Completion | Day 1: Drying Time |
|---|---|---|---|
| 1 | 0 | 1:50 PM | 2:50 PM |
| 2 | 5 | 1:54 PM | 2:54 PM |
| 3 | 10 | 2:58 PM | 3:58 PM |
| 4 | 20 | 3:02 PM | 4:02 PM |
| 5 | 30 | 3:02 PM | 4:02 PM |
| 6 | 40 | 4:01 AM | 5:01 AM |
| 7 | 50 | 4:06 AM | 5:06 AM |
| 8 | 60 | 5:16 AM | 6:16 AM |
| 9 | 80 | 5:20 AM | 6:20 AM |
| 11 | 100 | 6:26 AM | 7:26 AM |
| 12 | 150 | 6:31 AM | 7:31 AM |
| 13 | 200 | 7:38 AM | 8:38 AM |
| 14 | 250 | 7:42 PM | 8:42 PM |
| 15 | 300 | 8:46 PM | 9:46 PM |
| 16 | 400 | 9:55 PM | 10:55 PM |
| 17 | 500 | 9:58 PM | 10:58 PM |

Table 18: Calculated values for the standard arsenic solutions

| Solution Concentration (µg/L) | Absorbance Intensity | Standard Deviation | Relative Std. Dev. (%) | GF-AAS Concentration (µg/L) |
|---|---|---|---|---|
| 0 | 0.005456944 | 0.004492505 | 82.3263779 | 0.369397461 |
| 5 | 0.026307222 | 0.00284946 | 10.8314734 | 6.39088297 |
| 10 | 0.041531943 | 0.000187974 | 0.452601671 | 10.7877283 |
| 20 | 0.082905836 | 0.000327636 | 0.39519015 | 22.7363605 |
| 30 | 0.12335445 | 0.000659549 | 0.534677744 | 34.417778 |
| 50 | 0.162460834 | 0.000639402 | 0.393573195 | 45.7115593 |
| 60 | 0.198687226 | 0.000352434 | 0.177381262 | 56.1736145 |
| 70 | 0.255891114 | 0.00205427 | 0.802790761 | 72.6938934 |
| 80 | 0.301346391 | 0.001374162 | 0.456007302 | 85.8212128 |
| 100 | 0.365660548 | 0.001134447 | 0.310245812 | 104.394913 |
| 150 | 0.83985001 | 0.002563073 | 3.05182219 | 230.480194 |
| 200 | 0.84184445 | 0.000738665 | 0.877436996 | 231.056194 |
| 250 | 0.95621944 | 0.080338158 | 84.016449 | 264.087276 |
| 300 | 1.36565283 | 0.001287159 | 0.942522645 | 382.33017 |
| 400 | 1.62761673 | 0.001232003 | 0.756936908 | 457.984428 |
| 500 | 1.85936943 | 0.002267192 | 1.21933401 | 524.913788 |

Table 19: Imaging protocol

| Step # | Description |
|---|---|
| 1. | Place camera into associated slot and check placement with alignment lines |
| 2. | Load the saved camera settings |
| 3. | Place test strip on insert at specified location |
| 4. | Insert into image box slot |
| 5. | Calibrate the camera |
| 6. | Produce three images for each test strip |

*7.4.3 Equations*

The following calculation of the magnification ratio has been used to determine the marco lens conforms to an optimal position within the imaging apparatus.

$$1/f = 1/do + 1/di \qquad \text{Eq. 34}$$

Where di is the distance from the lens to the image, do is the distance from the lens to the object, f is the focal length and M is the magnification.

$$di = 1/(1/23 - 1/18.669) = - 99.143$$
$$M = - di/do = -(-99.143/18.669) = 5.3105$$

$$1/f = 1/do + 1/di$$
$$di = 1/(1/10 - 1/18.669) = - 21.535$$
$$M = - di/do = -(-21.535/18.669) = 1.15$$
$$1.15X < M < 5.3X$$

## 7.5 Additional/Incomplete Initiatives

### *7.5.1 Enrichment*

The full recovery of arsenic from a solution is of interest towards the accuracy of a colourimetric detection process, especially when dealing with lower concentrations. Through increasing the present concentration of a trace element, it is possible to detect the concentration more easily. Making note of this, a reliance may be placed on the use of pre-concentrated solutions that relate back to the actual concentration using developed ratios. This process of concentrating a given solute in solution may be referred to as enrichment or extraction.

Usually this extraction process is used solely to remove contaminates from solution and any detection requirements place a reliance on laboratory technologies. In reference to the works of Trung Do Q. et al., the use of chelating resins, loaded with iron, were found to recover 90-95% of the arsenite while a moderate adsorption of arsenate was also possible [10]. Thus the recovered traces of arsenic in a larger solution sample could be made detectable through the simple process of adsorption. Currently there are a number of different ways to enrich a solution but the focus here has been placed on solid phase extraction, others are listed in Figure 66 below.

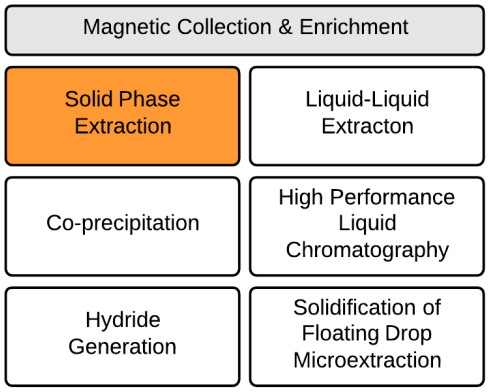


*Figure 66: Different methods to pre-concentrate a solution, the highlighted was chosen.*

Looking at the use of iron oxides for the collection of arsenic, it has been determined through studies that a molar ratio of Iron to Arsenic (Fe/As) of around seven is efficient in the adsorption of 50 to 200 ppb solutions. A much stronger influence can also be seen on the various species of arsenic when this ratio is larger than a value of ten [20], [80]–[82]. Although the collection of trace elements can be performed effectively with iron, it has yet been seen in application with simple colourimetric methods of detection. The current field of research has focused more on the removal of arsenic, thus effects of chemisorption have been ignorable. Chemisorption prevents desorption of arsenic from the iron oxides' surface, thus bound arsenic cannot be detected by colourimetric means. Before solid phase extraction may be used alongside colourimetry, the development of suitable particles must be discussed.

### *7.5.2 Super-paramagnetic Iron Oxide Nanoparticles for Solid Phase Extraction*

Super-paramagnetic nanoparticles are generally ferromagnetic, capable of magnetism when placed under the influence of an external magnetic field. In the absence of this field, the particles return to a relaxed state. This makes them useful towards the collection processes seen with solid phase extraction, in which solid particles are used to bind with a target for easy removal from solution. A reliance on the magnetic susceptibility of these nanoparticles makes it possible to bind specific targets in a homogenous solution and effortlessly collect the bound particles through magnetic aggregation. The larger surface area available on such nanoparticles makes it possible to more effectively bind trace elements in solution.

Currently such nanoparticles are used for biological applications and manufacturing pigments. The production of these particles may be achieved by various techniques, including coprecipitation, thermal decomposition and hydrothermal synthesis [77]. To prevent aggregation and increase their stability, these particles generally rely upon stabilizers, such as a fatty acid or amine, and the manipulation of the solvent's polarity. Consideration of the environmental conditions, such as the composition of the groundwater, may pose difficulties. Background ions pose complications, having an affinity for these nanoparticles, and natural organic matters (NOM) also affect kinetics in the collection of a desired trace element like arsenic [83].

In the application of iron oxide nanoparticles with arsenic, a more complex situation is faced. While pH only affects the charge associated with the iron oxide, it is the present oxidation state that holds concern. The oxidation state will determine the extent to which arsenic may be bound by the formation of physical or chemical attachment [84]. Here, strong chemical bonds prevent desorption of arsenic, needed if colourimetric detection is to be achievable.

Currently a number of different forms of iron oxide nanoparticles exist, specifically maghemite ($\gamma$-$Fe_2O_3$), magnetite ($Fe_3O_4$) and zero-valent Iron (nZVI or $Fe^0$). Each of these oxidation states possess a set of specific capabilities, caused by the change in chemical properties. Maghemite is currently applied to contaminant removal *via* physical adsorption. Maghemite nanoparticles can be feasibly desorbed and regenerated. While magnetite is applied in the same way, its regeneration is not highly effective as it produces a strong reduction and high occurrence of chemisorption. The zero-valent iron nanoparticles are the most effective, with high reducing capabilities, an ability to degrade a wide range of pollutants, and reversible adsorption, but unfortunately suffer from an unstable state that is tricky to maintain [83].

Through the measurement of optical opacity, illustrated in Figure 67, data had been collected to classify the adsorption and magnetic separation time scales for magnetite. An experimental protocol for creating the sample solutions and an opacity test system was designed without the use of coatings.

Table 20: Iron oxide aggregation protocol

| Step # | Description |
|---|---|

Part A. Iron Samples

1. Place Weighing paper on balance
2. Zero balance
3. Deposit iron oxide on weighing paper with micro-spatula
4. Add solvent (deionized water) to container
5. Transfer iron oxide to container
6. Sonification of sample
    - Intensity: 10%,
    - Pulse: 6 seconds ON, 3 seconds OFF
    - Note: Tip must not touch bottom of container
    - Clean probe when complete:
        i. Fill beaker with water
        ii. Sonicate sample for 1min
        iii. Spray probe with alcohol and dry with kim wipes
7. Repeat 1 to 6 for the creation of all samples

Part B. Collection Time

8. Confirm alignment of laser with optical detector
9. Place sample into opacity apparatus receptacle
10. Record gravitational dataset
11. Remove sample and insert magnet into inner well of receptacle
12. Begin recording before placing sample into receptacle for magnetic dataset

From the results collected for the varying concentrations and gravitational/magnetic response, the graphs of Figure 68 and Figure 69 were generated and passed along to the team at the University of Oxford, where they simulated the response to study the Hydrodynamic interactions placed upon iron oxide nanoparticles.

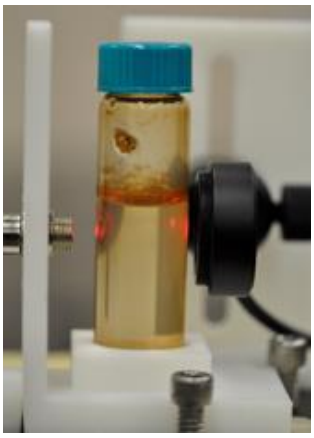

*Figure 67: Opacity System with iron oxide sample.*

*Magnetic Collection Results*

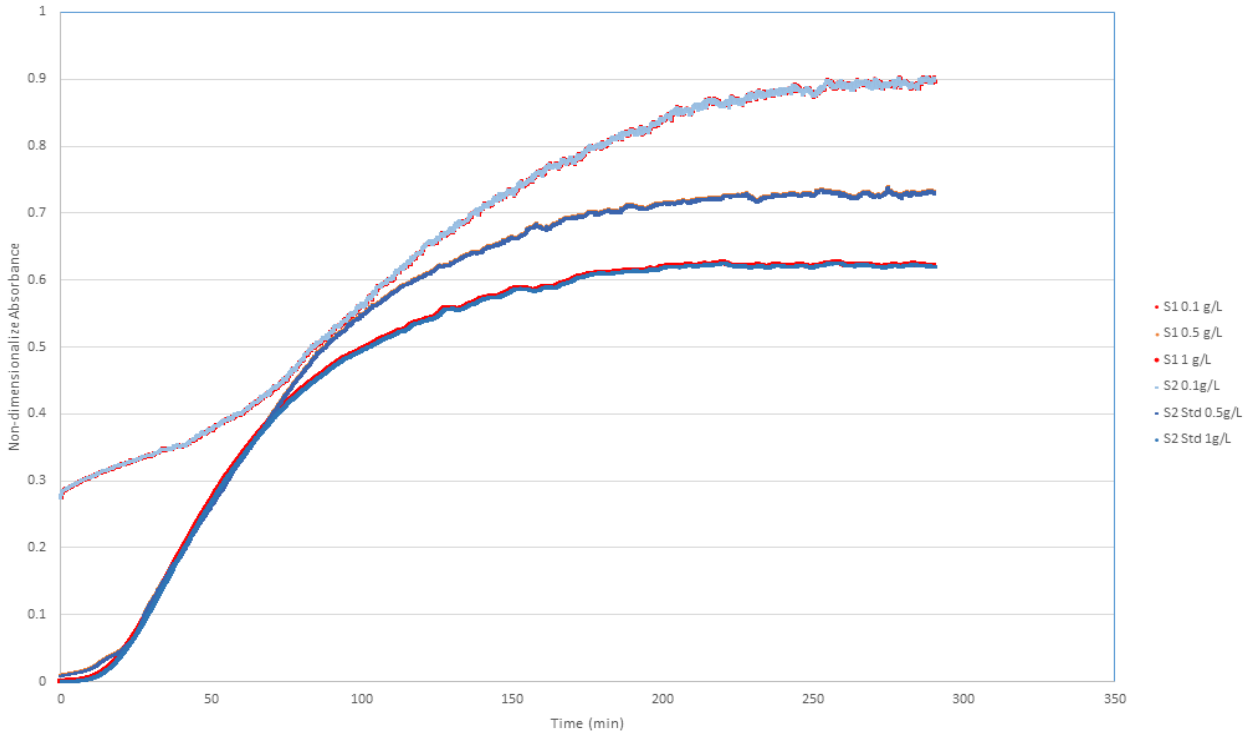


*Figure 68: Gravity Response of the iron oxide particles nanoparticles aggregation, for two datasets (S1 and S2).*

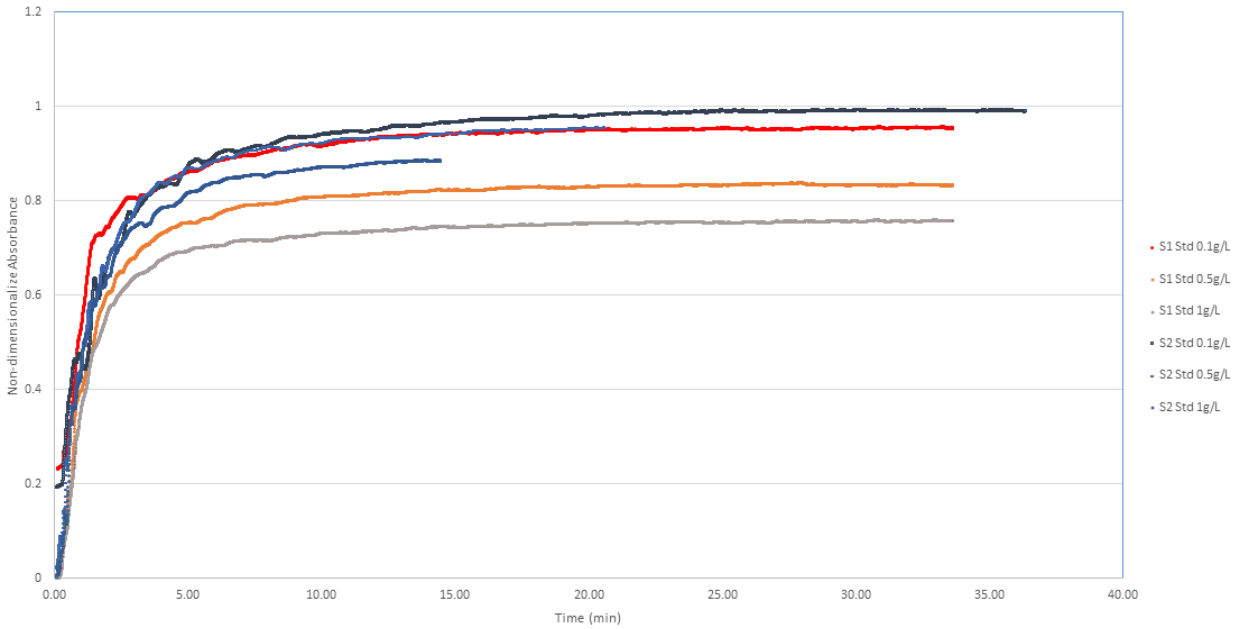


*Figure 69: The magnetic response of the iron oxide nanoparticles aggregation, for two datasets (S1 and S2).*

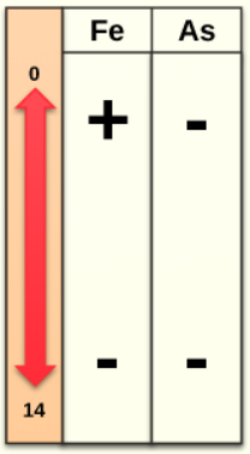


*Figure 70: Electrostatic interactions for iron oxides with arsenic.*

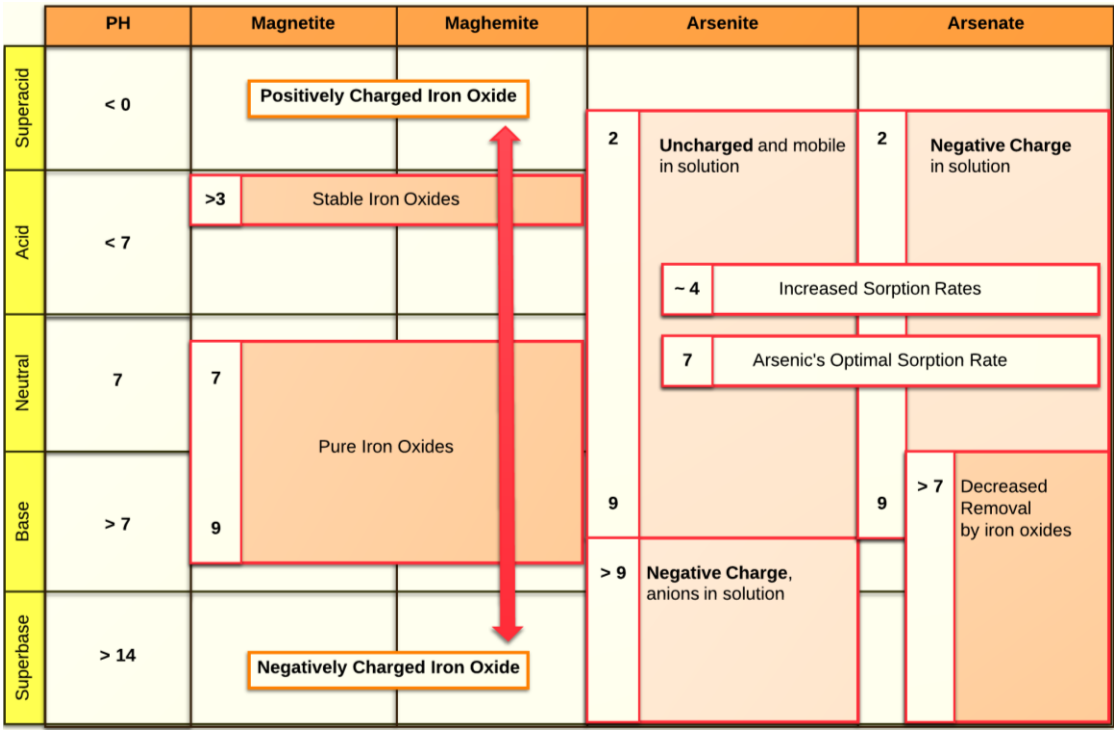


*Figure 71: Adsorption and recovery conditions for the various forms of Fe in relation to the arsenic present.*

From Figure 68 to Figure 72, it can be seen that iron oxides may be used in the collection and recovery of arsenic from solution, depending on the variation of the pH. The different forms of iron can affect this process making it more or less complex then need be. As this is the case, recent study has been on the use of iron oxides to still play a role in the magnetic collection but the use of coating to prevent the interference experienced through the chemical binding between arsenic and iron nanoparticles.

In addition to regulating the factors associated with the magnetic nanoparticles, the arsenic level in solution must also be controlled. A preference is placed on the conditions required for the increased presence of arsenate. The reason for this is shown in the diagram above. Arsenate holds a charge between the pH range of 2 to 9. Thus, electrostatic bonding becomes a driving force in arsenic removal. As arsenite cannot be collected out of solution easily, its conversion to arsenate must be made through the use of a reducing agents, such as Poly-Benzyl Pyridinium Tri-Iodide, and an increased pH to drive the process [85], [86]. Doing this also serves its use towards existing colourimetric test kits that make use of the Gutzeit Method, as they display better detection of arsenate. Regenerating these particles by desorption of the toxins can be achieved by one of three techniques:

1. Coatings: Applying different coatings to the particles makes it possible to use the ferromagnetic properties and electrostatic adsorption while lowing pH requirements and the occurrence of chemisorption.
2. Hard-soft acid-based theory: Placing a reliance on acid-base interactions to desorb particles can be chemically demanding, producing large quantities of waste.
3. Oxidization: This process requires well-controlled conditions to convert iron oxides to the stable maghemite state, in which pollutants may be desorbed by varying the pH.

### *7.5.3 Solid Phase Extraction*

From the adsorption studies and details given on the complexity of chemical bonds affecting the recovery process, regeneration is shown to be essential. The use of coatings shows the greatest success towards this attainable goal with recent literature posing a plausible aluminum coating for arsenic extraction. The generated Figure 72 below shows how this process is made possible. When the solution is acidic, the Aluminum coating repels the cationic Cetrimonium bromide (CTAB) surfactant, releasing the CTAB that has bound with Arsenic; the aluminum coated ferromagnetic particles may then be reused and the arsenic solution used with colourimetric analysis. The protocol that follows has been determined though the literature to create and test the use of such nanoparticles [87]–[90].

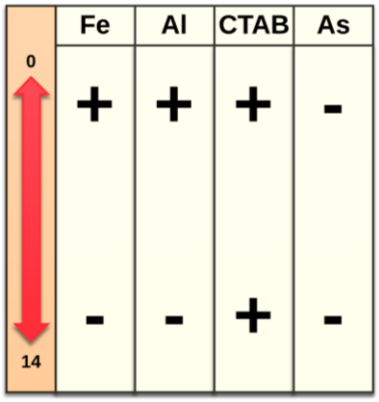


*Figure 72: Electrostatic interactions for the Aluminum coated nanoparticles.*

Table 21: Aluminum coated magnetic nanoparticle protocol

| Step # | Description |
|---|---|

Part A. Creation of MNPs

1. Create co-precipitation:
   - 25 mL of DI water,
   - 2.0 g of FeCl2 .4H20
   - 5.0 g of FeCl3 .6H20
   - 0.85 mL of HCl (12 mol/L)
2. Add co-precipitate dropwise:
   - 250 mL (1.5 mol/L) of NaOH
   - Nitrogen sparging
3. Separate MNPs with magnetic field
   - Wash with 200mL of DI water at least 4 times
   - Dry at 80 degrees Celsius

Part B. Coating MNPs with Aluminum

1. Place in beaker
   - 60 mL Ethanol
   - Add 1.0 g of Aluminum isopropoxide
2. Add to beaker:
   - 0.1 g of MNPs
   - Apply ultrasonic bath for 5 min
3. Add mixture drop wise:
   - 1:5 v/v (DI water: ethanol) while nitrogen sparging
   - Continue nitrogen sparging 30 min
   - Let stand for 1 hour before separating
   - Wash and suspend mixture with ethanol
   - Separate with magnet
4. Oven dry (calcined)
   - 500 degrees Celsius
   - 3 hours

Part C. Add CTAB to ACMNPs

- 50 mg CTAB
- 100 mg ACMNPs
- Adjust pH between 8.0 - 9.0
- 5 mL of NH3/NH4Cl
- 0.1 mol/L
- Shake for 5 minutes
- Apply magnet to side for Separation
- Rinse with 10 mL purified/DI water

Part D. CTAB-ACMNPs

- Study effects of binding time
- Determine Fe/As Ratio
- Demonstrate reusability
- Concentrate low ppb for calibration

### *7.5.4 Microfluidic Application*

*Experimental Techniques*

1. Inductively coupled plasma-optical emission spectroscopy (ICP-OES):
    - This tool will be applied to study the gaseous concentrations that are generated in the microfluidic platforms gaseous chamber collected in parallel to the production of colourimetric results for numerous trials, thus achieving a high level of correlation.
2. Digital Camera Apparatus:
    - The use of a digital camera that has been fixed into a confined structure will be used to control light conditions for the collection of colourimetric images.

*Modeling Techniques*

CAD tools, such as SOLIDWORKS, will be used to model the desired theoretical channel structure. The produced model will be reduced to a minimal number of layers by splitting the model into components of equal dimension. Once the separate components have been decided, COMSOL Multiphysics will be used to model the flow through each of them, specifically the movement in the aqueous channel, at the gas-liquid interface and the gaseous channel. Results of this analysis will be used to tune the theoretical model through various stages before actually producing components.

Furthermore, the use of analytical analysis will help in the development of the liquid-gas interface, studying the gaseous flow and determining the collection time expected of gaseous samples. To define the formation of air pillars and maximum pressure change that can be sustained by the microfluidic channel the Young-Laplace equation is used, as follows:

Young-Laplace:

$$\Delta P = P_l - P_a = \gamma_{LG}\left(\frac{1}{R_1} + \frac{1}{R_2}\right) \quad \text{Eq. 35}$$

Where $R_1$ and $R_2$ are the radii of curvature vertical and parallel to liquid stream, respectively, $\gamma_{LG}$ is the surface tension, $P_l$ is the liquid pressure and $P_a$ is the atmospheric pressure.

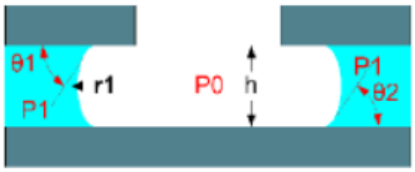


*Figure 73: Air pillar formation, adapted from* [71].

Convective transport of the bulk fluid is used to model gas using the following two dimensional, time-invariant, compressible equations [91].

Conservation of mass:

$$(\vec{u}\cdot\vec{\nabla})\rho + \rho\vec{\nabla}\cdot\vec{u} = 0 \quad \text{Eq. 36}$$

Conservation of momentum:

$$(\vec{u}\cdot\vec{\nabla})\vec{u} + \left(\frac{1}{\rho\vec{\nabla}\rho}\right) = 0 \quad \text{Eq. 37}$$

Conservation of energy:

$$(\vec{u}\cdot\vec{\nabla})p + \gamma p\vec{\nabla}\cdot\vec{u} = 0 \quad \text{Eq. 38}$$

Equation of state (for ideal gas):

$$p = \rho RT \quad \text{Eq. 39}$$

Where $\vec{u}$ is the velocity, $\gamma$ is the ratio of specific heats ($C_p/C_v$) for the gas mixture, $\rho$ is the density of the gas mixture, T is the temperature and R is the gas constant.

*Microfluidic Techniques*

To produce the multi-layered test model, as described by Figure 74, layer production will need to be considered. Model fabrication will be done with both layer-to-layer and layer-on-layer procedures. For the incorporation of test strips, layer-to-layer manufacturing would be best suited

as it involves the individual fabrication of layers followed by lamination. The use of a clamp may be incorporated in this design to insert/remove test strips. In a second model, paper-based analytics will be imbedded; the use of layer-on-layer fabrication may be used. While the second method avoids channel alignment issues, its layer production is performed one at a time, increasing the complexity [68].

As the lower layers in the platform would be used to insert reagents to the aqueous channel at set intervals, mix solution and provide a liquid-gas interface, material considerations must be taken. Layers above the interface must also be made impermeable to the gaseous phase, allowing for collection and interaction with paper-based analytics for optical detection in the platform [68].

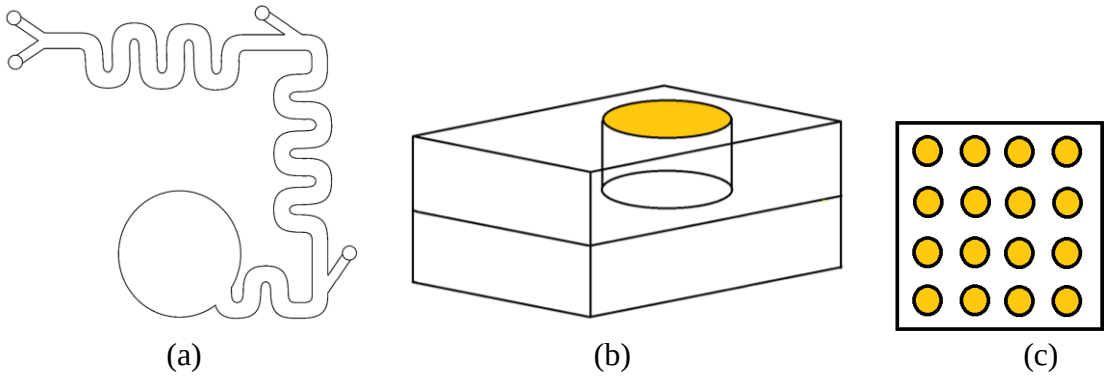

(a) (b) (c)

*Figure 74: Basic layout for gaseous colourimetric design (a) The addition of reagents will be diffused into the solution at various stages, where the last reagent added results in gaseous formation, (b) Gas is passed from the aqueous channel into collection chamber, (c) The use of mercuric-bromide impregnated filters (either existing test strips or multiplexed paper-based analytics) will be used to create colourimetric results.*

A second method in the formation of liquid-gas interfaces involves the production of air pillars. Before bonding the layers of a channel, holes are simply machined into the upper layer. Air pillars are a robust alternative, controlled by surface tension and associated pressures [71]. While liquid is flown at a constant rate through the channel, the pressure of the flow is balanced with the atmosphere at each interface. Analysis has shown that an increase in both the flow rate and number of air-pillars present may be achieved through uniform alignment [71]. Hydrophilic-hydrophobic substrates can also be incorporated into this design for better containment of the aqueous solution [70].

A final method for interfacing liquid and gaseous samples has been shown through the use of permeable membrane inserts. Commercially available membranes, such as polyvinylidene fluoride (PVDF) and Polytetrafluoroethylene (PTFE), have been widely used in the creation of devices for gas diffusion. The use of these membranes requires that a clamp is used to hold the layers together, the membrane being placed between the aqueous and gaseous channels [92].

Besides the fabrication of liquid-gas interfaces, the method used to control the flow and production of gaseous products needs to be considered. In the use of air pillars, hydrophilic-hydrophobic interfaces, and membranes, the gaseous products may be passed through simple aqueous channels that place a reliance on micro-pumping (with solenoid, pneumatic, peristaltic or active pumps) to control the flow of solution and reagents [93]. Another technique that has been shown to handle this process, removes the need for pumps and replaces it with the use of centrifugal force, Ymbern et al. has developed a simple device for such an application, in which gaseous products are formed and passed through a PVDF membrane [92]. This process has not been shown for use with air-pillars or hydrophilic-hydrophobic interfaces but it should be plausible, depending on how they are arranged, as existing membranes also incorporate holes in their structure.

The use of centrifugal force has an added bonus as it may be used to pre-concentrate gaseous species. While pre-concentration is normally performed beforehand with the sample solution, there has been significant advancement in the study of gaseous pre-concentration. Here a centrifuge may separate gaseous mixtures by the molecular weight of present elements. An example of this process has been demonstrated by Li et al., in which gas is simultaneously concentrated and separated into heavy and light species by the channel arrangement [91].

# 8. References


[1] D. R. Baldwin and W. J. Marshall, "Heavy metal poisoning and its laboratory investigation.," *Ann. Clin. Biochem.*, vol. 36 ( Pt 3), pp. 267–300, 1999.

[2] D. Melamed, "Monitoring arsenic in the environment: A review of science and technologies with the potential for field measurements," *Anal. Chim. Acta*, vol. 532, pp. 1–13, 2005.

[3] S. Kou, S. Nam, W. Shumi, M. H. Lee, S. W. Bae, J. Du, J. S. Kim, J.-I. Hong, X. Peng, J. Yoon, and S. Park, "Microfluidic detection of multiple heavy metal ions using fluorescent chemosensors," *Bull. Korean Chem. Soc.*, vol. 30, no. 5, pp. 1173–1176, 2009.

[4] B. K. Mandal and K. T. Suzuki, "Arsenic round the world: A review," *Talanta*, vol. 58, pp. 201–235, 2002.

[5] A. H. Smith and M. M. H. Smith, "Arsenic drinking water regulations in developing countries with extensive exposure," *Toxicology*, vol. 198, pp. 39–44, 2004.

[6] E. Diesel, M. Schreiber, and J. R. van der Meer, "Development of bacteria-based bioassays for arsenic detection in natural waters," *Anal. Bioanal. Chem.*, vol. 394, pp. 687 – 693, 2009.

[7] J. Anwar, Waheed-uz-Zaman, M. U. Shafique, and M. Salman, "Computational quantification of spot tests by image scanning: A new analytical technique for micro samples," *Anal. Lett.*, vol. 43, no. August 2009, pp. 367–371, 2010.

[8] N. Buffi, D. Merulla, J. Beutier, F. Barbaud, S. Beggah, H. van Lintel, P. Renaud, and J. R. van der Meer, "Development of a microfluidics biosensor for agarose-bead immobilized Escherichia coli bioreporter cells for arsenite detection in aqueous samples," *Lab Chip*, vol. 11, pp. 2369 – 2377, 2011.

[9] C. A. de Villiers, M. C. Lapsley, and E. A. H. Hall, "A step towards mobile arsenic measurement for surface waters," *R. Soc. Chem.*, 2015.

[10] C. D. Chin, V. Linder, and S. K. Sia, "Commercialization of microfluidic point-of-care diagnostic devices," *Lab Chip*, vol. 12, pp. 2118 – 2134, 2012.

[11] D. G. Kinniburgh and W. Kosmus, "Arsenic contamination in groundwater: Some analytical considerations," *Talanta*, vol. 58, pp. 165 – 180, 2002.

[12] A. Safarzadeh-Amiri, P. Fowlie, A. I. Kazi, S. Siraj, S. Ahmed, and A. Akbor, "Validation of analysis of arsenic in water samples using wagtech digital arsenator," *Sci. Total Environ.*, vol. 409, no. 13, pp. 2662–2667, 2011.

[13] J. Ma, M. K. Sengupta, D. Yuan, and P. K. Dasgupta, “Speciation and detection of arsenic in aqueous samples: A review of recent progress in non-atomic spectrometric methods,” *Anal. Chim. Acta*, vol. 831, pp. 1–23, 2014.

[14] S. K. Vashist, O. Mudanyali, E. M. Schneider, R. Zengerle, and A. Ozcan, “Cellphone-based devices for bioanalytical sciences,” *Anal. Bioanal. Chem.*, vol. 406, no. 14, pp. 3263–3277, 2014.

[15] R. V. Abrazheev, A. D. Zorin, N. P. Savinova, and Y. I. Sannikova, “An improved apparatus for determining microgram amounts of arsenic by the gutzeit method using computer-assisted data processing,” *J. Anal. Chem.*, vol. 57, no. 3, pp. 280–283, 2002.

[16] J. Jönsson and D. M. Sherman, “Sorption of As(III) and As(V) to siderite, green rust (fougerite) and magnetite: Implications for arsenic release in anoxic groundwaters,” *Chem. Geol.*, vol. 255, pp. 173 – 181, 2008.

[17] P. L. Smedley and D. G. Kinniburgh, “A review of the source, behaviour and distribution of arsenic in natural waters,” *Appl. Geochemistry*, vol. 17, no. 5, pp. 517–568, 2002.

[18] M. M. Uddin, a. K. M. Harun-Ar-Rashid, S. M. Hossain, M. A. Hafiz, K. Nahar, and S. H. Mubin, “Slow arsenic poisoning of the contaminated groundwater users,” *Int. J. Environ. Sci. Technol.*, vol. 3, no. 4, pp. 447–453, 2006.

[19] A. H. Smith, E. O. Lingas, and M. Rahman, “Contamination of drinking-water by arsenic in Bangladesh: A public health emergency,” *Bull. World Health Organ.*, vol. 78, no. 9, pp. 1093–1103, 2000.

[20] T. J. Sorg, A. S. C. Chen, and L. Wang, “Arsenic species in drinking water wells in the USA with high arsenic concentrations.,” *Water Res.*, vol. 48, pp. 156–169, Jan. 2014.

[21] D. Maddison, R. Catala-Luque, and D. Pearce, “Valuing the arsenic contamination of groundwater in Bangladesh,” *Environ. Resour. Econ.*, vol. 31, no. 4, pp. 459–476, 2005.

[22] M. F. Ahmed, S. Ahuja, M. Alauddin, S. J. Hug, J. R. Lloyd, A. Pfaff, T. Pichler, C. Saltikov, M. Stute, and A. van Geen, “Ensuring safe drinking water in Bangladesh,” *J. Sci.*, vol. 314, no. December, pp. 1687–1688, 2006.

[23] K. Cantrell, M. M. Erenas, I. De Orbe-Payá, and L. F. Capitán-Vallvey, “Use of the hue parameter of the hue, saturation, value color space as a quantitative analytical parameter for bitonal optical sensors,” *Anal. Chem.*, vol. 82, no. 2, pp. 531 – 542, 2010.

[24] D. Melamed, “Monitoring arsenic in the environment: A review of science and technologies for field measurments and sensors,” 2004.

[25] P. J. Potts, M. H. Ramsey, and J. Carlisle, “Portable x-ray fluorescence in the characterisation of arsenic contamination associated with industrial buildings at a heritage

arsenic works site near Redruth, Cornwall, UK.," *J. Environ. Monit.*, vol. 4, no. 6, pp. 1017–1024, 2002.

[26] K. Abbgy, A., Kelly, T., Lawrie, C., & Riggs, "Environmental technology verification report: Advanced monitoring systems center: Quick™ arsenic test kit," Columbus, 2002.

[27] M. H. Arbab-Zavar and M. Hashemi, "Evaluation of electrochemical hydride generation for spectrophotometric determination of As(III) by silver diethyldithiocarbamate," *Talanta*, vol. 52, no. 6, pp. 1007–1014, 2000.

[28] V. Lenoble, V. Deluchat, B. Serpaud, and J.-C. Bollinger, "Arsenite oxidation and arsenate determination by the molybdene blue method," *Talanta*, vol. 61, no. 3, pp. 267–276, 2003.

[29] T. Rupasinghe, T. J. Cardwell, R. W. Cattrall, M. D. L. De Castro, and S. D. Kolev, "Pervaporation-flow injection determination of arsenic based on hydride generation and the molybdenum blue reaction," *Anal. Chim. Acta*, vol. 445, pp. 229–238, 2001.

[30] P. K. Dasgupta, H. Huang, G. Zhang, and G. P. Cobb, "Photometric measurement of trace As(III) and As(V) in drinking water," *Talanta*, vol. 58, pp. 153 – 164, 2002.

[31] Z. L. Chen, J. M. Lin, and R. Naidu, "Separation of arsenic species by capillary electrophoresis with sample-stacking techniques," *Anal. Bioanal. Chem.*, vol. 375, no. 5, pp. 679 – 684, 2003.

[32] C. Casiot, M. C. Barciela Alonso, O. F. X. Donard, M. Potin-Gautier, M. C. Barciela Alonso, and J. Boisson, "Simultaneous speciation of arsenic, selenium, antimony and tellurium species in waters and soil extracts by capillary electrophoresis and UV detection," *Analyst*, vol. 123, no. 12, pp. 2887 – 2893, 1998.

[33] B. Sun, M. Macka, and P. R. Haddad, "Separation of organic and inorganic arsenic species by capillary electrophoresis using direct spectrophotometric detection," *Electrophoresis*, vol. 23, no. 1, pp. 2430 – 2438, 2002.

[34] R. T. Wainner, R. S. Harmon, a. W. Miziolek, K. L. McNesby, and P. D. French, "Analysis of environmental lead contamination: Comparison of LIBS field and laboratory instruments," *Spectrochim. Acta B*, vol. 56, no. 6, pp. 777–793, 2001.

[35] B. T. Fisher, H. A. Johnsen, S. G. Buckley, and D. W. Hahn, "Temporal gating for the optimization of laser-induced breakdown spectroscopy detection and analysis of toxic metals," *Appl. Spectrosc.*, vol. 55, no. 10, pp. 1312 – 1319, 2001.

[36] A. M. Beccaglia, C. A. Rinaldi, and J. C. Ferrero, "Analysis of arsenic and calcium in soil samples by laser ablation mass spectrometry," *Anal. Chim. Acta*, vol. 579, no. 1, pp. 11 – 16, 2006.

[37] R. Feeney and S. P. Kounaves, “Voltammetric measurement of arsenic in natural waters,” *Talanta*, vol. 58, pp. 23 – 31, 2002.

[38] H. Huang and P. K. Dasgupta, “A field-deployable instrument for the measurement and speciation of arsenic in potable water,” *Anal. Chim. Acta*, vol. 380, pp. 27 – 37, 1999.

[39] V. M. Sbarato and H. J. Sánchez, “Analysis of arsenic pollution in groundwater aquifers by x-ray fluorescence,” *Appl. Radiat. Isot.*, vol. 54, no. 5, pp. 737–740, 2001.

[40] V. Thomsen and D. Schatzlein, “Advances in field-portable XRF,” *Spectroscopy*, vol. 17, no. 7, pp. 14 – 21, 2002.

[41] F. F. Roberto, J. M. Barnes, and D. F. Bruhn, “Evaluation of a GFP reporter gene construct for environmental arsenic detection,” *Talanta*, vol. 58, no. 1, pp. 181–188, 2002.

[42] J. Stocker, D. Balluch, M. Gsell, H. Harms, J. Feliciano, S. Daunert, K. A. Malik, and J. R. van der Meer, “Development of a set of simple bacterial biosensors for quantitative and rapid measurements of arsenite and arsenate in potable water,” *Environ. Sci. Technol.*, vol. 37, no. 20, pp. 4743–4750, 2003.

[43] C. M. Steinmaus, C. M. George, D. A. Kalman, and A. H. Smith, “Evaluation of two new arsenic field test kits capable of detecting arsenic water concentrations close to 10 μg/L,” *Environ. Sci. Technol.*, vol. 40, no. 10, pp. 3362–3366, 2006.

[44] S. P. Pande, L. S. Deshpande, and S. N. Kaul, “Laboratory and field assessment of asrenic testing field kits in Bangladesh and West Bengal, India,” *Environ. Monit. Assess.*, vol. 68, pp. 1–18, 2001.

[45] J. Kearns and J. Tyson, “Improving the accuracy and precision of an arsenic field test kit: increased reaction time and digital image analysis,” *Anal. Methods*, vol. 4, pp. 1693–1698, 2012.

[46] J. F. Tyson, *Development of measurement technologies for low-cost, reliable, rapid, on-site determination of arsenic compounds in water, in contamination of groundwater: mechanism, analysis, and remediation*. New York: Wiley, 2008.

[47] M. Jakariya, M. Vahter, M. Rahman, M. A. Wahed, S. K. Hore, P. Bhattacharya, G. Jacks, and L. Å. Persson, “Screening of arsenic in tubewell water with field test kits: Evaluation of the method from public health perspective,” *Sci. Total Environ.*, vol. 379, no. 3, pp. 167 – 175, 2007.

[48] M. M. Rahman, D. Mukherjee, M. K. Sengupta, U. K. Chowdhury, D. Lodh, C. R. Chanda, S. Roy, M. Selim, Q. Quamruzzaman, A. H. Milton, S. M. Shahidullah, R. M. Tofizur, and D. Chakraborti, “Effectiveness and reliability of arsenic field testing kits: Are the million dollar screening projects effective or not?,” *Environ. Sci. Technol.*, vol. 36, no. 24, pp. 5385–5394, 2002.

[49] M. Kompany-Zareh, M. Mansourian, and F. Ravaee, “Simple method for colorimetric spot-test quantitative analysis of Fe(III) using a computer controlled hand-scanner,” *Anal. Chim. Acta*, vol. 471, pp. 97–104, 2002.

[50] Q. Wei, R. Nagi, K. Sadeghi, S. Feng, E. Yan, S. J. Ki, and R. Caire, “Detection and spatial mapping of mercury contamination in water samples using a smart-phone,” *Am. Chem. Soc.*, vol. 8, no. 2, pp. 1121–1129, 2014.

[51] A. van Geen, Z. Cheng, A. A. Seddique, M. A. Hoque, A. Gelman, J. H. Graziano, H. Ahsan, F. Parvez, and K. M. Ahmed, “Reliability of a commercial kit to test groundwater for arsenic in bangladesh,” *Environ. Sci. Technol.*, vol. 39, pp. 299–303, 2005.

[52] S. Paciornik, A. V. Yallouz, R. C. Campos, and D. Gannerman, “Scanner image analysis in the quantification of mercury using spot-tests,” *J. Braz. Chem. Soc.*, vol. 17, no. 1, pp. 156–161, 2006.

[53] A. Lapresta-Fernández, R. Huertas, M. Melgosa, and L. F. Capitán-Vallvey, “Colourimetric characterisation of disposable optical sensors from spectroradiometric measurements,” *Anal. Bioanal. Chem.*, vol. 393, no. 4, pp. 1361 – 1366, 2009.

[54] E. Hirayama, T. Sugiyama, H. Hisamoto, and K. Suzuki, “Visual and colorimetric lithium ion sensing based on digital color analysis,” *Anal. Chem.*, vol. 72, no. 3, pp. 465 – 474, 2000.

[55] V. V. Apyari and S. G. Dmitrienko, “Using a digital camera and computer data processing for the determination of organic substances with diazotized polyurethane foams,” *J. Anal. Chem.*, vol. 63, no. 6, pp. 530–537, 2008.

[56] M. Salman, M. Athar, Waheed-uz-Zaman, U. Shafique, J. Anwar, R. Rehman, S. Ameer, and M. Azeem, “Micro-determination of arsenic in aqueous samples by image scanning and computational quantification,” *Anal. Methods*, vol. 4, p. 242, 2012.

[57] D.-J. Lee, J. K. Archibald, Y.-C. Chang, and C. R. Greco, “Robust color space conversion and color distribution analysis techniques for date maturity evaluation,” *J. Food Eng.*, vol. 88, pp. 364–372, 2008.

[58] “Color Theory,” 2012. [Online]. Available: http://learn.colorotate.org/color-models/#.U_EjYvldWAV. [Accessed: 13-Jul-2014].

[59] J. G. Proakis and D. G. Manolakis, *Digital signal processing-principles, algorithms and applications*. 2006.

[60] M. E. Johnson, “Rapid, simple quantitation in thin-Layer chromatography using a flatbed scanner,” *J. Chem. Educ.*, vol. 77, no. 3, p. 368, 2000.

[61] S. V. Bannur, S. V. Kulgod, S. S. Metkar, S. K. Mahajan, and J. K. Sainis, "Protein determination by ponceau S using digital color image analysis of protein spots on nitrocellulose membranes.," *Anal. Chem.*, vol. 267, pp. 382 – 389, 1999.

[62] O. Mudanyali, S. Dimitrov, U. Sikora, S. Padmanabhan, I. Navruz, and A. Ozcan, "Integrated rapid-diagnostic-test reader platform on a cellphone," *Lab Chip*, vol. 12, no. 15, pp. 2678 – 2686, 2012.

[63] L. Shen, J. A. Hagen, and I. Papautsky, "Point-of-care colorimetric detection with a smartphone," *Lab Chip*, vol. 12, no. 21, pp. 4240–4243, 2012.

[64] A. Ozcan, "Mobile phones democratize and cultivate next-generation imaging, diagnostics and measurement tools.," *Lab Chip*, vol. 14, pp. 3187–3194, 2014.

[65] W. Bishara, U. Sikora, O. Mudanyali, T.-W. Su, O. Yaglidere, S. Luckhart, and A. Ozcan, "Holographic pixel super-resolution in portable lensless on-chip microscopy using a fiber-optic array," *Lab Chip*, vol. 11, no. 7, pp. 1276 – 1279, 2011.

[66] A. F. Coskun and A. Ozcan, "Computational imaging, sensing and diagnostics for global health applications," *Curr. Opin. Biotechnol.*, vol. 25, pp. 8–16, 2014.

[67] K. R. Mathews, J. D. Landmark, and D. F. Stickle, "Quantitative assay for starch by colorimetry using a desktop scanner," *J. Chem. Educ.*, vol. 81, no. 5, p. 702, 2004.

[68] A. Waldbaur, H. Rapp, K. Länge, and B. E. Rapp, "Let there be chip - towards rapid prototyping of microfluidic devices: One-step manufacturing processes," *Anal. Methods*, vol. 3, no. 12, pp. 2681–2716, 2011.

[69] P. Lisowski and P. K. Zarzycki, "Microfluidic paper-based analytical devices (μPADs) and micro total analysis systems (μTAS): Development, applications and future trends," *Chromatographia*, vol. 76, no. 19–20, pp. 1201–1214, 2013.

[70] S. S. Sridharamurthy and H. Jiang, "A microfluidic device to acquire gaseous samples via surface tension held gas-liquid interface," *IEEE Sens. J.*, vol. 7, no. 9, pp. 1315–1316, 2007.

[71] J. D. Greenwood, Y. Liu, D. E. Busacker, D. Cheng, and H. Jiang, "Collection of gaseous and aerosolized samples using microfluidic devices with gas-liquid interfaces," *IEEE Sensors*, vol. 10, no. 5, pp. 952 – 959, 2010.

[72] J. Greenwood, D. Cheng, Y. Liu, and H. Jiang, "Air to liquid sample collection devices using microfluidic gas/liquid interfaces," in *IEEE Sensors*, 2008, pp. 720 –723.

[73] V. C. Ezeh and T. C. Harrop, "A sensitive and selective fluorescence sensor for the detection of arsenic(III) in organic media," *Inorg. Chem.*, vol. 51, no. 3, pp. 1213 – 1215, 2012.

[74] K. Hylton and S. Mitra, “A microfluidic hollow fiber membrane extractor for arsenic(V) detection,” *Anal. Chim. Acta*, vol. 607, no. 1, pp. 45 – 49, 2008.

[75] D. M. Cate, P. Nanthasurasak, P. Riwkulkajorn, C. L’Orange, C. S. Henry, and J. Volckens, “Rapid detection of transition metals in welding fumes using paper-based analytical devices,” *Ann. Occup. Hyg.*, vol. 58, no. 4, pp. 413 – 423, 2013.

[76] P. Niedzielski and M. Siepak, “Analytical methods for determining arsenic, antimony and selenium in environmental samples,” *Polish J. Environ. Stud.*, vol. 12, no. 6, pp. 653–667, 2003.

[77] Y. Ju-Nam and J. R. Lead, “Manufactured nanoparticles: An overview of their chemistry, interactions and potential environmental implications,” *Sci. Total Environ.*, vol. 400, no. 1–3, pp. 396–414, 2008.

[78] “Mean Vector and Covariance Matrix.” [Online]. Available: http://www.itl.nist.gov/div898/handbook/pmc/section5/pmc541.htm. [Accessed: 09-Dec-2013].

[79] A. Baghel, B. Singh, P. Pandey, and K. Sekhar, “A rapid field detection method for arsenic in drinking water,” *Anal. Sci.*, vol. 23, no. February, pp. 135 – 137, 2007.

[80] M. Bissen and F. H. Frimmel, “Arsenic a review part II: Oxidation of arsenic and its removal in water treatment,” *Acta Hydrochim. Hydrobiol.*, vol. 31, pp. 97 – 107, 2003.

[81] J. G. Hering, P.-Y. Chen, J. A. Wilkie, and M. Elimelech, “Arsenic removal from drinking water during coagulation,” *Environ. Eng.*, vol. 12, pp. 800 – 807, 1997.

[82] R. Mamtaz and D. H. Bache, “Low-cost technique of arsenic removal from water and its removal mechanism,” *... Technol. Dhaka Univ. ...*, pp. 43–58, 2001.

[83] S. C. N. Tang and I. M. C. Lo, “Magnetic nanoparticles: essential factors for sustainable environmental applications.,” *Water Res.*, vol. 47, no. 8, pp. 2613–32, May 2013.

[84] S. R. Wickramasinghe, B. Han, J. Zimbron, Z. Shen, and M. N. Karim, “Arsenic removal by coagulation and filtration: Comparison of groundwaters from the United States and Bangladesh,” *Desalination*, vol. 169, pp. 231–244, 2004.

[85] M. Borho and P. Wilderer, “Optimized removal of arsenate(III) by adaptation of oxidation and precipitation processes to the filtration step,” *Water Sci. Technol.*, vol. 34, no. 9, pp. 25–31, 1996.

[86] S. J. A.-L. Hug O., “Iron-catalyzed oxidation of arsenic (III) by oxygen and by hydrogen peroxide: pH-dependent formation of oxidants in the fenton reaction,” *Environ. Sci. Technol.*, vol. 37, no. 12, pp. 2734 – 2742, 2003.

[87] M. A. Karimi, A. Mohadesi, A. Hatefi-mehrjardi, S. Z. Mohammadi, J. Yarahmadi, and A. Khayrkhah, "Separation/preconcentration and speciation analysis of trace amounts of arsenate and arsenite in water samples using modified magnetite nanoparticles and molybdenum blue method," *Chemistry (Easton).*, pp. 1 –9, 2014.

[88] M. A. Karimi, A. Hatefi-Mehrjardi, S. Z. Mohammadi, A. Mohadesi, M. Mazloum-Ardakani, M. R. Hormozi Nezhad, and A. A. Kabir, "Solid phase extraction of trace amounts of Pb(II) in opium, heroin, lipstick, plants and water samples using modified magnetite nanoparticles prior to its atomic absorption determination," *Iran. Chem. Soc.*, vol. 9, pp. 171–180, 2012.

[89] Y. Jin, F. Liu, M. Tong, and Y. Hou, "Removal of arsenate by cetyltrimethylammonium bromide modified magnetic nanoparticles," *J. Hazard. Mater.*, vol. 227–228, pp. 46 – 468, 2012.

[90] M. A. Karimi, S. Z. Mohammadi, A. Mohadesi, A. Hatefi-Mehrjardi, M. Mazloum-Ardakani, L. Sotudehnia Korani, and A. Askarpour Kabir, "Determination of silver(I) by flame atomic absorption spectrometry after separation/preconcentration using modified magnetite nanoparticles," *Sci. Iran.*, vol. 18, no. 3, pp. 790–796, 2011.

[91] S. Li, J. C. Day, J. J. Park, C. P. Cadou, and R. Ghodssi, "A fast-response microfluidic gas concentrating device for environmental sensing," *Sensors and Actuators*, vol. 136, no. 1, pp. 69–79, 2007.

[92] O. Ymbern, N. Sández, A. Calvo-López, M. Puyol, and J. Alonso-Chamarro, "Gas diffusion as a new fluidic unit operation for centrifugal microfluidic platforms," *Lab a \Chip*, vol. 14, no. 5, pp. 1014–1022, 2014.

[93] T. Becker, S. Mühlberger, C. Bosch-v.Braunmühl, G. Müller, A. Meckes, and W. Benecke, "Microreactors and microfluidic systems: An innovative approach to gas sensing using tin oxide-based gas sensors," *Sensors and Actuators*, vol. 77, no. 2, pp. 48 – 54, 2001.